OVERLAP OF CARGO ADAPTOR BINDING SITES ON MYOSIN V COORDINATES THE INHERITANCE OF DIVERSE CARGOES

by

Patrick Taylor Eves

A dissertation submitted in partial fulfillment
of the requirements for the degree of
Doctor of Philosophy
(Cellular and Molecular Biology)
in the University of Michigan
2012

Doctoral Committee:

Professor Lois S. Weisman, Chair
Professor Peter Arvan
Professor Robert S. Fuller
Professor Joel A. Swanson
Associate Professor Kristen J. Verhey

DEDICATION

This thesis is dedicated to the memory of Donna and Daniel Leon, and Helen Margaret Feather, whom I lost while I was pursuing my dreams.

ACKNOWLEDGMENTS

I would like to first thank my mentor Dr. Lois Weisman. More than anything else, she has introduced me to the amazing world of cell biology. She possesses many qualities that make her an exceptional mentor, both intellectually and on a personal level. Dr. Weisman has been a continual positive motivator in my thesis work and I deeply value her encouragement and commitment to my success.

I want to thank current and former lab members that have helped me on many different levels during my time in the lab: Dr. Yui Jin, Emily Kauffman, Dr. Natasha Pashkova, Dr. Connie Yutian Peng, Dr. Yanling Zhang, Dr. Sergey Zolov, Dr. Natsuko Jin, Dr. Raj Valiathan, Matthew Brunner and Richard Yau.

I also thank the members of my committee for their significant contribution to my work. Their guidance kept me on track with my thesis and it was very gratifying having their shared involvement in my work. I also thank Dr. Jessica Schwartz for her advice and guidance in completing my thesis. As well, I thank Cathy Mitchell for her skilled administration of CMB. The CMB program provided funding for my thesis work for two years, and I am grateful for this contribution.

I wish to thank Mark Nance (Tesmer Lab, UM) for guidance on protein expression and purification. I also thank Dr. Levi Blazer (Neubig Lab, UM) for assistance with the FCPIA assay, Dr. Jeff Moore (Cooper Lab, Wash U, St. Louis) for Tub1-GFP

plasmids and advice, Dr. Janet Shaw (U of Utah) for mitoGFP/RFP plasmids and Dr. Amir Khan (U of Dublin) for *in vitro* expression vectors.

Most importantly, I cannot thank my family enough for their unconditional love, support and understanding as I have pursued my education. I am thankful for all my friends that shared the past six years with me.

I acknowledge Eves *et al*., (manuscript under review) with contributions from Dr. Lois Weisman.

TABLE OF CONTENTS

LIST OF FIGURES

Figure

LIST OF TABLES

Table

LIST OF ABBREVIATIONS

AD	activation domain
ARM	armadillo repeat
BD	binding domain
BR	binding region
BSA	bovine serum albumin
CBD	cargo binding domain
CC	coiled-coil
DMSO	dimethyl sulfoxide
DTT	dithiothreitol
ER	endoplasmic reticulum
ERMES	endoplasmic reticulum-mitochondrial encounter structure
FM4-64	*N*-(3-triethylammoniumpropyl)-4-(6-(4-(diethylamino)phenyl) hexatrienyl)pyridinium dibromide
GFP	green fluorescent protein
GST	glutathione S-transferase
GTD	globular tail domain
GTP	guanosine triphosphate
KHC	kinesin heavy chain
KLC	kinesin light chain

MBP	maltose binding protein
MT	microtubule
NaOH	sodium hydroxide
ORF	open reading frame
PEST	proline glutamate serine and threonine
$PI3,5P_2$	phosphatidylinositide 3,5-bisphosphate
SDS-PAGE	sodium dodecyl sulfate-polyacrylamide gel electrophoresis
SV	secretory vesicle
TCA	trichloroacetic acid
TEV	tobacco etch virus
TM	transmembrane domain
TOR	target of rapamycin
YEPD	yeast extract-peptone-dextrose

ABSTRACT

Membrane-bound organelles are essential components of eukaryotic cells. Similar to chromosomes, specific mechanisms exist to ensure that partitioning of each organelle to the daughter cell occurs. Moreover, the proper amount of each organelle is distributed to a specific location in the daughter.

The budding yeast *Saccharomyces cerevisiae*, provides a unique model to determine the mechanisms of organelle inheritance. Unlike other organisms, where organelle movement requires an interplay between two cytoskeletal systems, actin and microtubules, most cytoplasmic organelles in budding yeast move solely on actin. Moreover, virtually all of the cytoplasmic organelles are moved by a single myosin V, Myo2. Despite the fact that one motor is involved, the itinerary and ultimate location of each organelle is unique. These itineraries are regulated in part through specific cargo adaptor proteins that link Myo2 to each organelle. The existence of specific cargo adaptors, suggested the possibility that cargo adaptors provide the main regulation of cargo movement, while the Myo2 motor provides an inert platform for cargo binding. In further support of this postulate, the vacuole-specific adaptor Vac17, and the secretory vesicle-specific Rabs Ypt31/Ypt32, bind to distinct sites on Myo2. This suggested that each adaptor might bind a unique location on the Myo2 cargo binding domain.

Here we demonstrate that Mmr1 is a cargo adaptor that links the mitochondria membrane to Myo2. Notably, the binding site for Mmr1 overlaps with the binding site for Vac17, a member of the cargo adaptor complex that links the vacuole membrane to Myo2. Importantly, we find that Vac17 and Mmr1 compete for binding at this site. This competition had the unexpected result of regulating the volume of vacuoles and mitochondria inherited by the daughter cell. We find that eight of the nine known Myo2 cargo adaptors overlap at either of two sites. Vac17 and Mmr1 overlap at one site, while Ypt11 and Kar9 bind subsets of residues that also bind Ypt31/Ypt32, Sec4 and Inp2. Thus, competition for access to Myo2 may be a common mechanism to coordinate the inheritance of diverse cargoes.

CHAPTER 1

INTRODUCTION

Eukaryotic cells are distinguished from their prokaryotic ancestors by the presence of membrane-bound organelles. Organelles perform distinct yet cooperative tasks. For instance, mitochondria specialize in ATP production, while lysosomes produce hydrolytic enzymes that break down discarded or damaged cellular proteins. Together, organelles allow the cell to persist as a single synergistic unit using a division of labor to provide specialized products (Shimizu and Haken 1983).

A common untested assumption is that the total amount, volume and position of each organelle is defined for each cell type. Analysis of electron micrographs reveals that different cell types have different ratios of organelle volume, surface area and copy numbers relative to other cells. These ratios likely reflect their functions (Warren and Wickner 1996). For example, secretory cells contain a larger proportion of secretory organelles, such as the endoplasmic reticulum (ER) and Golgi network. The intracellular space is also heterogeneous, where intracellular compartments are positioned to meet functional requirements. For instance, insulin-secreting cells in the pancreas receive chemical messages at their basolateral membranes and transport vesicle away from the cell nucleus, toward the apical membrane (Watson and Pessin 2001; Hou *et al*., 2009). Here, the vesicle contents are released into ducts. This intracellular asymmetry is critical to cell function (Pruyne *et al*., 2004; Neumüller and Knoblich 2009).

The evolution of eukaryotes meant increasingly complex functions and structures for each organelle. The *de novo* formation of an organelle may have demanded too much time and energy. Rather than generate new organelles with each round of cell division, efficiency was maintained by transporting portions of each organelle from the mother into the daughter cell (Lowe and Barr 2007). This process, by which the mother cell contributes a portion of each organelle to the daughter cell, is called organelle inheritance (Warren and Wickner 1996).

Until recently there was little understanding of how cells control the inheritance of their organelles, an essential process for many organelles. An exciting notion in the field of organelle inheritance is that similar mechanisms govern the initiation of movement, transport, and retention of membrane-bound compartments during cell division (Munson and Novick 2006; Weisman 2006). Because all eukaryotes have similar characteristics at the cellular level, *Saccharomyces cerevisiae* has played a vital role in understanding mechanisms of organelle inheritance. While metazoans and some yeast species coordinate movement on both microtubule and actin cytoskeletons for transport of many cargoes, *S. cerevisiae* utilize actin for relatively long range transport. Thus studies of this yeast can contribute to the actin-based portion of organelle motility.

Organelle inheritance in budding yeast

Saccharomyces cerevisiae, or budding yeast, consists of a single cell that is highly asymmetric. Initially, a small bud forms on the plasma membrane surface which grows and becomes the daughter cell (Figure 1.1). Once the bud has reached sufficient size, the

cell cycle is completed by separating the daughter from the mother cell. As a result, the daughter cell will become a new mother cell, and both mother cells produce new buds.

In the early phase of the cell cycle, a bud site is selected. Both actin-nucleating proteins, Bni1 and Arp2/3 complex, and the regulatory proteins Cdc24 and Cdc42 localize to the nascent bud site (Pruyne and Bretscher 2000; Moseley and Goode 2006). Actin cables assemble at the bud tip and bud neck and extend deep into the mother cell. Actin cables consist of bundles of actin filaments which are polarized toward the bud tip, known as the "plus" end of the actin cable (Moseley and Goode 2006). The bud emerges with concurrent growth in actin cable length by the addition of actin monomers at the "plus" end, which grow toward the "minus" end (i.e., opposite end from the bud tip), and the fusion of secretory vesicles to the plasma membrane at the bud tip. It is important to note that any position along an actin cable is in constant flow toward the "minus" end of the cable (retrograde flow) due to addition of actin monomers at the "plus" end.

As the bud expands in volume, organelle cargoes are carried along actin cables to the bud. A drawing representing a single budding yeast cell undergoing organelle inheritance is shown in Figure 1.1. The cargoes individually pass from the mother to the bud by crossing through the mother-bud neck. The cargoes are then delivered to the correct position in the daughter cell. In budding yeast, sister chromatids are separated within the nuclear envelope compartment that remains intact. This process is distinguished from metazoan cells in which the nuclear envelope breaks down (Hetzer 2010). Since the nucleus has a diameter many times the size of the mother-bud neck, a small tubule forms and stretches into the bud (Merlini and Piatti 2011). The vacuole,

which is often larger than the nucleus, must also form small tubules that progress through the mother-bud neck (Weisman 2003).

Organelles are inherited to ensure propagation in the daughter cell. However the inheritance of only some organelles is essential, while other organelles can be made *de novo*. The inheritance of at least three distinct organelles is essential: the nucleus, mitochondria (Garcia-Rodriguez *et al*., 2009) and the ER (Du *et al*., 2004). The nuclear envelope, along with a single copy of the genome, must be inherited from the mother. Second, mitochondria contain a single chromosome that encodes mitochondrial proteins not encoded in the nuclear genome. Thus inheritance of mitochondria is also essential. Third, the ER is the site of membrane protein insertion and the site of membrane genesis. ER inheritance, or at least a small portion of it, is essential (Estrada de Martin *et al*., 2005). While the inheritance of these three organelles is essential, they each have redundant mechanisms to ensure their proper partitioning to the daughter cell.

Other organelles, though inherited in wild-type cells, can be generated *de novo* in the absence of an active inheritance pathway. The Golgi, peroxisomes and the vacuole can form from preexisting organelles or be generated *de novo*. In addition, while some bud-targeted mRNAs are inherited from the mother cell, this process is not essential and can be translated from mRNAs originating in the bud.

Vacuole inheritance

The yeast vacuole functions similarly to the mammalian lysosome (Armstrong 2010). The vacuole serves several critical functions. It receives and enzymatically degrades discarded or dysfunctional proteins and membranes. The vacuole is also a major storage

site for water, phosphate, amino acids and specific metal ions. Though the vacuole is an essential organelle, inheritance of the vacuole is not essential. In cases when the vacuole is not inherited, the cell cycle is delayed until a vacuole is formed *de novo* (Weisman and Wickner 1992).

Budding yeast undergoing vacuole inheritance often display a long vacuole tubule stretched across the cell into the small bud (Weisman 2003). This appearance of the vacuole is called the segregation structure. Occasionally the vacuole is seen moving into the bud as individual vesicles, though this may be the result of light-induced vesiculation (unpublished observations). Once the correct proportion of vacuole reaches the bud, vacuole inheritance is terminated and the vacuole is anchored in the bud. Isolation of yeast mutants that were defective in vacuole inheritance lead to the discovery that vacuole inheritance was actin-based and required the myosin V motor protein, Myo2 (Catlett and Weisman 2000).

Understanding the molecular basis for organelle inheritance

Myo2: a myosin V motor

Treating cells with latrunculin-A, an actin polymerizing inhibitor, disrupts actin filament formation within minutes. Interestingly latrunculin-A also disrupts localization of Sec4, an essential GTPase that regulates transport of secretory vesicles to the exocyst complex (Ayscough *et al*., 1997). This and similar findings founded the hypothesis that transport of intracellular cargo was based on actin filaments. A temperature-sensitive screen for mutants that affected the yeast cell cycle identified *cdc66*, a mutant which had an unbudded phenotype at the restrictive temperature of 36°C (Prendergast *et al*., 1990).

The allele was identified as a mutation within *MYO2*, an essential gene required for transport of secretory vesicles, and renamed *myo2-66* (Johnston *et al*., 1991).

The *MYO2* gene encodes a 180 kilodalton (kDa) heavy chain protein which dimerizes to form the active motor protein (Figure 1.2). Each heavy chain consists of four functional domains (Trybus 2008). The N-terminus of the protein contains the motor domain, which includes the highly conserved actin-binding and ATP-binding (i.e., the P-loop) domains. Following ATP binding, hydrolysis of the terminal phosphate causes a swinging movement of the lever arm which produces the power stroke that shifts the motor forward (Veigel *et al.,* 2002). One swing of the head domain produces a step size of 72 nm on an actin filament (36 nm between motor domains) (Walker *et al*., 2000; Yildiz *et al*., 2003).

As a dimer, Myo2 likely functions as a processive motor similar to its mammalian myosin V counterparts (Dunn *et al*., 2007; Hammer and Sellers 2012). Processivity is a mechanism by which a motor remains attached to an actin cable for a series of steps, rather than falling off after just one or two. One study demonstrating Myo2 is non-processive (Reck-Peterson *et al*., 2001) is routinely cited, yet this study utilized *in vitro* motility assays to make their conclusion and does not reflect an *in vivo* environment. Smy1, a Myo2-binding protein with kinesin homology that lacks motor function (Lillie and Brown 1998), may help Myo2 remain attached to actin through Smy1 electrostatic interactions with actin (Hodges *et al*., 2011). This may explain the observation that Smy1 overexpression increases viability of a *myo2* mutation that disrupts motor function (Beningo *et al*., 2000).

Adjacent to the head domain, Myo2 has six IQ motif tandem repeats, named for the increased proportion of isoleucines (I) and glutamines (Q) present in this motif. Collectively, the IQ motifs form the lever-arm; some deletions of this domain affect the velocity of the motor (Schott *et al*., 2002). Each IQ motif has a consensus sequence IQxxxRGxxxR, where 'x' denotes any amino acid (Terrak *et al*., 2005). IQ motifs interact with the myosin light chain protein Mlc1, a member of the calmodulin family of proteins, and provide rigidity to the lever arm. Though several co-crystal structures of Mlc1 bound to IQ motifs of Myo2 are solved (Terrak and Dominguez 2003; Terrak *et al*., 2005; Houdusse *et al*., 2006), it is not clear which IQ motif functions *in vivo* to bind Mlc1. Determining the correct IQ motif(s) which bind Mlc1 *in vivo* is important because the rate limiting step of the ATPase cycle is significantly affected depending on which IQ motif is bound to myosin light chain (De La Cruz *et al*., 2000).

The third domain, the dimerization or coiled-coil (CC) domain, allows Myo2 heavy chains to dimerize. This is thought to be an essential part of motor function. In myosin Va and Vb, the dimerization domain also contains a PEST domain, however no identifiable PEST sequence is present in Myo2, Myo4 or myosin Vc. PEST domain function in myosin V is not understood (Rodriguez and Cheney 2001).

The C-terminus of Myo2 is the cargo binding domain (CBD), also known as the globular tail domain (GTD). It comprises the last 487 residues of the Myo2 heavy chain. The CBD interacts with at least eight different cargo adaptor proteins (Fagarasanu and Rachubinski 2010). Cargo adaptors allow myosin V motors to connect to organelles and other cargoes. Studies initially defined the Myo2 CBD using trypsin proteolysis (Pashkova *et al*., 2005), from which a stable protein product is obtained. The crystal

structure of the Myo2 CBD was solved at high resolution (2.2 Å) and was the first cargo binding domain structure of any molecular motor to be solved (Pashkova *et al*., 2006). This structure has provided insight into how cargoes attach to Myo2. The CBD is composed of fifteen anti-parallel helices that fit together in a compact globular fold, ending with a long loop containing two helices. The loop wraps back to the N-terminus of the CBD. The crystal structure of the CBD revealed that mutations in Myo2 that disrupted vacuole inheritance were clustered at a specific region on the surface of Myo2. Moreover, residues that disrupted secretory vesicle transport mapped to the opposite face of the CBD (Pashkova *et al*., 2006; Lipatova *et al*., 2008) (Figure 1.2).

Two interesting findings suggest alternative yet important ways in which cargo transport by myosin V motors are regulated. It was found that in the absence of calcium and cargo, myosin Va can assume a folded, inactive state, whereby the motor domain bends toward the CBD (Liu *et al*., 2006). This hypothesis suggests that the motor may bind to the CBD, making it inaccessible to binding partners. It is appealing to speculate that Myo2 may be recycled after cargo delivery. Release of a cargo induces the motor to fold and "turn off", the motor gets recycled by binding a plus-end motor protein, where it begins a new round of cargo transport (Taylor 2007). Second, the Myo4 CBD crystal structure was recently solved and exhibits high structural similarity to Myo2 CBD (Heuck *et al*., 2010). Despite sequence and structural homology, the mechanism by which Myo2 and Myo4 attach to cargoes appear to differ considerably (Mueller *et al*., 2011; Heuck *et al*., 2007).

Cargo adaptor proteins play a major role in the regulation of cargo attachment and detachment from myosin V

Myo2 carries the majority of cargoes within budding yeast, with the exception of cortical ER and some messenger RNAs, which are moved by Myo4. Myo2 transports each cargo by binding to a specific cargo adaptor protein. Myo2 transports vacuoles by binding to Vac17, which binds to Vac8 on the vacuole membrane (Ishikawa *et al*., 2003; Tang *et al*., 2003). Post-Golgi secretory vesicles are moved via Myo2 binding of Ypt31/Ypt32, Sec15 and Sec4 (Jin *et al*., 2011; Santiago-Tirado *et al*., 2011). Peroxisomes bind to Myo2 through Inp2 (Fagarasanu *et al*., 2009). Mitochondria bind to Myo2 via Mmr1 and/or Ypt11 (Itoh *et al*., 2002; Itoh *et al*., 2004; Fortsch *et al*., 2011). A Myo2-dependent role for Golgi transport was identified (Rossanese *et al*., 2001b). Evidence suggests this occurs through Ypt11 (Aria *et al*., 2008), though a more definitive understanding of Ypt11's role is needed. Myo2 orients the bud-directed terminus of the mitotic spindle via Kar9, ensuring that the dividing nucleus is properly polarized toward the bud (Beach *et al*., 2000; Korinek *et al*., 2000; Yin *et al*., 2000).

In several cases, cargo adaptors are post-translationally modified. Several different classes of modification provide a platform for achieving proper cargo transport. These include phosphorylation (Peng and Weisman 2008; Fagarasanu *et al*., 2009), SUMOylation (Leisner *et al*., 2008) and covalent attachment to lipids for membrane recruitment (Segev 2001; Peng *et al*., 2006). Modifications of these adaptors are likely to be important for spatial and temporal control of organelle movement. These modifications will be discussed with the relevant cargo adaptors in this section.

Vac17/Vac8 Complex

One of the better characterized myosin V cargo adaptor complexes is the vacuole-specific transport complex, in which the cargo adaptor Vac17, is sandwiched between the Myo2 motor and Vac8 on the vacuole. *VAC17* was initially identified in a screen which sought genes other than *MYO2* that, when over-expressed, suppressed the vacuole inheritance defect of a *myo2* point mutant, *myo2-2* (*myo2*-G1248D) (Ishikawa *et al*., 2003). An additional independent screen sought extragenic mutants of *MYO2* that suppressed the vacuole inheritance defect of *myo2*-N1304S, identified a *VAC17* mutant, *vac17*-S57F (Ishikawa *et al*., 2003).

Some functional domains within Vac17 have been identified (Weisman 2006). A central PEST domain of ~50 amino acids is key for Vac17 turnover. PEST domains are enriched in proline (P), glutamate (E), serine (S) and threonine (T) residues, and are often found in proteins degraded in a ubiquitin-dependent manner (Rechsteiner and Rogers 1996). Vac17 mutants with a deletion of the PEST domain, or specific point mutations within the PEST domain, elevate Vac17 protein ~10-fold (Tang *et al*., 2003; Tang *et al*., 2006). Moreover, the Vac17-ΔPEST mutant is constitutively attached to Myo2 and the vacuole throughout its itinerary, causing mislocalization of the vacuole to the mother-bud neck region (Tang *et al*., 2003).

Vac17 contains two putative coiled-coil domains (CC1 and CC2), one at each terminus of the protein; their functions are not presently known. A point mutation in CC1, *vac17*-S57F, which is outside of the Myo2 binding domain, is able to restore vacuole inheritance of all *myo2* point mutants. However, interaction between *myo2* point mutants and *vac17*-S57F is still disrupted (Ishikawa *et al*., 2003). This observation raises

the possibility that additional proteins function in the vacuole-specific transport complex with Myo2. Inclusion of either domain into constructs for *in vitro* expression purposes produces high molecular weight aggregates (unpublished results), thus their functions are difficult to pursue using *in vitro* studies. Vac17 also interacts with Atg18, a regulator of phosphatidylinositide 3,5-bisphosphate ($PI3,5P_2$) (Efe *et al*., 2007). The function of this interaction is presently unknown.

In addition to Myo2, Vac17 also binds to Vac8, a peripheral vacuole membrane protein. Vac8 is palmitoylated and myristoylated, modifications that attach Vac8 to the vacuole membrane (Peng and Weisman 2006). Vac8 is an Armadillo (ARM) repeat-containing protein containing eleven ARM domains. ARM domains are often found in proteins that act as molecular signaling scaffolds (Tewari *et al*., 2010; Peifer *et al*., 1994). In addition to binding to Vac17, Vac8 has at least three additional, independent functions. Vac8 is a member of the Cvt (the cytoplasm-to-vacuole targeting) pathway and the Nvj (nucleus-to-vacuole junction) pathway (Tang *et al*., 2006). Vac8 also interacts with Tco89, a subunit of the TOR complex 1 (TORC1) (Tang *et al*., 2006). Thus Vac8 integrates several pathways that converge on the vacuole membrane.

In cells with a *vac8* deletion, Vac17 localizes to the bud tip in small and medium budded cells, and the mother-bud neck in large budded cells (Peng and Weisman 2008), the site where Myo2 localizes. That Vac17 is bound to Myo2 in the absence of Vac8 suggests that Vac17 need not be connected to Vac8 nor the vacuole in order to bind Myo2. Conversely, in *myo2* mutations that disrupt interaction with Vac17, Vac17 localizes strictly to the vacuole membrane. Thus the order of the binding of Vac17 with Myo2 and Vac8 in wild-type cells, remains to be determined.

Mmr1

The mitochondrial Myo2-receptor related protein 1 (Mmr1) was identified as a mitochondrial peripheral membrane protein which localized to mitochondria in the tips of small budded cells (Itoh *et al*., 2004). It binds to Myo2 both *in vivo* and *in vitro* (Itoh *et al*., 2004). In cells deleted for *MMR1*, mitochondria distribution is abnormal and mitochondria are often missing from small buds. In *mmr1*Δ cells, the mitochondrial network is fragmented and may therefore have additional roles in mitochondrial fusion (Swayne *et al*., 2011). In *mmr1*Δ yeast, as the bud size increases, mitochondria distribution is partially corrected, indicating that additional mechanisms of inheritance/distribution are involved.

Point mutations in Myo2 that disrupt Vac17 interaction with Myo2, for example, *myo2*-N1304D, also disrupt mitochondria inheritance (Altmann *et al*., 2008). Since *myo2*-N1304D is a surface residue, this might suggest that a protein factor binds at the same site of Vac17 to coordinate the inheritance of mitochondria. Furthermore, a Myo2 mutant, *myo2-573*, which contains six point mutations in the CBD, disrupted Mmr1 binding to Myo2 (Itoh *et al*., 2004). Together, these studies implicated Mmr1 as a mitochondria cargo adaptor that binds to a surface region of Myo2 that overlaps with the Vac17 binding site.

An alternative hypothesis has been proposed that Myo2 does not actively transport mitochondria. According to this hypothesis, Mmr1 protein is transported to the bud tip where it interacts with Myo2 to capture or "tether" mitochondria (Shepard *et al*.,

2003; Peraza-Reyes *et al*., 2010; Swayne *et al*., 2011). These findings however, do not directly address whether Mmr1 functions with Myo2 for transport of mitochondria.

Ypt11

Ypt11 is a small Rab GTPase. It is the most distantly related of eleven Rab GTPases in budding yeast. At 417 amino acids in length, it is almost twice the size as other Rabs, and interacts directly with the Myo2 CBD (Itoh *et al*., 2002). Studies that relate Ypt11's GTPase activity to its function have not been performed. Ypt11 has been implicated in the inheritance of three organelles: mitochondria, the ER and the late Golgi. Each is discussed below.

A role for Ypt11 in mitochondria inheritance came from the finding that deletion of Ypt11 produced a mitochondria inheritance defect (Itoh *et al*., 2002). Conversely over-expression of Ypt11 resulted in bud accumulation of mitochondria in ~80% of budded cells. In these cells, vacuole inheritance was normal. A *myo2* mutant that disrupts mitochondria inheritance, *myo2-338*, disrupted interaction with Ypt11 (Itoh *et al*., 2002). Thus Ypt11 interaction with Myo2 plays a role in mitochondria inheritance.

Interestingly, *YPT11* deletion has strong synthetic effects with *MMR1* or *GEM1* deletion (Frederick *et al*., 2008). Gem1 is a Rho-type GTPase that has very recently been found to be part of the ERMES (ER-mitochondrial encounter structure; formerly called the Mitochore) complex (Kornmann *et al*., 2011), which physically links the ER with mitochondria and functions independently of Myo2. ERMES mutants severely disrupt mitochondria morphology (Kornmann *et al*., 2009). It was also shown that mutations in Myo2 that disrupt vacuole inheritance (*myo2*-L1301P and *myo2*-Q1233R) are

synthetically lethal with *YPT11* deletion (Förtsch *et al*., 2011). One complication of these studies is that Ypt11 is also involved in mitochondria inheritance, yet its molecular role is not known.

Ypt11 is reported to localize to the ER *in vivo*. In yeast, the ER exists at two distinct pools, a nuclear pool that surrounds the nucleus, and a cortical pool adjacent to the plasma membrane. A study in which seven of the eleven small Rab GTPases in yeast were tagged with fluorescent markers revealed that Ypt11 extensively co-localized with the ER near the cell cortex (Buvelot Frei *et al*., 2006). Ypt11 was also cloned into a mammalian expression vector. Similar to yeast, it co-localized with ER compartments and KDEL-positive compartments (ERGIC compartments) (Buvelot Frei *et al*., 2006). Because mitochondria and the ER are physically linked through the ERMES complex, the transport of mitochondria may be coupled to ER transport, and the Myo2/Ypt11 complex may jointly carry both organelles.

Ypt11 plays an additional role in Golgi inheritance. Unlike metazoans, budding yeast Golgi are not arranged in parallel stacks. Instead, the Golgi cisternae are spread throughout the cytoplasm (Fagarasanu and Rachubinski 2007). Whereas early Golgi elements localize to the bud in an actin-independent and Myo2-independent manner, late Golgi elements require actin, Myo2 and Cdc1 (Rossanese *et al*., 2001). It was reported that overexpression of Ypt11, using a *GAL1* promoter, caused the accumulation of Ret2-containing Golgi vesicles in the bud (Arai *et al*., 2008). This effect was dependent on Myo2; a *myo2* mutant that disrupts Ypt11 binding inhibited the accumulation of Golgi vesicles in cells overexpressing *YPT11*. Thus, Ypt11 functions in the transport of several organelles.

Ypt31/Ypt32, Sec4 and Sec15

During the budding yeast cell cycle, new growth is targeted almost exclusively to the bud (Pruyne *et al*., 2004). Secretory vesicles move along actin cables toward the bud and fuse with the exocyst at the PM. Transport from the late Golgi to the plasma membrane is regulated by Rab GTPases Ypt31/Ypt32 and Sec4, which form a "cascade" (Grosshans *et al*., 2006). In the Rab cascade, Ypt31/Ypt32 recruits Sec2, a guanine nucleotide exchange factor (GEF) that activates and recruits Sec4. Notably, all of these Rab GTPases bind to Myo2 (Jin *et al*., 2011; Santiago-Tirado *et al*., 2010) and are essential for Myo2 attachment to secretory vesicles. A subunit of the exocyst, Sec15, binds Myo2 CBD (Jin *et al*., 2011). Interestingly, Ypt31/Ypt32 and Sec4 bind to a single overlapping region on the Myo2 CBD whereas Sec15 binds on the opposite side.

The regulation of Rab attachment to Myo2 and Rab detachment from Myo2 are unique to the Rab GTPase cargo adaptors. For Rab GTPases, the C-terminal prenyl group has a direct affect on Rab localization to a specific membrane. Ypt31, Ypt32 and Sec4 insert their hydrophobic tails into the lipid bilayer, where a membrane-associated GEF activates the Rab (Grosshans *et al*., 2006). The binding of guanine-nucleotide dissociation inhibitors, or GDIs, which mask the prenyl group when not attached to the membrane, is coupled with a Rab's GTP/GDP cycle. Once the Rab GTPase hydrolyzes GTP to GDP, the Rab becomes inactive. It is not clear if an inactivated Rab protein directly causes dissociation from Myo2 or GDI-binding of the Rab GTPase causes Myo2 dissociation.

Inp2

Inp2 functions in the inheritance of peroxisomes. Inp2 is a single-pass integral membrane protein on the outer peroxisome membrane, and directly links peroxisomes to Myo2 (Fagarasanu *et al*., 2006). Further, Inp2 expression is coordinated with the cell cycle. Inp2 expression rises during peroxisome inheritance and falls at its conclusion (Fagarasanu *et al*., 2009). Mutations in Myo2 that disrupt Inp2 binding cause a cause a rise in steady-state levels in Inp2 protein.

Similar to Vac17, Inp2 is phosphorylated (Fagarasanu *et al*., 2009). Peak phosphorylation occurs during peroxisome inheritance. Consensus Cdk1 sites have also been identified in Inp2 (Peng and Weisman 2008) suggesting phosphorylation of Inp2 may be positively associated with Inp2 binding to Myo2 and peroxisome inheritance.

Kar9

In yeast, the actin cytoskeleton and Myo2 play a major role in nuclear segregation. Lat-A, an inhibitor of actin polymerization, disrupts nuclear orientation early in the cell cycle, however this is corrected at later stages (Theesfeld *et al*., 1999), due to an independent dynein pathway (Grava *et al*., 2006; Eshel *et al*., 1993).

KAR9 (for Karyogamy 9) was identified as a gene whose mutation resulted in misoriented microtubules, and increased frequency of binucleated cells (Kurihara *et al*., 1994). Kar9 acts as a cargo adaptor that links Bim1, a protein that caps the end of spindle microtubules, to Myo2 (Beach *et al*., 2000; Korinek *et al*., 2000; Lee *et al*., 2000; Miller *et al*., 2000; Yin *et al*., 2000). The Myo2/Kar9/Bim1 complex functions to orient the mitotic spindle before nuclear division so that the dividing nucleus is polarized toward

the bud. The force behind separating the nucleus occurs via dynein motors (Grava *et al*., 2006). Initially Kar9 localizes to the bud-proximal spindle microtubule (i.e., the aster). Later, when the nucleus is dividing, Kar9 localizes to the distal microtubule of the mother cell.

This asymmetric localization of Kar9 has been attributed to phosphorylation and SUMOylation. At least two residues on Kar9 are phosphorylated (Liakopoulos *et al*., 2003; Maekawa *et al*., 2003). Both sites are phosphorylated by Cdc28, however cyclin specificity for these two sites differs. S197 is phosphorylated by Cdc28/Clb4, while S496 is phosphorylated by Cdc28/Clb5 (Moore and Miller 2007). Phosphorylation at serine 197, adjacent to the Bim1 binding region, and serine 496 (Figure 1.3), inhibits attachment to the distal spindle pole body which ensures that Kar9 only attaches to the SPB oriented toward the mother-bud neck.

Kar9 is SUMOylated on four lysine residues (Leisner *et al*., 2008). SUMO is ligated to a lysine (K) within the consensus sequence ΨKXD/E of the target protein, where Ψ represents an aliphatic hydrophobic residue, and X represents any residue. SUMO has typically been studied in the context of transcription regulation, in which a transcription factor is shuttled between the cytoplasm and nucleus via interaction with a binding partner containing a nuclear localization sequence (Verger and Crossley 2002). SUMO directly regulates this interaction. In the case of Kar9, SUMO promotes asymmetric localization of Kar9 to the bud-proximal SPB (Leisner *et al*., 2008; Meednu *et al*., 2008). Thus, while Kar9 is phosphorylated and SUMOylated, evidence is lacking whether these modifications work independently or in concert to coordinate Kar9 localization.

Mechanisms that coordinate organelle inheritance

Ultimately, the transport of all organelles and cargoes is coordinated so that inheritance is completed prior to cytokinesis. Studies of Vac17 have yielded insight into how yeast initiates vacuole inheritance. Vac17 is a direct target of the cell cycle control protein, Cdk1. Cdk1 phosphorylates Vac17 and this phosphorylation peaks when vacuole inheritance peaks (Peng and Weisman 2008). Mutation of consensus Cdk1 sites in Vac17 decreases Vac17 interaction with Myo2 and causes vacuole inheritance defects. That Kar9, Mmr1 and Inp2 also contain putative Cdk1 consensus sites (Peng and Weisman 2008) or are already known to be phosphorylated by Cdk1, suggests that inheritance of most organelles is coordinated with the cell cycle.

There is recent evidence that a cell cycle check point exists for some organelles, for example, the cortical ER (Babour *et al*., 2010) and mitochondria (Garcia-Rodriguez *et al*., 2009). A spindle assembly checkpoint was previously identified (Amon 1999). Mammalian organelle-related checkpoints are also known. For example, in addition to several cell cycle checkpoints, a Golgi fragmentation checkpoint prior to partitioning into daughter cells has been determined (Colanzi *et al*., 2007). Whether all organelles have similar checkpoints remains to be determined, though several regulators of budding yeast ER and mitochondria checkpoints are conserved in metazoans.

Variety of cargo attachment in the myosin family

All myosin motors characterized to date bind to actin cables via similar mechanisms. With one exception, myosin motors travel toward the plus-end of actin cables, toward the

cell periphery. Interestingly, myosin VI, a minus-end directed motor, travels in the opposite direction. Studies have confirmed, however, that myosin VI interacts with actin cables similarly to other myosins. The reverse directionality originates from two additional inserts that cause the lever arm to swing in the opposite direction (Ménétrey *et al*., 2005).

Based on the strict sequence conservation of the motor domain, two methods have been proposed to classify myosin genes. One highly cited study grouped myosins into twenty-four families based upon phylogenetic analysis of the motor domain (Foth *et al*., 2006). Another study, arguably more useful, categorized myosins into thirty-six groups based on sequence similarity to protein domains outside of the motor domain (Richards and Cavalier-Smith 2005). The benefit of this approach is that it correlates with a motor's molecular function. A caveat to this, however, is that many motors currently have protein domains of unknown functions.

Though the various motor domains of myosins interact with actin via the same mechanism throughout the family, analysis of the cargo binding domains revealed that the mechanisms employed to attach motors to their cargoes is highly diverse (Mooseker and Foth 2008). The primary reason for this is likely because the cargoes themselves are varied and numerous, and differ among cell types. Moreover, a single motor may have multiple cargoes. Interestingly, the C-terminal cargo binding region of the ~twenty-four classes of myosins varies in length and composition considerably. For example, *T. gondii* myosin XIVa has one of the shortest cargo binding domains, approximately 35 residues, while *C. elegans* myosin XII has a cargo binding domain more than double the length of the myosin V CBD (Foth *et al*., 2006).

At both a genetic and biochemical level, the cargo binding domain of class V myosins are the best characterized in the myosin family (Schliwa and Woehlke 2003). In mammalian melanocytes, myosin V interacts with the small Rab GTPase Rab27a which also interacts with melanophilin to enable distribution of melanosomes to the cell cortex. Since budding yeast Myo2 contains a small Rab GTPase site as well, and since the residues which are required for Ypt31/Ypt32 binding are conserved between yeast and humans (Jin *et al*., 2011), it is likely that, though untested, Rab27a binds to the same region on myosin Va as Ypt31/Ypt32 binds to Myo2. Thus it is possible that while individual cargo adaptor proteins may have distinct functions between different species, the binding sites on the CBD of myosin V function similarly for similar cargoes.

Kinesins share some similarities to myosins

Kinesins also contain a conserved motor domain that interacts with microtubule filaments, and a highly variable cargo binding domain, or tail. Notably, eukaryotic organisms such as animals have established an accessory subunit, the kinesin light chain (KLC), which directly binds to the tail of a single kinesin heavy chain (KHC). These serve to mediate distinct molecular interactions with cargo (Vale 2003). The KLC tetracopeptide region interacts with several proteins, including Jun-N-terminal kinase (JNK)-interacting protein 1 (JIP1) (Verhey *et al*., 2001; Byrd *et al*., 2001) JIP2 and JIP3 (Hirokawa and Takemura 2005), amyloid precursor protein (APP) (Kamal *et al*., 2000) and vaccinia viral protein (Rietdorf *et al*., 2001). Moreover, the KHC interacts with GRIP1, a glutamate receptor-interacting protein (Setou *et al*., 2002), the neurofibromatosis protein (Hakimi *et al*., 2002) and RNA-containing granules (Kanai *et*

al., 2004). Because many cargo binding domain binding partners are as yet unidentified, it is likely that a single kinesin motor interacts with multiple cargoes in the same cell at overlapping times, and that more complex mechanisms to coordinate cargo movement exist.

It has been shown that several kinesins have a mechanism to suppress cargo transport in the absence of cargo (Verhey and Hammond 2009). This occurs via a folding mechanism in which the motor bends and the KLC interacts with the KHC motor domain and/or the microtubule. This motor is considered "autoinhibited" because the ATPase activity of the motor is turned off (Wong and Rice 2010). Conversely, when cargo is present, kinesin has the ability to processively move along filaments bound to the cargo. For example, by attaching a glass bead to the tail of *D. melanogaster* kinesin-1 purified *in vitro*, the motor is able to walk processively along microtubules (Coy *et al*., 1999). It was further shown that *in vivo*, two inhibitory regions of the kinesin tail exist. Binding of both Fez1, which binds to the KHC, and Jip1, which binds to the KLC, are necessary to overcome autoinhibition and drive processive movements (Blasius *et al*., 2007). Therefore, at least some kinesins, with their attached lights chains, are bound to two cargo proteins at the same time.

An autoinhibitory state was also shown for myosin V (Liu *et al*., 2006; Taylor 2007) however it is not known to what extent this occurs *in vivo*. Both kinesins and myosins have the ability to shut off transport in the absence of cargo. A region of the tail domain in either myosins or kinesins has not yet been identified that interacts with the motor domain. It is reasonable to speculate that when the tail domain is bound to the motor, the binding sites for cargo would be less accessible to other cargo.

Focus of the thesis

At least eight cargo adaptor proteins are known to interact with the myosin V motor, Myo2, cargo binding domain. Each cargo adaptor acts directly in the transport of at least one organelle or cargo. Interestingly, inheritance of organelles by Myo2 occurs at distinct yet overlapping times during the cell cycle, and each cargo itinerary is unique. Together, these observations suggest a complex mechanism for the attachment of cargoes to Myo2. A model in which all cargo adaptors freely attach to Myo2 at the correct time in the cell cycle had been assumed. This model suggests that Myo2 freely associates with cargo adaptors, and that cargo adaptors interact with Myo2 when correctly positioned or modified (i.e., phosphorylated). Studies described in this thesis are the result of findings that cargo adaptor proteins have overlapping binding sties on Myo2. Moreover, these findings suggest that shared Myo2 binding sites provide an important mechanism of regulating cargo transport and regulate organelle volume, as well as, the timing of organelle inheritance.

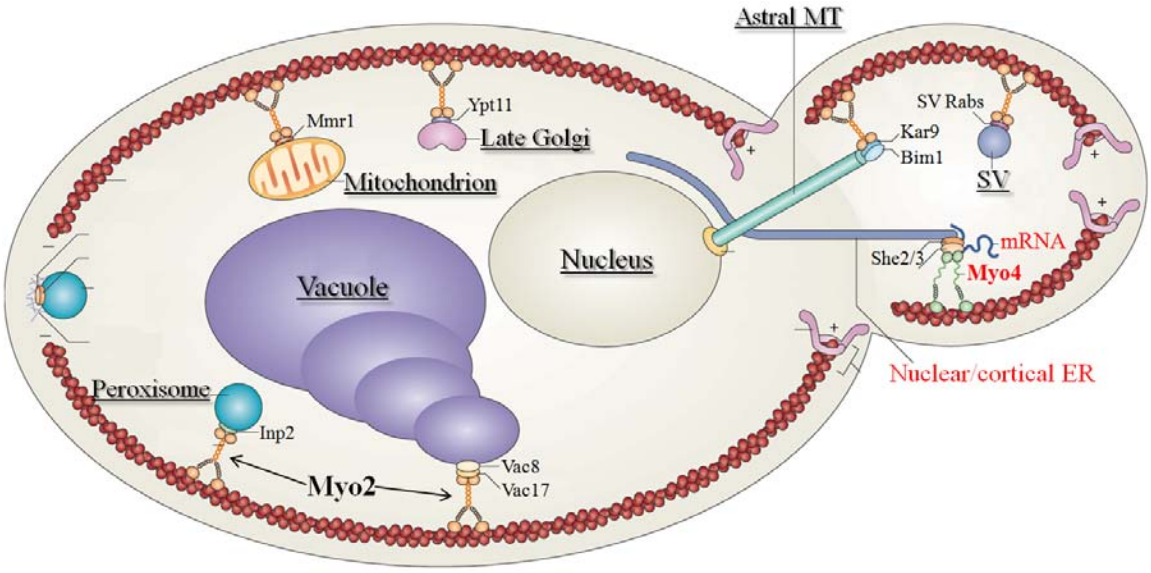

Figure 1.1
Budding yeast, *Saccharomyces cerevisiae*, divides asymmetrically by budding. Each cargo is carried individually to the emerging bud at a defined time in the cell cycle, where the cargo is release and retained. Cargoes transported by the myosin V motor, Myo2, are underlined. This includes: the vacuole, peroxisomes, mitochondria, late Golgi, secretory vesicles (SV) and astral microtubules (MT). Cargo adaptor proteins for each cargo are indicated. Cargoes of Myo4, the other myosin V motor in budding yeast, are indicated in red font. Image modified from Fagarasanu *et al*., 2010.

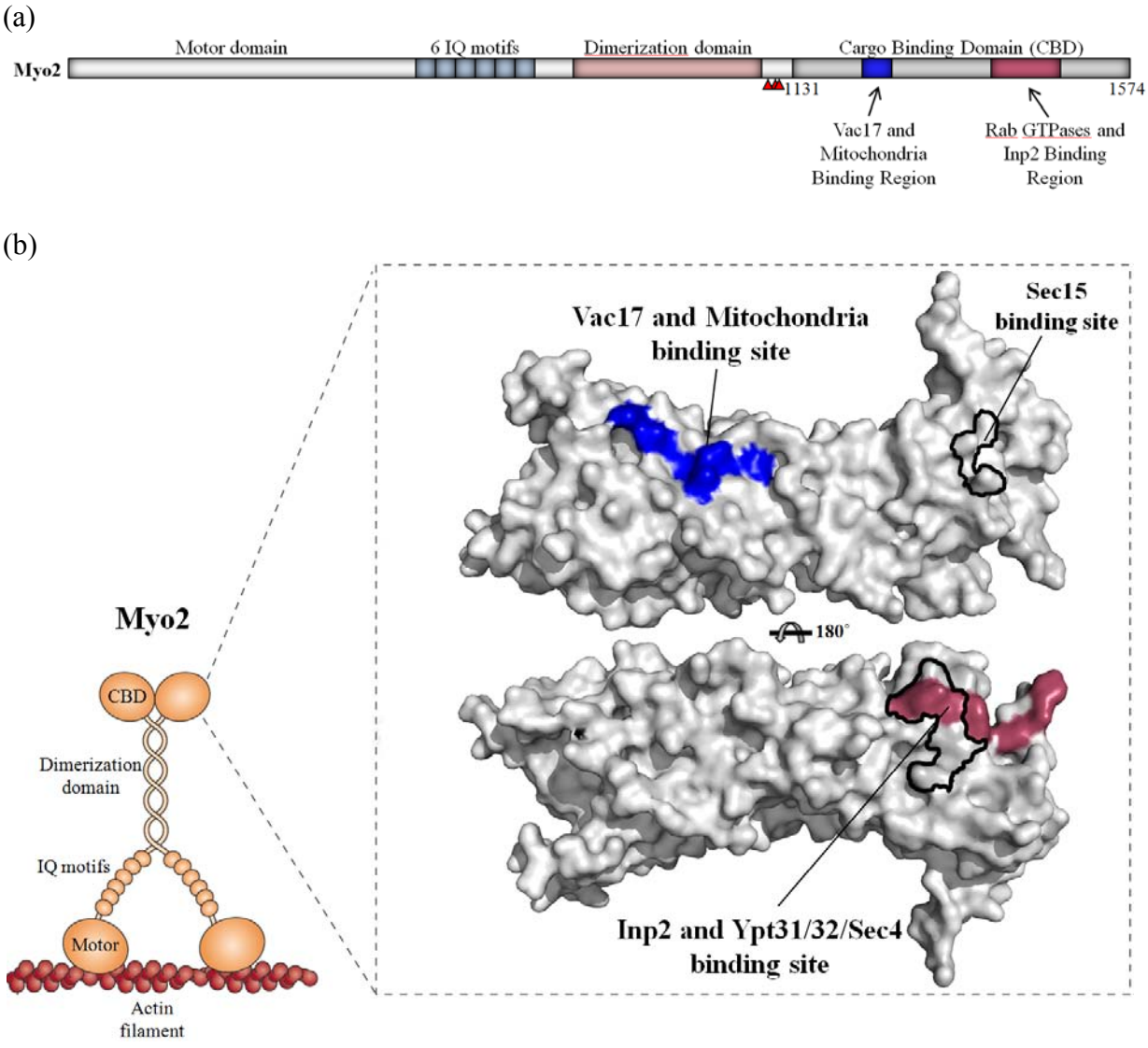

Figure 1.2
Surface representations of the crystal structure of the Myo2 Cargo Binding Domain. (a) Linear schematic of Myo2. Red arrow heads denote phosphorylation sites. (b) *Top*: The Vac17 binding site has been identified (Ishikawa *et al*., 2003 and Pashkova *et al*., 2006). Some of these residues, when mutated, also cause a mitochondrial inheritance defect (Altmann *et al*., 2008). Vac17 binding residues and the "mitochondria" binding residues are indicated in blue. Sec15 binding site of Myo2 was identified (Jin *et al*., 2011). *Bottom*: The Inp2 binding region has been identified (Fagarasanu *et al*., 2009). Some of these residues overlap with residues the bind the Rab GTPases, Ypt31/Ypt32 and Sec4 (Lipatova *et al*., 2006; Santiago-Tirado *et al*., 2010; Jin *et al*., 2011). The Rab GTPase binding site is indicated in black outline. The Vac17, mitochondria and Sec15 binding sites are located on the opposing side of the CBD from the Rab GTPase and Inp2 binding region.

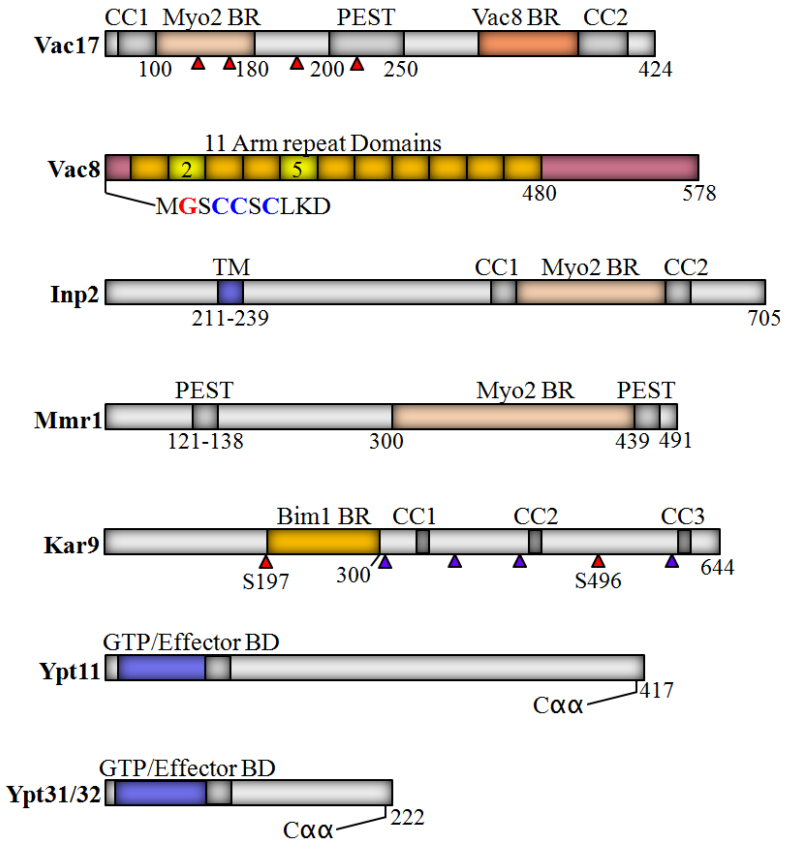

Figure 1.3
Linear schematics of Myo2 cargo adaptor proteins. All proteins depicted interact directly with Myo2 except Vac8. Regulatory or structural domains are indicated for each protein. The Myo2 binding region is indicated in cases in which it has been identified. Red arrow heads denote phosphorylation sites that have been tested *in vivo*; Kar9 is SUMOylated on 4 residues indicated by purple arrow heads: K301, K333, K381 and K529. Vac8 is myristoylated at Glycine 2 (red) and palmitoylated at Cysteines 4, 5 and 7 (blue). Arm repeats 2 and 5 are important for all known Vac8 functions and deletion of these two domains disrupts Vac17 interaction. Ypt11/31/32: The grey box next to the GTP/Effector BD indicates the Switch I/II regions. Yeast Rab GTPases are attached to membranes using a geranylgeranyl (20 carbons) unsaturated group on a Cysteine residue followed by two aliphatic residues (Cαα) at the C-terminus of the protein. CC = coiled cold domain; BR = Binding Region; BD = Binding Domain; TM = Transmembrane domain.

CHAPTER 2

OVERLAP OF CARGO ADAPTOR BINDING SITES ON MYOSIN V COORDINATES THE INHERITANCE OF DIVERSE CARGOES

Introduction

Multiple cellular functions are executed via cytoplasmic organelles. The volume of each organelle likely depends upon several factors, including type of cell, its functions, metabolic status, and stage in the cell cycle. Moreover, during cell division, organelle volume must be coordinated with the transient change in cell volume. However little is known about how cells control organelle size.

In the yeast *Saccharomyces cerevisiae*, the mother cell generates a bud that becomes the daughter cell. During budding, a portion of each cytoplasmic organelle is transported across the mother-bud neck to a distinct location in the bud. In yeast, the myosin V motor, Myo2, transports most cytoplasmic organelles as well as other cargoes. Myo2 carries secretory vesicles (Govindan *et al*., 1995), the vacuole (Catlett and Weisman, 1998; Hill *et al*., 1996), mitochondria (Itoh *et al*., 2002), peroxisomes (Fagarasanu *et al*., 2006; Hoepfner *et al*., 2001), the late Golgi (Rossanese *et al*., 2001a), and astral microtubules (Beach *et al*., 2000; Yin *et al*., 2000). This raises the question of how Myo2 carries diverse cargoes to the proper place at the right time.

Insight into how Myo2 selects cargoes comes from analysis of a high-resolution crystal structure of the Myo2 cargo binding domain (CBD) (Pashkova *et al*., 2006). The

CBD consists of the C-terminal 487 residues of the motor heavy chain, which fold into a globular protein of fifteen anti-parallel helices, ending with a long loop containing two helices. The loop wraps back to the "beginning" of the CBD. Residues identified as critical for the inheritance of the vacuole map to a single region on the surface of the CBD (Catlett *et al*., 2000; Pashkova *et al*., 2006). Mutation of these Myo2 residues disrupted Myo2 interaction with Vac17, the vacuole-specific cargo adaptor protein (Ishikawa *et al*., 2003). Vac17 also binds Vac8, a vacuole membrane protein (Tang *et al*., 2003). Thus, the Myo2/Vac17/Vac8 complex attaches Myo2 to the vacuole. These studies suggested that specificity for an individual Myo2 cargo derives in part, from adaptor proteins that link the cargo to the Myo2 CBD (Weisman, 2006).

Indeed several adaptor proteins have been identified. In yeast, the peroxisomal protein Inp2 binds Myo2 and is required for proper inheritance of peroxisomes (Fagarasanu *et al*., 2006). Kar9 links Myo2 to the plus ends of microtubules via direct interaction with the capping protein Bim1 (Korinek *et al*., 2000; Miller *et al*., 2000). Myo2/Kar9 interaction is important for the correct orientation of the mitotic spindle during the cell cycle (Beach *et al*., 2000; Yin *et al*., 2000). While the Myo2 CBD exhibits high conservation with most eukaryotic myosin V CBDs, the adaptor proteins are not uniformly conserved (Mast *et al*., 2011), which suggests that modes of attachment to myosin V rapidly evolve, while the mechanisms employed by the CBD itself are conserved.

Mmr1 was proposed to be an adaptor protein that links Myo2 to mitochondria. The mitochondrial protein, Mmr1, binds directly to Myo2 (Itoh *et al*., 2004) and has a role in mitochondrial distribution to the bud (Frederick *et al*., 2008; Itoh *et al*., 2004). In

cells deleted for *MMR1*, mitochondria are often missing from small buds. Mmr1 may have additional roles related to mitochondria fusion; in *mmr1*Δ yeast, the mitochondrial network is mildly fragmented.

In *mmr1*Δ yeast, as the bud size increases, mitochondria distribution is partially corrected, indicating that additional mechanisms of inheritance/distribution are involved. One additional mechanism involves the ERMES/mitochore complex, which forms junctions between mitochondria and the endoplasmic reticulum (ER) (Kornmann *et al*., 2009). The ERMES complex functions independently of Myo2 and is critical for the proper distribution of mitochondria. The GTPase, Gem1, required for distribution of mitochondria to the bud (Frederick *et al*., 2004), is part of the ERMES complex (Kornmann *et al*., 2011).

The Rab GTPase, Ypt11, which has a role in mitochondrial inheritance or retention, also interacts with Myo2 (Boldogh *et al*., 2004; Fortsch *et al*., 2011; Frederick *et al*., 2008; Itoh *et al*., 2002). However, Ypt11 localizes to the ER (Buvelot Frei *et al*., 2006) and late Golgi vesicles (Arai *et al*., 2008), which raises questions about whether Ypt11 directly attaches mitochondria to Myo2. Given its localization, Ypt11 may move the ER and/or late Golgi. Moreover Ypt11 likely functions outside of the Mmr1 pathway; a double deletion of *YPT11* and *MMR1* has a synthetic negative effect on mitochondrial distribution (Frederick *et al*., 2008).

Adaptor proteins that attach Myo2 to secretory vesicles have been identified (Jin *et al*., 2011; Lipatova *et al*., 2008; Santiago-Tirado *et al*., 2011). The Rab GTPases Ypt31/32 and Sec4 bind a site on Myo2 that is offset 180° from the Vac17 binding site. Mutation of any residue that disrupts Rab GTPase binding produces a severe growth

defect due to a defect in secretory vesicle transport to the plasma membrane. Sec15, a subunit of the exocyst tethering complex, binds an additional region on Myo2, on the opposing side from the Rab GTPase binding site (Jin *et al*., 2011). Binding of both Sec15 and the Rab GTPases are required for the normal distribution of secretory vesicles.

Here we map the binding sites of the other known cargo adaptors for Myo2. Together with previous studies, we find that eight adaptor proteins bind to either of two overlapping binding sites (Fagarasanu *et al*., 2009; Jin *et al*., 2011; Lipatova *et al*., 2008). The binding sites for Mmr1 and Vac17 overlap at a "simpler" region. These proteins compete for access to Myo2 *in vivo* and *in vitro*. Surprisingly, mutations that affect Myo2 interaction with Mmr1 only, result in an increase in the volume of vacuoles in the bud. Similarly, mutations that affect Myo2 interaction with Vac17 only, result in an increase in the volume of mitochondria in the bud. Thus overlap of the Vac17 and Mmr1 binding sites on Myo2 likely has a role in regulating organelle volume. Similarly, the other adaptor proteins overlap on the opposite side of Myo2. The Ypt11 and Kar9 binding sites overlap with each other and with the secretory vesicle Rab GTPases and Inp2 binding sites. Furthermore, the Rab GTPase/Kar9/Inp2 binding region, Mmr1/Vac17 binding region and the Sec15 binding site are potentially connected through shared helices and loops. This raises the possibility that the binding of any single cargo adaptor may enhance or inhibit binding of adaptor proteins at spatially distinct regions. Thus the CBD of Myo2 may be a focal point to integrate the distribution of all of its cargoes.

Results

Mmr1 is a cargo adaptor protein for mitochondria, and binds Myo2 at a site that overlaps with the Vac17 binding site.

Several organelle cargo adaptor proteins interact with the Myo2 cargo binding domain (CBD) (Figure 2.1a). Mmr1 is required for normal distribution of mitochondria to the yeast bud. Movement of mitochondria is disrupted by mutation of specific surface residues on the Myo2 CBD (Altmann *et al*., 2008). These residues overlap with residues required for Myo2 interaction with Vac17, the vacuole-specific adaptor protein (Ishikawa *et al*., 2003). Thus we tested whether *myo2* mutations in this region disrupted the interaction between Myo2 and Mmr1 and/or Myo2 and Vac17 (Figure 2.1b). In addition, we tested each of the six residues mutated in *myo2-573*, a mutant defective in binding Mmr1 and mitochondria inheritance (Itoh *et al*., 2004). Using a yeast two-hybrid test, we identified several mutants, including *myo2*-N1304D, which disrupted interactions between both Myo2 and Mmr1 and between Myo2 and Vac17 (Figure 2.2; purple). Mutation of adjacent residues, *myo2*-E1293K and *myo2*-D1297N, only affected the ability of Myo2 to interact with Vac17, and not Mmr1 (Figure 2.2; blue). *myo2*-P1529A/S, was the single residue in *myo2-573* that disrupted Myo2 interaction with Mmr1 (Figure 2.2, red). This mutant did not affect Myo2 interaction with Vac17. An additional two mutants, *myo2*-I1308A and *myo2*-K1312A, interacted with Vac17 but not Mmr1 (Figure 2.2; red).

These point mutations in the context of full length *MYO2* did not affect Myo2 expression levels (Fig. 2.3), actin cable organization (Figure 2.3), cell viability (Figure 2.4), or mitochondria function, measured by the ability of mutant strains to grow on a non-fermentable carbon source, glycerol (Figure 2.4). Surface mutations near this region did not disrupt binding to any cargo adaptor protein tested (Figure 2.5; Table 1).

Selected mutations that blocked Myo2 interaction with Vac17 and/or Mmr1 in a yeast two-hybrid test, were assayed for their ability to support vacuole and mitochondria inheritance *in vivo* (Figure 2.6 and 2.7, respectively). Mutations that disrupted interaction with both Vac17 and Mmr1 in the yeast two-hybrid test, disrupted inheritance of both vacuoles (Figure 2.6) and mitochondria (Figure 2.7). Thus, a central region on helix six, and part of helix four of the Myo2 CBD contain residues important for inheritance of both vacuoles and mitochondria.

The *myo2*-E1293K and *myo2*-D1297N mutants, which affected Myo2 interaction with Vac17 but not Mmr1, disrupted the inheritance of vacuoles only. Conversely, the *myo2*-I1308A, *myo2*-K1312A and *myo2*-P1529A/S mutants only disrupted mitochondria inheritance. Together, these data support the hypothesis that Vac17 and Mmr1 interact with Myo2 at overlapping but not identical regions on the Myo2 CBD. Disruption of the interaction between Myo2 and either Vac17 or Mmr1 results in fewer vacuoles or mitochondria in the daughter cell, respectively.

myo2-P1529S disrupted the interaction of Myo2 with Mmr1 (Figure 2.8) and caused a mitochondrial inheritance defect. However, substitution of a proline may disrupt secondary and tertiary structure. Thus, whether P1529 contributes directly to the Mmr1 binding site remains an open question.

That the Vac17 and Mmr1 binding sites overlap raised the possibility that Vac17 and Mmr1 may function together with Myo2 to move vacuoles and mitochondria. We tested if the absence of either Vac17 or Mmr1 affected the inheritance of mitochondria or vacuoles, respectively. The *mmr1*Δ mutant has a mitochondrial inheritance defect (Figure 2.9). However, vacuole inheritance was normal. Conversely, in *vac17*Δ cells, mitochondria were inherited normally but vacuole inheritance was disrupted (Figure 2.9). Thus, inheritance of mitochondria requires Mmr1, while the inheritance of vacuoles requires Vac17. Further, these studies suggest that Vac17 binds Myo2 in the absence of Mmr1, and conversely, Mmr1 binds Myo2 in the absence of Vac17.

Prior to testing the functional significance of the overlap of the Mmr1 and Vac17 binding sites on Myo2, we tested the relative importance of Mmr1 and Ypt11 for inheritance of mitochondria. Similar to Mmr1, Ypt11 binds directly to the Myo2 CBD, but at a distinct site from Mmr1/Vac17. We found that the *mmr1*Δ mutant had a greater mitochondrial inheritance defect than the *ypt11*Δ mutant (49% versus 21% buds had no detectable mitochondria; Fig. 2.10). Thus, we chose to study Vac17 and Mmr1 independent of potential contributions from Ypt11.

Vac17 and Mmr1 localize to the leading edge of vacuoles and mitochondria in the bud and mother cell.

To determine functions of Vac17 and Mmr1, we determined the localization of these proteins in wild-type cells and in *myo2* mutants. Vac17-3xGFP localized on the leading edge of vacuoles in the bud, as well as to portions of vacuoles in the mother cell that are near the mother-bud neck (Figure 2.11). In wild-type cells, the regulated

degradation of Vac17 protein occurs following vacuole inheritance (Tang *et al*., 2003). Notably in the *myo2*-D1297N mutant, there is a vacuole inheritance defect and an unpolarized accumulation of Vac17-3xGFP protein on the vacuole membrane in the mother cell (Figure 2.12). Similarly, Vac17 protein levels are elevated on the mother cell vacuole in *myo2*-N1304S, a mutant that is defective in binding to Vac17 (Tang *et al*., 2003). These findings support the hypothesis that Myo2 and Vac17 bind vacuoles in the mother, and that Vac17 together with the attached portion of the vacuole, moves to the bud via Myo2. Vac17-3xGFP did not accumulate in *myo2*-I1308A, which does not have a vacuole inheritance defect.

We tested Mmr1 using assays that paralleled those used for Vac17. Two postulated roles for Mmr1 function are consistent with the observation that Mmr1 directly contacts Myo2. Mmr1 may connect Myo2 to mitochondria to facilitate their transport (Frederick *et al*., 2008; Itoh *et al*., 2004). Alternatively, Mmr1 protein may be transported to the bud tip via Myo2 where it functions as a tether to capture and retain mitochondria (Peraza-Reyes *et al*., 2010; Shepard *et al*., 2003; Swayne *et al*., 2011). These hypotheses are not mutually exclusive. For the purposes of this study, we focused on whether the Mmr1/Myo2 complex moves mitochondria across the mother-bud neck.

Mmr1-GFP localized to portions of mitochondria in the bud, as well as mitochondria in the mother cell near the mother-bud neck (Figure 2.13). Importantly, mitochondria at the rear of the mother cell, opposite the bud, lack Mmr1-GFP (Figure 2.13; arrows). Thus, localization of both Vac17 and Mmr1 are consistent with their roles as adaptor proteins which link Myo2 to those portions of vacuoles and mitochondria that are moving into the bud. In further support of this hypothesis, in the *myo2*-I1308A

mutant, which cannot bind Mmr1, Mmr1 was distributed throughout the mitochondrial surface. In small budded cells, Mmr1 accumulated on mitochondria in the mother cell (Figure 2.14). There was also an increase in Mmr1-GFP fluorescence. Elevation of Mmr1-GFP did not occur in cells containing *myo2*-D1297N, which disrupts Vac17 but not Mmr1 interaction with Myo2 (Figure 2.14). By western blot analysis Mmr1 protein was elevated five to seven-fold in *myo2* mutants that are defective in binding Mmr1 (Figure 2.15). Both Vac17 and Mmr1 are elevated in *myo2*-N1304D, which has a vacuole and mitochondrial inheritance defect (Figures 2.12 and 2.14). That Mmr1 and Vac17 accumulate in specific *myo2* mutants in the mother cell on mitochondria and vacuoles, respectively, strongly suggests that Mmr1 and Vac17 interact with the organelles in the mother, and interact with Myo2 to transport mitochondria and vacuoles across the mother-bud neck. In the case of mitochondria, other transport mechanisms may be present as well (Boldogh *et al*., 2001; Frederick *et al*., 2008; Kornmann *et al*., 2011; Shepard *et al*., 2003; Swayne *et al*., 2011).

Vacuole and mitochondrial inheritance occur early in the cell cycle, at similar but not identical times.

To further test the role of Mmr1 and Vac17 interactions with Myo2, we performed *in vivo* time-lapse imaging. Cells with buds initially devoid of mitochondria and vacuoles were visualized until both mitochondria (mitoGFP) and vacuole (FM4-64) tubules moved into the bud (Figure 2.16). Each red and green pair represents one cell. We found that the time the vacuole or mitochondria crossed the mother-bud neck occurred independently; this was designated time zero for the first organelle that moved into the

bud. The black arrowhead between each red-green pair indicates when the second organelle crossed the mother bud neck. As an example, in Figure 2.16 (I), the green bar at top indicates that mitochondria moved into the bud first and crossed the mother-bud neck approximately one minute from the start of imaging. After approximately four minutes, the vacuole also crossed the mother-bud neck, indicated by the arrowhead.

To maximize the number of time-courses analyzed, we utilized time-lapse series, ranging from 13 s between each image up to 180 s between each image. For the majority of the ten cells imaged, both vacuoles and mitochondria crossed into the bud within seven minutes after the start of imaging. After moving across the mother-bud neck, the organelles frequently retracted back into the mother cell and then recrossed from the mother to the bud (Figure 2.17; red and green arrow heads). This was observed in six of the ten time-lapse series. Moreover, for the two cells in which images were acquired less than 60 seconds apart (Figure 2.16 , I and V) the vacuole tubule crossed the mother-bud neck seven and nine times, respectively, and the mitochondrial tubule crossed the mother-bud neck eleven and five times, respectively.

The time lapse series revealed several aspects regarding the inheritance of vacuoles and mitochondria: (1) There is not a designated order for whether vacuoles or mitochondria enter the bud first. Mitochondria moved into the bud before vacuoles in four of the ten cells analyzed, while vacuoles moved first in the other six cells. (2) While the precise time that each organelle crossed the mother bud neck was independent of the other, mitochondria and vacuoles moved into the bud at similar times in the cell cycle. Thus, there is not a chronological order to binding of Vac17 versus Mmr1 to Myo2 yet binding of each is regulated by the cell cycle. (3) The movement of vacuoles and

mitochondria into the bud is a combination of anterograde and retrograde events (rocking) across the mother-bud neck. The timing of rocking of each organelle was independent of the other.

To further test whether Mmr1/Myo2 move mitochondria across the mother bud neck, we acquired time-lapse images for *myo2*-I1308A, which is defective in binding Mmr1 (Figure 2.18). In the six examples imaged, five cells had either a pronounced delay (approximately 32 minutes; Figure 2.18 (I-III)) or complete defect (observed for >40 min each; Figure 2.18 (IV-V) open arrow heads) in movement of mitochondria into the bud. While mitochondria in *myo2*-I1308A mutants frequently moved to a position near the mother-bud neck, they did not move into the bud (Figure 2.19a; white arrow). That mitochondria eventually crossed the mother-bud neck in three of the six *myo2*-I1308A mutants fits the postulate that there are redundant mechanisms to move mitochondria across the mother-bud neck (Boldogh *et al*., 2001; Frederick *et al*., 2008). Alternatively, *myo2*-I1308A may be only partially defective in binding Mmr1. Note that the time required for buds to inherit the vacuole in six of the *myo2*-I1308A mutants was similar to wild-type cells; approximately 7 minutes. Together the defects observed in *myo2*-I1308A cells support the hypothesis that Mmr1 links the mitochondrial membrane to Myo2 for transport across the mother-bud neck.

One of the *myo2*-I1308A mutants had normal inheritance of mitochondria (Figure 2.18 (VI)). Moreover, in this example the vacuole was inherited late, with a delay of 12.3 minutes. This example raises the possibility that Vac17 may also interact with Myo2 residue I1308, although this residue is not a major contributor to Vac17 binding (Figure 2.1).

Based on studies of populations of cells, Vac17 was proposed to act as an adaptor protein that links vacuoles to Myo2 for movement of vacuoles across the mother-bud neck. To further test this hypothesis, we acquired time-lapse images of the *myo2*-D1297N mutant, which fails to bind Vac17 (Figure 2.19b). In each of the five time-lapse series, the vacuole was not inherited for the duration of imaging (cells observed 20 to 35 min; Figure 2.18 (VII-XI)). This result strongly suggests that Myo2 interaction with Vac17 is essential for vacuole movement across the mother-bud neck.

Notably, in the *myo2*-D1297N mutant, where vacuole inheritance is defective, mitochondrial tubules moved into the bud earlier. On average mitochondria moved into the bud within 2 to 3 minutes from the start of imaging (Figure 2.18) compared with 5 to 6 minutes for the wild-type strain (Figure 2.16). In addition, in time lapse images acquired less than 60 seconds apart, there was less rocking, mitochondria crossed the mother-bud neck, an average of 3 times in the *myo2*-D1297N mutant. Conversely, vacuoles crossed the mother-bud neck an average of 3.4 times in the *myo2*-I1308A mutant. These observations strongly suggest that in Myo2 mutants where Vac17 binding is compromised, Mmr1 has greater access to Myo2. Conversely in mutants where Mmr1 binding is compromised, there is a greater likelihood of Vac17 attachment to Myo2. Thus, Vac17 and Mmr1 may compete for access to Myo2.

Mmr1 and Vac17 compete for access to Myo2, in vivo.

To determine whether Mmr1 and Vac17 compete for access to Myo2 *in vivo*, we examined images from a large population of cells, to test if *myo2*-D1297N, which has a defect in binding Vac17, has increased amounts of mitochondria in the bud. Conversely,

we tested if *myo2*-I1308A, which has a defect in binding Mmr1, has increased amounts of vacuoles in the bud. We measured the ratio of bud fluorescence to mother fluorescence for individual cells for both mitochondria (mitoGFP) and vacuoles (FM4-64). A minimum of one hundred small budded cells for each strain was analyzed (Figure 2.20). *myo2*-D1297N cells had lower vacuole fluorescence levels in the bud compared to wild-type cells (0.029±0.004 versus 0.178±0.010, respectively; $p<0.001$), consistent with observations that *myo2*-D1297N has a vacuole inheritance defect. Conversely, *myo2*-D1297N had an increase in mitochondrial fluorescence in the bud compared to wild-type cells (0.151±0.006 versus 0.115±0.002, $p<0.001$). Thus, when Vac17 cannot bind Myo2, transport of mitochondria into buds is increased, which suggests that Mmr1 has greater access to Myo2.

In *myo2*-I1308A mutant cells, which have a defect in Mmr1 binding to Myo2, there was a significantly lower ratio of mitochondria fluorescence in buds compared to wild type cells (Figure 2.20; 0.040±0.002 versus 0.115±0.002, $p<0.001$). This provides further support for the hypothesis that Mmr1 interaction with Myo2 is important for mitochondria inheritance. Interestingly, buds in the *myo2*-I1308A mutant had an increase in vacuole fluorescence compared to wild-type cells (0.213±0.010 versus 0.178±0.010, $p<0.05$). These data are consistent with the postulate that when Myo2 cannot bind to Mmr1, a larger population of Myo2 binds Vac17, and thus transport of vacuoles to the bud is increased. *myo2*-N1304D, a mutation at the center of both the Vac17 and Mmr1 binding sites, results in decreased inheritance of both vacuoles and mitochondria.

The excess volume of vacuoles or mitochondria inherited by small buds of the *myo2* point mutants persisted in large budded and unbudded cells (Figure 2.21). Thus the

changes in both vacuole and mitochondrial volume that occurred early in the cell-cycle in the *myo2*-I1308A and *myo2*-D1297N mutants were not corrected to wild-type volumes at the point of cytokinesis. Thus, competition between Mmr1 and Vac17 for access to Myo2 is a major contributor to the modulation of organelle volume.

Additional evidence for competition between Mmr1 and Vac17 came from studies of wild-type cells that over-expressed either *MMR1* or *VAC17* (Figure 2.22a). Compared with wild-type cells, when *MMR1* was over-expressed, mitochondria accumulated in the bud (Figure 2.22b and 2.22c), with a corresponding significant decrease ($p<0.05$) in the amount of vacuoles present (Figure 2.22b). Conversely, over-expression of Vac17 led to higher levels of vacuoles but fewer mitochondria in the bud (Figure 2.22b and 2.22c).

Over-expression of either *MMR1* or *VAC17* had additional consequences. Over-expression of Vac17 led to abnormal positioning of vacuoles in the mother cell to the forward part of the cell, near the mother-bud neck (Figure 2.22c; asterisk). Similarly, over-expression of *MMR1* disrupted the cortical distribution and caused an accumulation of mitochondria in the forward part of the mother cell near the mother-bud neck (Figure 2.22c; arrowhead). These results provide further support for the hypotheses that Vac17 and Mmr1 link Myo2 to vacuoles and mitochondria, respectively, for transport of these organelles across the mother-bud neck.

Together, analysis of mutations in *myo2* that block either binding of Mmr1 or Vac17, as well as analysis of over-expression of Mmr1 or Vac17, strongly suggest that Myo2 transports both mitochondria and vacuoles, and further, that the volume of mitochondria and vacuoles inherited is partially determined by access of Mmr1 and Vac17 to Myo2.

Mmr1 and Vac17 compete for access to Myo2, in vitro.

We tested and found that recombinant Myo2 CBD pulls-down both Vac17-GFP and Mmr1-HA expressed in yeast cell lysates (Figure 2.23). To determine whether Myo2 interactions with Vac17 or Mmr1 can be assayed *in vitro*, we expressed full-length Vac17 and Mmr1 in *E. coli*, but found that neither protein was soluble (data not shown). Thus, we used yeast two-hybrid analysis to identify peptides of Vac17 and Mmr1 that interact with Myo2 (Figure 2.24). We performed further tests on Mmr1(378-430), because it interacted well with wild-type *MYO2*, but not *myo2*-N1304D or *myo2*-I1308A, mutant alleles that do not interact with full-length Mmr1. Similarly, we chose Vac17(112-157), which interacted with wild-type *MYO2* and *myo2*-I1308A, but did not interact with *myo2*-N1304D, which does not bind full-length *VAC17*. The Mmr1 and Vac17 peptides were expressed as fusion proteins containing an N-terminal maltose binding protein (MBP) tag.

Purified Myo2 CBD interacted with MBP-Vac17(112-157). Proteins were added in a 1:1 molar ratio and analyzed by size-exclusion chromatography. Myo2 CBD (50.5 kD) and MBP-Vac17 peptide (53 kD) eluted as a single complex of approximately 115 kD (Figure 2.25a; red line). Similarly, we found that the Myo2 CBD interacts with MBP-Mmr1(378-430) (55 kD) and migrates on gel filtration as a bimolecular complex of approximately 120 kD (Figure 2.25b). As a control, MBP added to Myo2 CBD in a 1:1 ratio eluted as unbound monomers (Figure 2.25a and 2.25b, dotted line).

To determine if Vac17 and Mmr1 peptides compete for Myo2 *in vitro*, we formed a Myo2-Mmr1 complex and added MBP-Vac17 peptide (Figure 2.26). Increasing

amounts of MBP-Vac17 resulted in the formation of Myo2/Vac17 complexes with the concomitant displacement of Mmr1 (Figure 2.26, black boxes on gels). Thus Mmr1 and Vac17 compete for access to Myo2 *in vitro*. Note that MBP-Vac17 peptide does not interact with MBP-Mmr1 peptide; these eluted as unbound monomers (Figure 2.26; chromatogram dotted line).

The binding surfaces for Ypt11, Kar9, Inp2 and additional Rab GTPases partially overlap with each other.

Ypt31/Ypt32 and Sec4 bind a site on Myo2 that is offset 180° from the Vac17/Mmr1 binding site. Notably, Inp2, which functions in peroxisome inheritance, binds a subset of these Myo2 residues plus one additional residue in this region (Fagarasanu *et al*., 2009).

We tested proteins known to interact with Myo2 whose binding sites were unknown; Kar9, Ypt11 and Smy1 (Figure 2.27a). These proteins bound to each of the Myo2 mutants of the Vac17/Mmr1 binding region. The one exception was *myo2*-L1301P, which was defective in binding to Smy1 and Kar9 (Figure 2.27a). Since other mutations in this region bound to these proteins, it is likely that Smy1 and Kar9 binding are affected due to a conformational change due to the substitution of leucine with proline. Note that a conformational change may affect only a subset of surface residues. For example, mutation of a buried residue, *myo2*-G1248D, affects Vac17 binding but does not affect binding of Rab GTPases (Catlett and Weisman, 1998; Pashkova *et al*., 2006).

To test whether Ypt11, Smy1 or Kar9 bind Myo2 near the Ypt31/Ypt32, Sec4 or Inp2 binding sites, we generated and tested sixteen additional mutations near Myo2-

Y1415, a surface residue whose mutation disrupts binding of each of these proteins (Figure 2.27b). Smy1 bound to all of the mutants tested in that region, therefore the Smy1 binding region remains to be determined. Ypt11 binding was disrupted by most of the mutations that disrupt Myo2 interaction with the Rab GTPases Ypt31/Ypt32 and Sec4 (Figure 2.28, blue and brown residues). However, Myo2-L1331, which is important for binding Ypt31/Ypt32 and Sec4 is not important for Ypt11 interaction with Myo2 in a yeast two-hybrid test (Figure 2.28; green). We tested the viability of cells with *myo2*-L1331S as the sole source of *MYO2* in the cell, and found a modest growth defect (Figure 2.29), consistent with a role for Myo2-L1331 being important for Ypt31/Ypt32 and/or Sec4 binding. This growth defect was not due to an altered expression level of *myo2*-L1331S (Figure 2.30). Thus, Myo2-L1331 may uniquely bind Ypt31/Ypt32 and Sec4, while residues L1411, Y1415, and K1444, are required for the binding all of the Rab GTPases that interact with Myo2.

Note that growth defects due to mutation of Rab GTPase-binding residues are unlikely to be due to disruption of the ability of Ypt11 to bind to Myo2. Deletion of Ypt11 does not affect yeast growth (Figure 2.29).

Using a yeast-two hybrid test we found that Kar9 failed to interact with two mutants defective in binding Rab GTPases, *myo2*-L1331S and *myo2*-Y1415E. In addition, Kar9 failed to interact with *myo2*-F1334A, *myo2*-K1408A and *myo2*-Y1483A. To test the functional significance of this interaction, we measured spindle orientation. Note that even in the absence of Kar9, the defect in spindle orientation is partial. This is because a parallel dynein-dependent pathway divides a subset of the nuclei along the

correct axis (Grava *et al*., 2006). Thus *kar9*Δ cells are viable and do not display a temperature sensitive growth defect.

Importantly mutations identified in the yeast two-hybrid test as defective in binding to Kar9, were also defective in binding Kar9 *in vivo*, as assessed by their function in the orientation of the mitotic spindle. An asynchronous population of *myo2*Δ cells expressing a plasmid encoding wild-type or mutant *myo2* was scored according to five categories. Orientations assigned to categories III, IV and V are not informative and thus while recorded, were excluded from the analysis. Categories I and II are informative and about 35-50% of cells in both the mutants and wild-type were assigned to one of these two groups (Figure 2.31). Wild-type *MYO2* plasmid-containing cells had a 2.5-fold higher percentage of correctly oriented spindle microtubules compared to *kar9*Δ cells. Strikingly, there was a direct correlation between mutations that disrupted Myo2-Kar9 interaction in the yeast two-hybrid test and those that cause the misorientation of spindle microtubules *in vivo*. Mutations of residues adjacent to these mutations did not affect spindle orientation or Kar9 binding. A mutation that disrupts vacuole and mitochondria inheritance, *myo2*-N1304D, also did not affect spindle orientation (Figure 2.31). Together, these results demonstrate that Kar9, Inp2, Sec4, Ypt11 and Ypt31/Ypt32 bind to overlapping regions on the Myo2 CBD. Thus, of nine proteins known to interact with the Myo2 CBD, six overlap in this region.

Conclusions

Characterization of organelle-specific cargo adaptors, which directly link cargoes to myosin V motors, revealed that organelle transport occurs via direct regulation of cargo adaptor proteins (Fagarasanu *et al*., 2009; Moore and Miller, 2007; Peng and Weisman, 2008). An example is Vac17, where initiation of vacuole movement begins with Cdk1-dependent phosphorylation of Vac17 (Peng and Weisman, 2008). This promotes Vac17 binding to Myo2 and results in vacuole movement. Regulation of Vac17 is also required for the termination of vacuole movement (Tang *et al*., 2003). When the vacuole reaches the bud, a pathway that utilizes the Vac17 PEST sequence promotes detachment of Vac17 from Myo2 and the degradation of Vac17. These events deposit the vacuole at its correct position (Tang *et al*., 2003). Additionally, Vac17 expression is coordinated with the cell cycle (Tang *et al*., 2003). Vac17 levels peak when the vacuole is moving into the bud (Peng and Weisman, 2008).

Discovery of multiple modes of regulation of Vac17 suggested that cargo adaptors provide the main regulation of cargo movement, while the motor provides an inert platform for cargo binding. In further support of this postulate, two types of cargo adaptors, Vac17, and the secretory vesicle-specific Rabs Ypt31/Ypt32, bound distinct sites on Myo2. Thus it was assumed that binding of each Myo2 adaptor could be independently regulated.

An indication that the CBD of myosin V plays an active role in the selection of cargoes came from discoveries that *Xenopus* myosin V and yeast Myo2 undergo reversible phosphorylation. Three residues in the Myo2 CBD are phosphorylated (Legesse-Miller *et al*., 2006). Interestingly, phosphorylation of the conserved myosin V CBD in *Xenopus* oocytes regulates cargo interactions (Karcher *et al*., 2001; Rogers *et al*., 1999). Thus phosphorylation of the myosin V CDB may facilitate the attachment or detachment of select cargoes.

A further indication that the cargo binding of Myo2 may regulate cargo selection, was the observation that the Inp2 binding site overlaps with the Rab GTPase binding site (Fagarasanu *et al*., 2009). The results contained in this thesis show that Kar9 and Ypt11 also interact with residues at this region (Figure 2.28). Similarly, Mmr1 binds to a second site, which overlaps with the Vac17 binding site (Figure 2.2). The overlap of at least eight cargo adaptors at two distinct sites suggested that this extensive overlap is functionally significant.

Indeed the overlap of the binding sites of Mmr1 and Vac17 contributes to the inheritance of mitochondria and vacuoles (Figure 2.20). An initial hypothesis was that competition between Mmr1 and Vac17 for access to Myo2 could provide temporal order for the inheritance of these organelles. However, mitochondria and vacuoles moved into the bud at similar times (Figure 2.16). Moreover, either the vacuole or mitochondria moved first, or both crossed the mother-bud neck simultaneously. Thus Mmr1 and Vac17 appear to have equal access to Myo2.

Despite similar access to Myo2, Mmr1 and Vac17 compete with each other *in vivo* and *in vitro* (Figure 2.20 and 2.26). The major significance of this competition is

regulation of the volume of vacuoles and mitochondria that are inherited by the bud. Little is known about the processes that regulate organelle volume (Chan and Marshall, 2010). It had been assumed that organelle volume is primarily regulated via a combination of organelle biogenesis and autophagy/turnover (Diaz and Moraes, 2008; Hutchins *et al*., 1999; Veenhuis *et al*., 2000). Our studies reveal an additional determinant of organelle volume, which is based on the competition between cargo adaptor proteins for Myo2. A mutant that blocks mitochondrial inheritance, *myo2*-I1308A, has an increased amount of vacuoles in the bud. Conversely, a mutant that blocks vacuole inheritance, *myo2*-D1297N, has an increased amount of mitochondria in the bud. Note that the inheritance of a greater amount of mitochondria or vacuoles persisted, and was observed in large budded and unbudded cells from *myo2*-D1297N and *myo2*-I1308A mutants (Figure 2.21). This finding leads to the model that the competition between Mmr1 and Vac17 for access to Myo2 plays a major role in regulation of the volume of mitochondria and vacuoles that are inherited (Figure 2.32).

Both mitochondria and vacuoles undergo retrograde, as well as, anterograde movements across the mother bud neck. One possibility, is that in general Myo2 stochastically releases cargoes through a loss of Myo2 attachment to the cargo adaptor. Indeed, in both the *myo2*-D1297N and *myo2*-I1308 mutants, there are fewer retrograde movements of the inherited organelle (Figure 2.18). One interpretation of these observations, is that in those mutants the likelihood of reinitiation of Myo2 binding to Vac17 (for *myo2*-I1308A) or Mmr1 (for *myo2*-D1297N) is higher because there is no longer competition from the other cargo adaptor protein.

Mutants with defects in moving mitochondria or vacuoles often had portions of each organelle poised at the mother-bud neck for several minutes. This suggests that in the *myo2*-I1308A and *myo2*-D1297N mutants, attachment of the organelle to Myo2 is not completely blocked. Further, the intracellular environment in the mother-bud neck may be distinct from the cytoplasm in the mother cell; a higher level of force might be needed to move organelles through this region of the cell. It is tempting to speculate that fewer motors are required to bring a portion of the organelle to the mother-bud neck, and then additional motors are required for movement through the mother-bud neck. The environment in the neck may contribute to the rocking motion.

Eventually, the retrograde and anterograde rocking ceases, and a stable pool of both mitochondria and vacuoles persist in the bud. Tethering proteins likely anchor the organelles in the bud. Mmr1 and Ypt11, as well as ERMES tethering of mitochondria to the endoplasmic reticulum may perform this function for mitochondria. Similarly, there are likely tethers for the vacuole. Interestingly we observed that over-expression of either *VAC17* and *MMR1* overcomes a tethering mechanism in the mother cell for vacuoles or mitochondria, respectively (Figure 2.22c).

That mitochondria and vacuoles move across the mother-bud neck at similar times and that Mmr1 and Vac17 appear to have equal access to a common binding region on Myo2, suggests that the cell cycle-dependent regulation of Vac17 and Mmr1 may be similar. Mmr1 may be the target of the same Cdk1/cyclin complex(es) that target Vac17 (Peng and Weisman, 2008). Note that Mmr1 has seven Cdk1 consensus sites. Along similar lines, we predict that detachment of Mmr1 from Myo2 may utilize a similar mechanism to that observed with Vac17 (Tang *et al*., 2003). Vac17 detachment from

Myo2 requires the Vac17 PEST sequence. Similarly Mmr1 contains two predicted PEST sequences (Figure 2.24). Moreover, like Vac17, Myo2 mutations that block mitochondrial inheritance result in elevation of Mmr1 protein (Figure 2.15).

Determination of the molecular consequences of the overlap of six cargo adaptors at the Rab GTPase binding site, will be challenging. In addition to the Rab GTPase Ypt11 and the secretory vesicle Rab GTPases Ypt31/Ypt32 and Sec4, both Kar9 and Inp2 bind at this region. Moreover, the overlap of cargo binding sites may be even more complex. All cargo adaptor binding sites may modulate each other through structural changes in the Myo2 CBD.

Binding of the Rab GTPases Ypt31/Ypt32 and Sec4 may impact the Sec15 binding site and vice versa. Analysis of the CBD structure reveals a loop containing an important Sec15-binding residue (Figure 2.33b; Loop H) that connects to helix nine, which has several residues that are important for Kar9, Inp2 and the Rab GTPase interactions. In addition, helix twelve contributes residues to Sec15 binding. The loop extending from this helix contains residues important for Kar9 and Inp2 binding (Figure 2.33b; Loop L). Thus binding of Inp2, Kar9 and/or Rab GTPases has the potential to change the Sec15 binding site, or vice versa. This may be critical to the regulation of Myo2 attachment to secretory vesicles.

Along similar lines the Vac17/Mmr1 binding region may connect with the Rab GTPase binding region. The Mmr1 and Vac17 binding region lies on helix six, which spans the CBD. Helix six contains most of the critical Vac17/Mmr1 binding residues and contains a loop at the C-terminus (Figure 2.33b; Loop F) with residues important for the Rab GTPase binding site. Thus, binding of a Rab may affect the binding of Vac17 and

Mmr1, and vice versa. Evidence in support of this hypothesis comes from a mutation of *myo2*-L1301 on Helix 6. As expected, mutation of L1301 to proline disrupts Myo2 interaction with Mmr1 and Vac17. Notably, this mutation also disrupts the ability of Kar9 and Smy1 to bind to Myo2 (Figure 2.33). Further, that Ypt11 binding was not affected in *myo2*-L1301P suggests that this mutation did not drastically alter the globular structure of the CBD. It is tempting to speculate that Ypt31/Ypt32 and Sec4, may have priority to occupy the CBD. Thus, cargo transport may be coordinated in part through structural changes in the myosin V CBD that occur through long-distance communication between each of the adaptor binding sites.

(a)

(b)

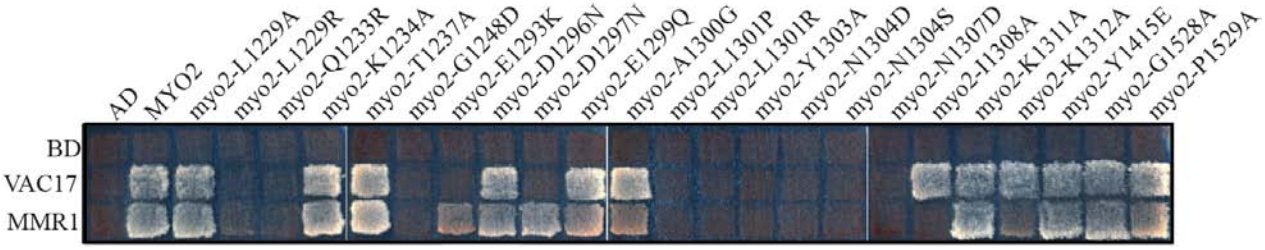

Figure 2.1
Mutations on the Myo2 cargo binding domain surface reveal an overlapping binding region for interactions with Vac17 and Mmr1. (a-b) Yeast two-hybrid plates incubated at 24˚C for 3 or 4 days until growth was seen on all control test squares. Top and left-most test squares in for each panel are empty vector controls. (a) Vac17, Mmr1, Kar9, Ypt11, Inp2 and Smy1 interact with Myo2 cargo binding domain. (b) Myo2 mutations that define the binding region for Vac17 and Mmr1. This analysis was conducted on the basis of initial findings from Matthew J. Brunner and Dr. Yui Jin. pGBD-Vac17, Ishikawa *et al*., 2003. pGBD-Mmr1 was constructed by Dr. Jin.

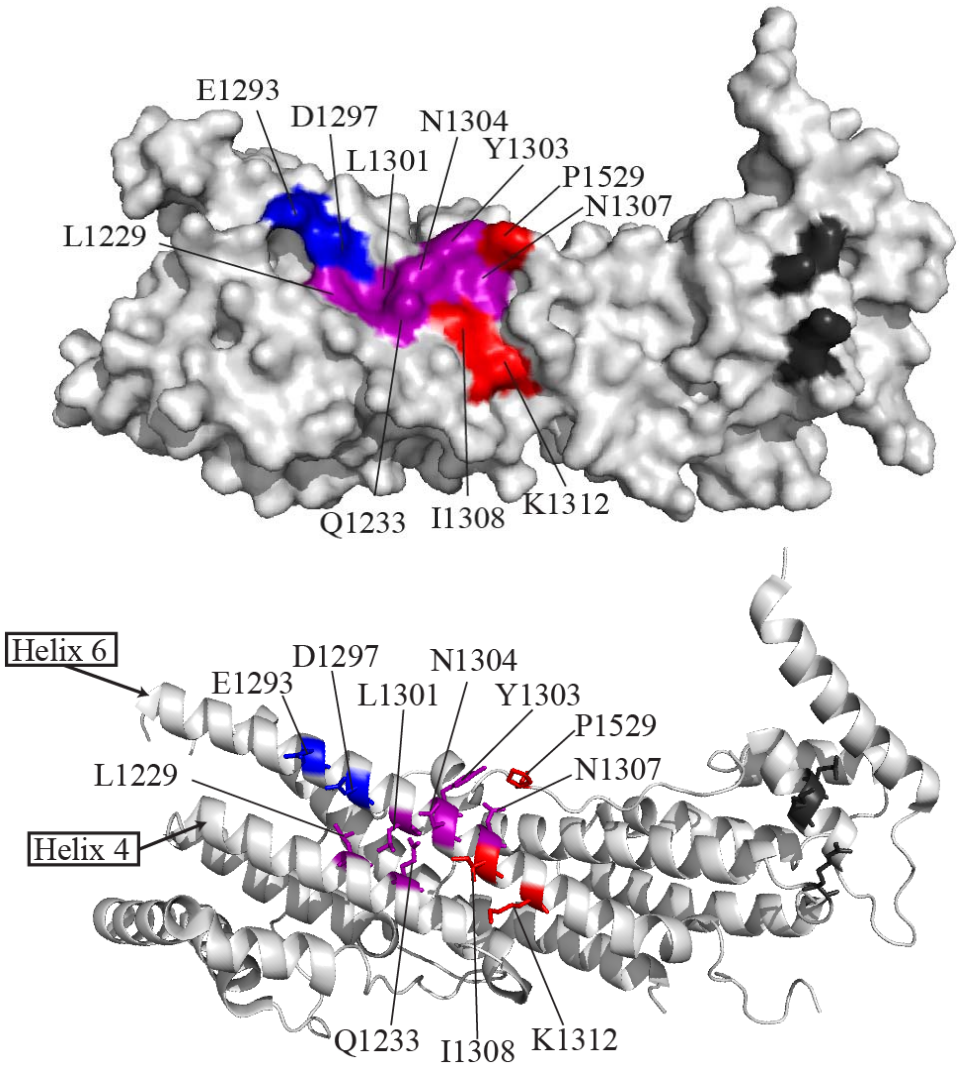

Figure 2.2
Surface (top) and ribbon (bottom) representations of the Myo2 cargo binding domain. The Myo2 CBD structures (i.e., globular tail domain, Pashkova *et al*., 2006) depict residues of indicated binding proteins shown in color. Blue: only important for Vac17 interaction; Red: only important for Mmr1 interaction; Purple: important for interactions with both Vac17 and Mmr1. Colors represent residues which, when mutated, disrupt the binding between Myo2 and the cargo adaptor. Dark grey: Sec15 binding site (Jin *et al*., 2011).

(a)

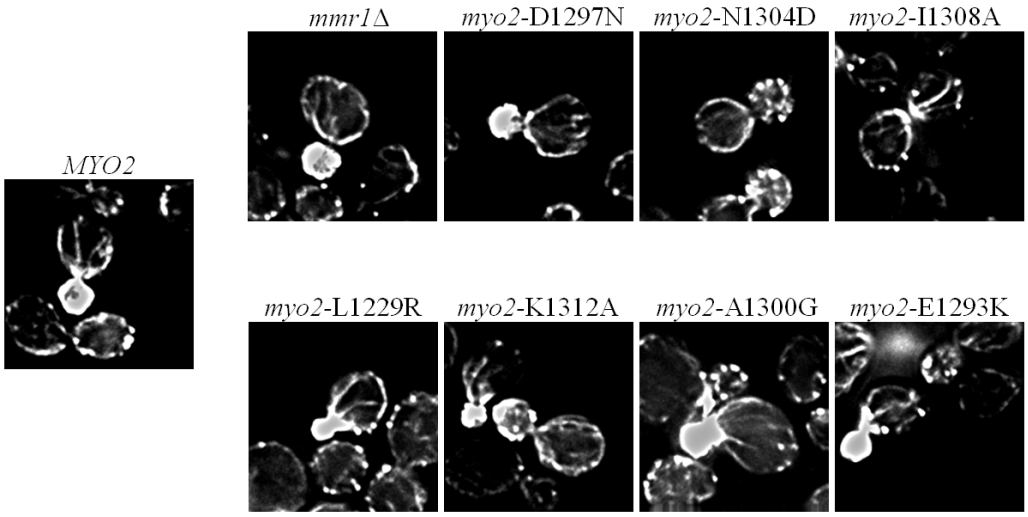

(b)

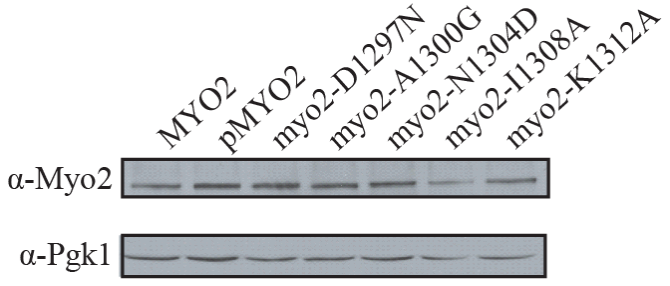

Figure 2.3
Specific mutations in full length Myo2 do not disturb actin filament formation or cortical actin patch localization, or Myo2 expression levels. (a-b) Cells, in which a wild-type (*MYO2*) or mutant *myo2* allele was transformed into cells lacking the endogenous *MYO2* gene, were grown in log phase for six to seven doubling times. (a) Cells were fixed and stained as described (Hill *et al*., 1996). (b) Cells were washed once and prepared for protein analysis using the TCA/NaOH precipitation method (Methods). Cells were immunoblotted with anti-Myo2 goat primary antibody (Catlett *et al*., 2000). Pgk1, phosphoglycerate kinase 1; loading control.

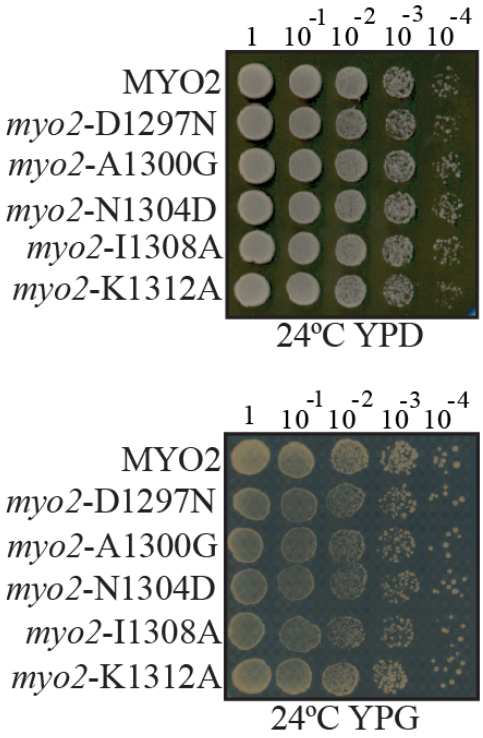

Figure 2.4
Myo2 mutations that cause a defect in vacuole or mitochondria inheritance do not noticeably affect cell viability or mitochondria function and integrity. The endogenous *MYO2* ORF was deleted and wild-type (MYO2) or *myo2* allele transformed on a plasmid. Cells were grown in log phase for approximately at least six doubling times before performing 1:10 serial dilutions as indicated. (Top) Cells were spotted onto glucose-rich media. (Bottom) Cells were spotted onto glycerol-containing plates as the sole carbon source.

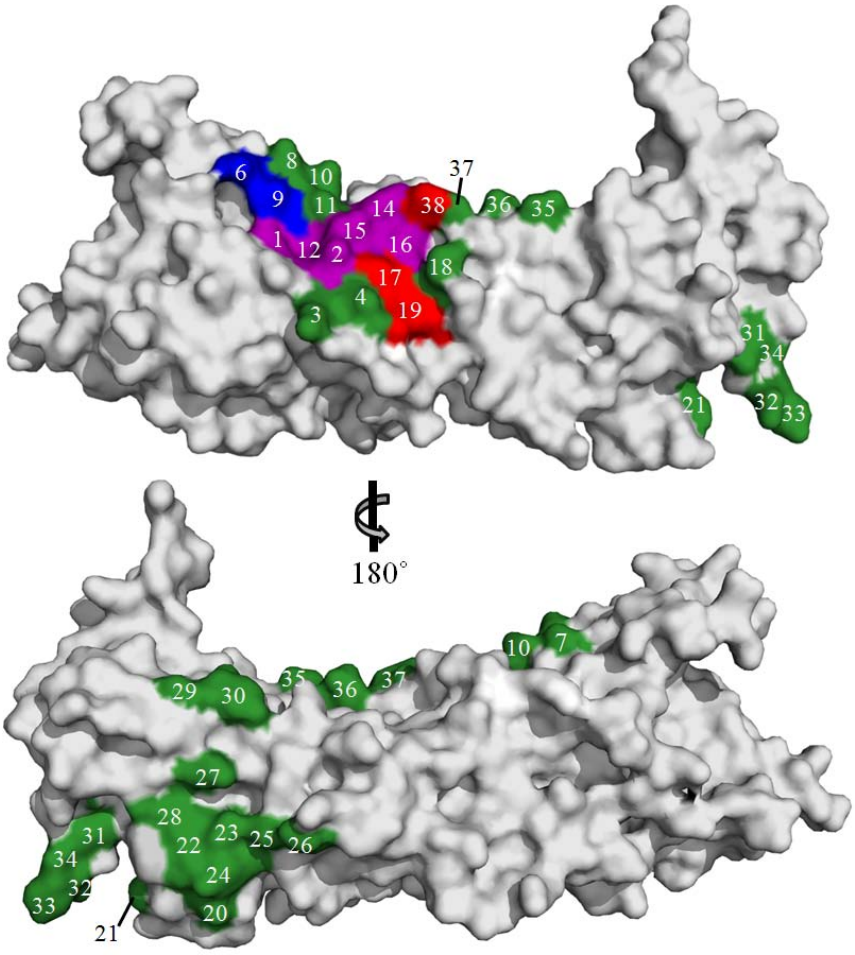

Figure 2.5
Surface representation of the crystal structure of the Myo2 CBD. Colored residues indicate residues that were mutated and tested for Mmr1 or Vac17 interaction in a yeast two-hybrid test. Blue: binds Vac17 only; Red: binds Mmr1 only; Purple: binds Vac17 and Mmr1; Green: Mutations that did not perturb any of the interactions or phenotypes tested. Residues indicated as follows: 1, 1229; 2, 1233; 3, 1234; 4, 1237; 5, 1248 (myo2-2; internal residue); 6, 1293; 7, 1295; 8, 1296; 9, 1297; 10, 1299; 11, 1300; 12, 1301; 13, 1302; 14, 1303; 15, 1304; 16, 1307; 17, 1308; 18, 1311; 19, 1312; 20, 1331; 21, 1408; 22, 1411; 23, 1414; 24, 1415; 25, 1418; 26, 1422; 27, 1444; 28, 1447; 29, 1461; 30, 1464; 31, 1480; 32, 1482; 33, 1483; 34, 1484; 35, 1525; 36, 1526; 37, 1528; 38, 1529.

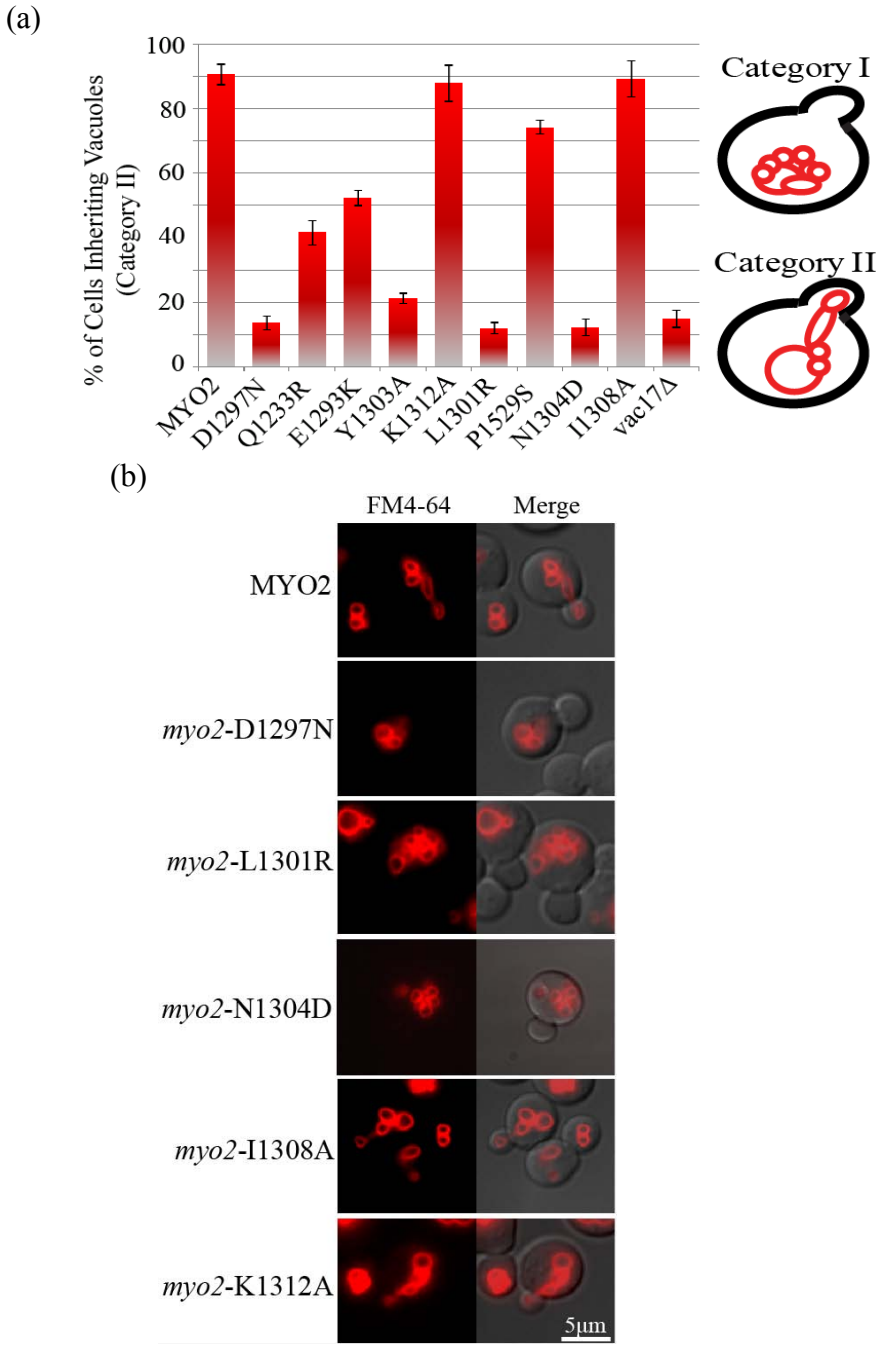

Figure 2.6
Specific mutations in *MYO2* cause a vacuole inheritance defect. (a) Cells in which the endogenous *MYO2* ORF was deleted and the *myo2* allele transformed on a plasmid were scored for vacuole inheritance. Cells were grown in log phase for approximately seven doubling times, washed, and labeled with FM4-64 fluorophore (red) and chased with fresh media. Cells not in focus were not scored nor cells that were not sufficiently labeled with FM4-64. (b) Representative micrograph images of cells labeled as in (a).

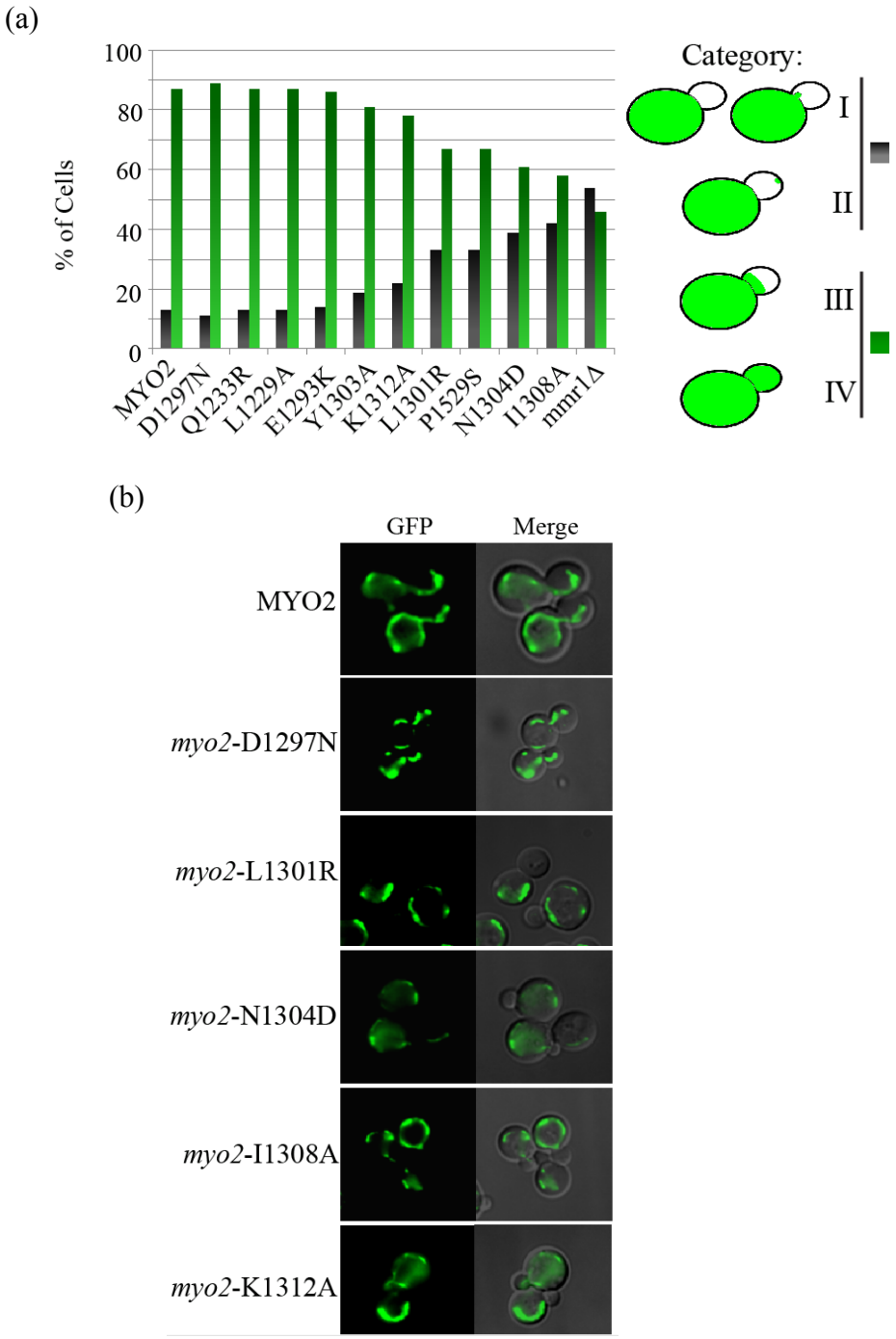

Figure 2.7
Specific mutations in *MYO2* cause a mitochondria inheritance defect. (a) Cells in which the endogenous *MYO2* ORF was deleted and the indicated *myo2* allele was doubly transformed with mitoGFP(LEU2) plasmid. Cells were grown in log phase for approximately seven doubling times, imaged and scored for mitochondrial inheritance according to four categories; categories I and II were mutant, categories III and IV were wild-type. Cells not in focus were not scored. (b) Micrograph images of cells from (a). The *mmr1*Δ strain was created by Dr. Yui Jin.

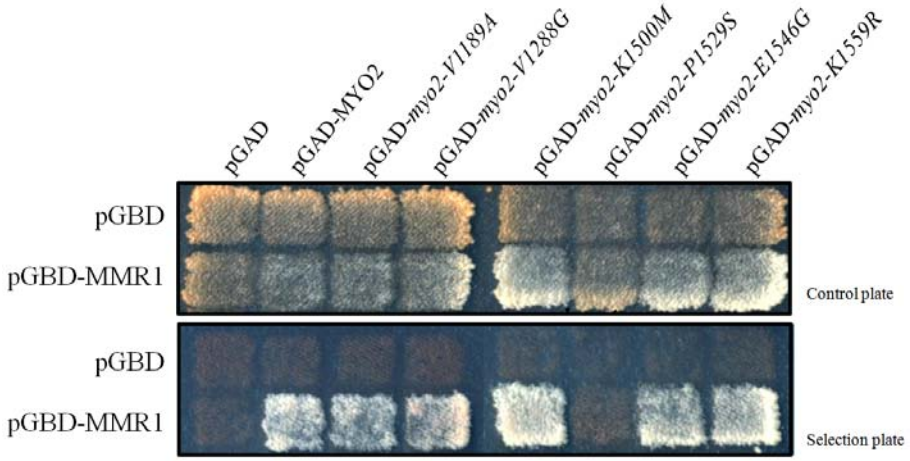

Figure 2.8
The P1529S mutation is the sole mutation that disrupts interaction of Mmr1 with Myo2 in the *myo2-573* mutant. The *myo2-573* mutant was found to disrupt interaction with Mmr1 and disrupt polarized localization of Mmr1 *in vivo* (Itoh *et al*., 2002 and Itoh *et al*., 2004). Control plate, sc-leu-trp. Selection plate, sc-leu-trp-ade-his+3-aminotriazole. Plates incubated 2 to 5 days at 24˚C.

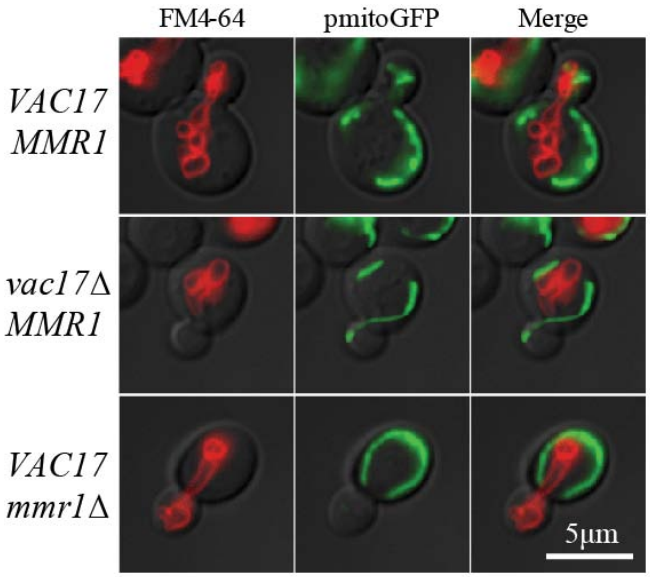

Figure 2.9
Deletion of *MMR1* ORF preserves vacuole inheritance and deletion of *VAC17* ORF preserves mitochondrial inheritance. Both the MMR1 and VAC17 ORFs were deleted in the LWY7235 (wild-type) yeast strain using the PCR method of recombination as described previously (Jin *et al*., 2008; Ishikawa *et al*., 2003; Tang *et al*., 2003). Cells were transformed with mitoGFP (2u, LEU2). Cells were grown in log phase for seven doubling times, washed, and labeled with FM4-64 fluorophore (red) and chased with fresh media for one doubling period.

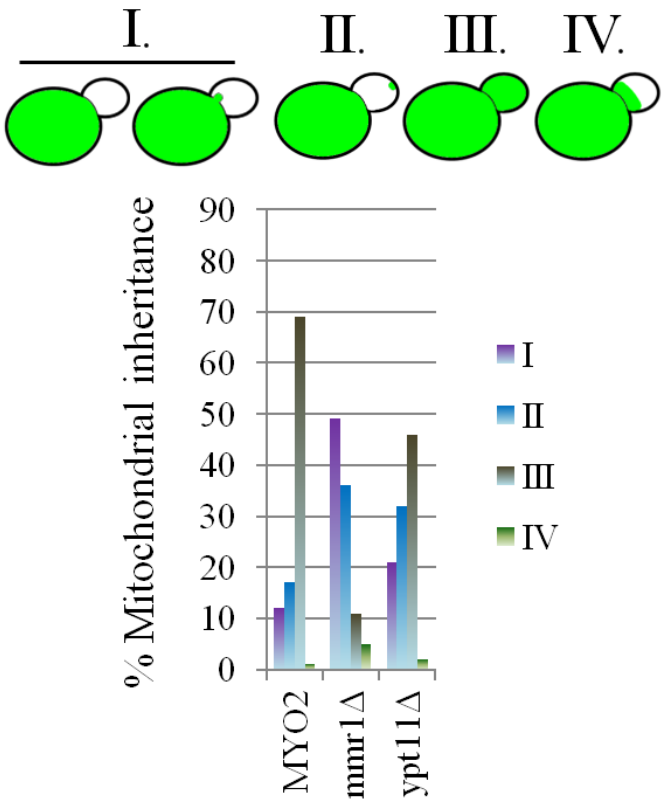

Figure 2.10
Deletion of *MMR1* causes a stronger mitochondrial inheritance defect than deletion of *YPT11*. Cells were transformed with mitoGFP (2μ, LEU2) and grown in sc-leu media in log phase for at least six doubling periods. Mitochondrial inheritance was scored according to four categories. Categories III and IV were wild-type phenotypes. The *ypt11*Δ strain was generated by Dr. Yui Jin.

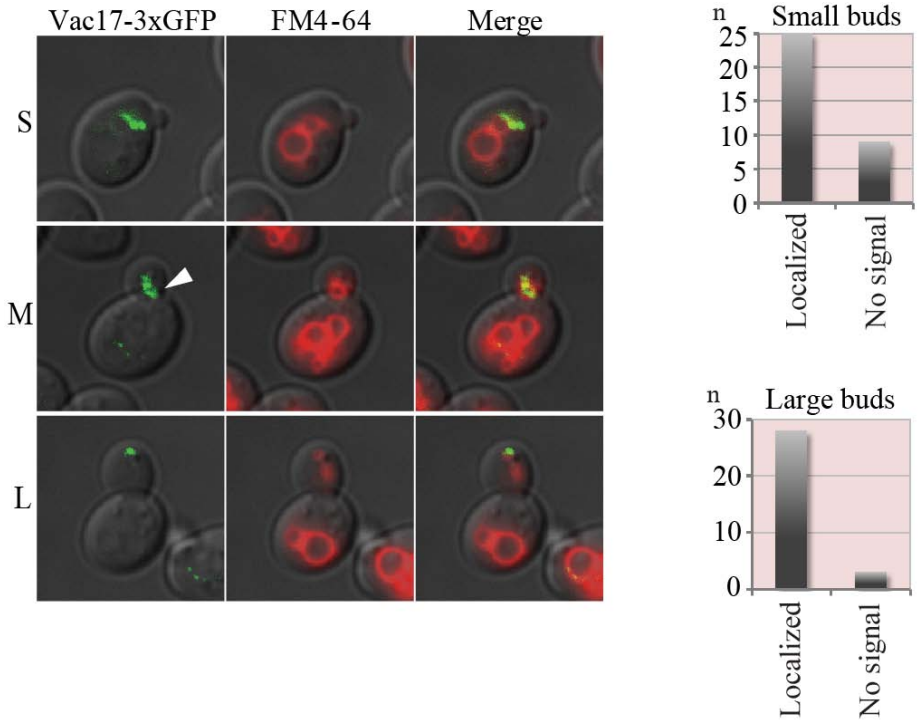

Figure 2.11
Vac17 localizes to the leading portion of the vacuole membrane. Vac17 was tagged at the C-terminus with three tandem GFP modules (Jin *et al*., 2009). Representative small (S), medium (M) and large (L) budded cells are shown. Cells were grown in log phase for at least six doubling times, washed, and labeled with FM4-64 fluorophore (red) and chased with fresh media for one doubling period. (Right) Small budded (*n*=34) and large budded (*n*=31) cells were scored. In cases where GFP signal was detected, the signal was localized to the vacuole membrane closest to the bud or toward the bud tip.

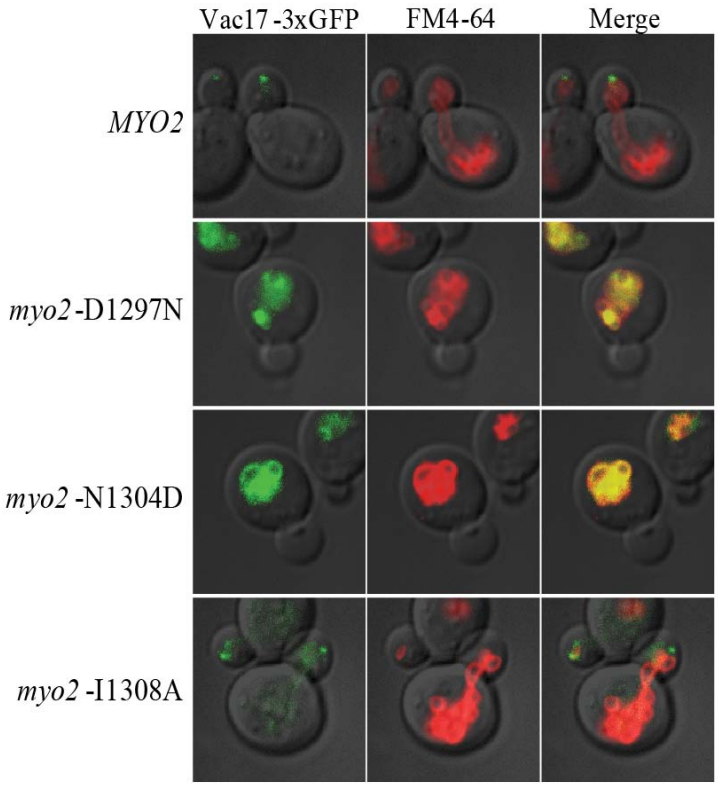

Figure 2.12
myo2 mutants that disrupt Vac17 interaction with Myo2 have elevated levels of Vac17-3xGFP. *myo2*Δ cells with wild-type or the indicated *myo2* mutant expressed from a plasmid (CEN, HIS3) as the sole copy of *MYO2*. Vac17-3xGFP was expressed from its endogenous locus. Cells were grown in log phase for at least five doubling times, washed, and labeled with FM4-64 fluorophore (red) and chased with fresh media for one doubling period before imaging.

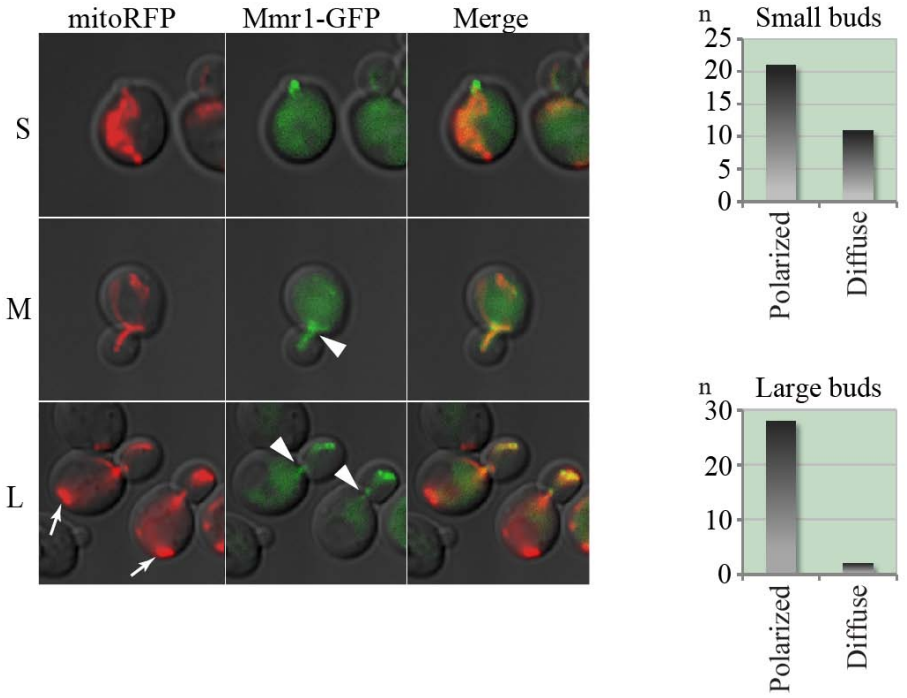

Figure 2.13
Mmr1 concentrates to the leading portion of mitochondria. Cells expressing Mmr1-GFP from its endogenous locus, transformed with mitoRFP (2μ, LEU2). Small budded (top graph; *n*=32) and large budded (bottom graph; *n*=30) cells were scored for the presence of polarized GFP signal on the mitochondrial membrane or a diffuse GFP signal that was not polarized. Cells were grown for at least five doublings before imaging. Mmr1-GFP strain was made by Dr. Yui Jin.

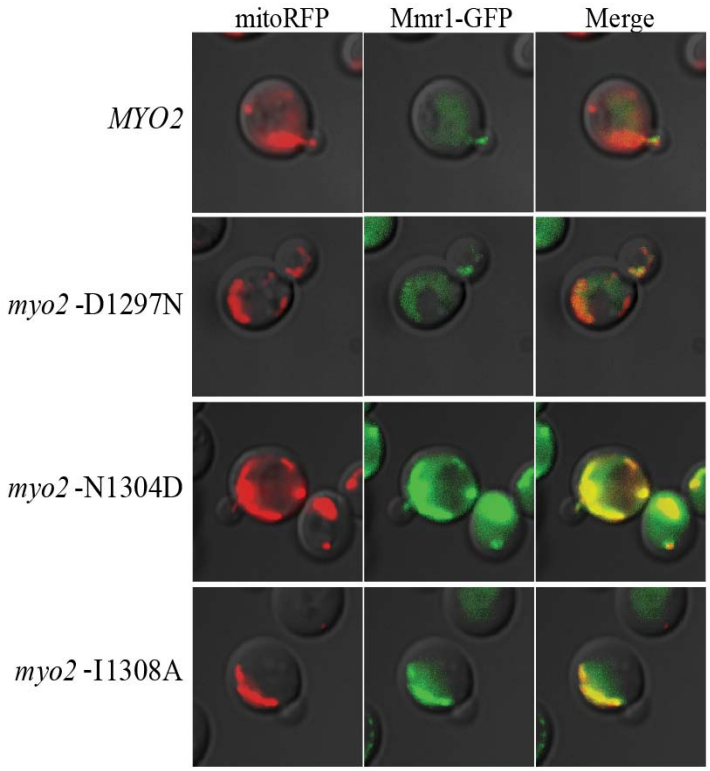

Figure 2.14
myo2 mutants that disrupt Mmr1 interaction with Myo2 have elevated levels of Mmr1-GFP. *myo2*Δ cells with wild-type or the indicated *myo2* mutant expressed from a plasmid (CEN, HIS3) as the sole copy of *MYO2*. Mmr1-GFP was expressed from its endogenous locus. Cells were transformed with mitoRFP (2μ, LEU2) grown in log phase for at least five doubling times

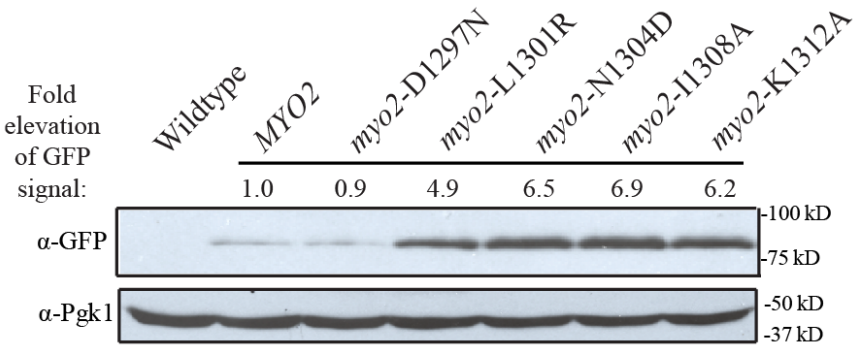

Figure 2.15
Mmr1-GFP protein levels are elevated approximately six-fold in *myo2* mutants that disrupt Mmr1 binding. Cells were washed once and prepared for protein analysis using the TCA/NaOH precipitation method (Methods). Protein extracts were separated via SDS-PAGE and blots were probed with monoclonal anti-GFP and anti-Pgk1. Fold elevation of GFP signal was quantified using NIH ImageJ software.

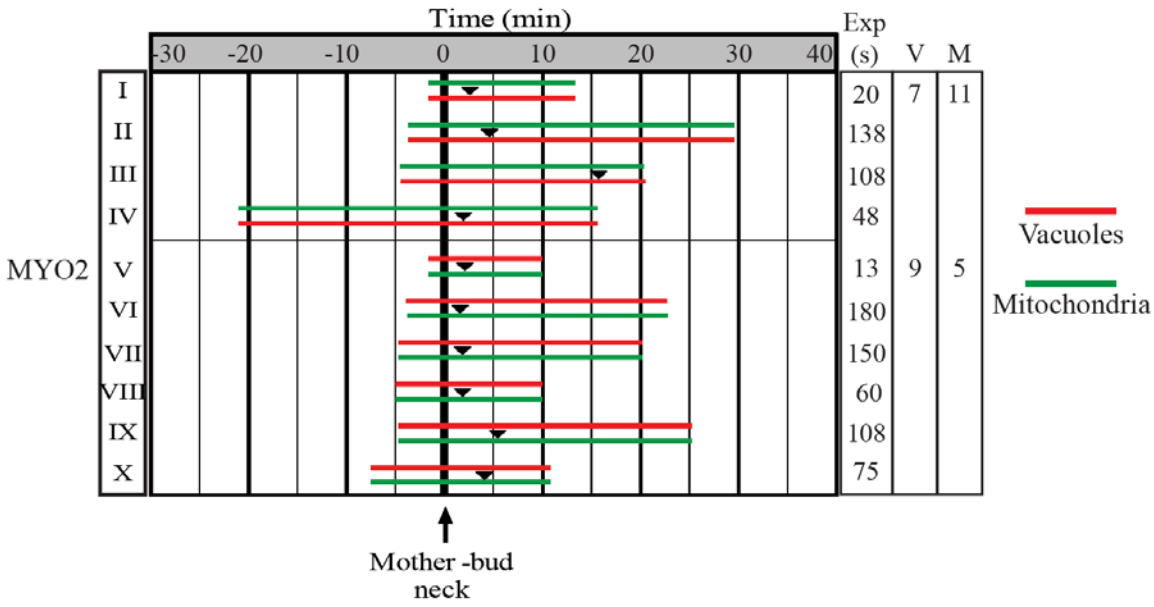

Figure 2.16
Vacuole and mitochondrial inheritance occur at similar times during the cell cycle. Each pair of bars, green (mitochondria) and red (vacuoles), represents one cell. Total length of bar indicates total time of the time-lapse series. Zero (t=0) indicates the time that the first organelle (top bar) entered the bud. Black arrowheads indicate the time the lagging organelle entered the bud. Right columns: Time (seconds) between each time-lapse exposure for the series; 'V' or 'M' indicate the number of times a vacuole tubule (V) or mitochondria tubule (M) crossed the mother-bud neck for the two time-lapse series that had less than 60 seconds between collected images. Wild-type cells were transformed with pmitoGFP and grown in log phase for a minimum of six doubling times, labeled with FM4-64, chased for one doubling time and imaged at room temperature (23.5 to 24.5ºC). Small buds initially devoid of both mitochondria and vacuoles were analyzed for organelle inheritance. Buds that emerged outside the focal plane were not analyzed further. Only cells in which both mitochondria and vacuoles were visible in the region around the mother-bud neck were analyzed.

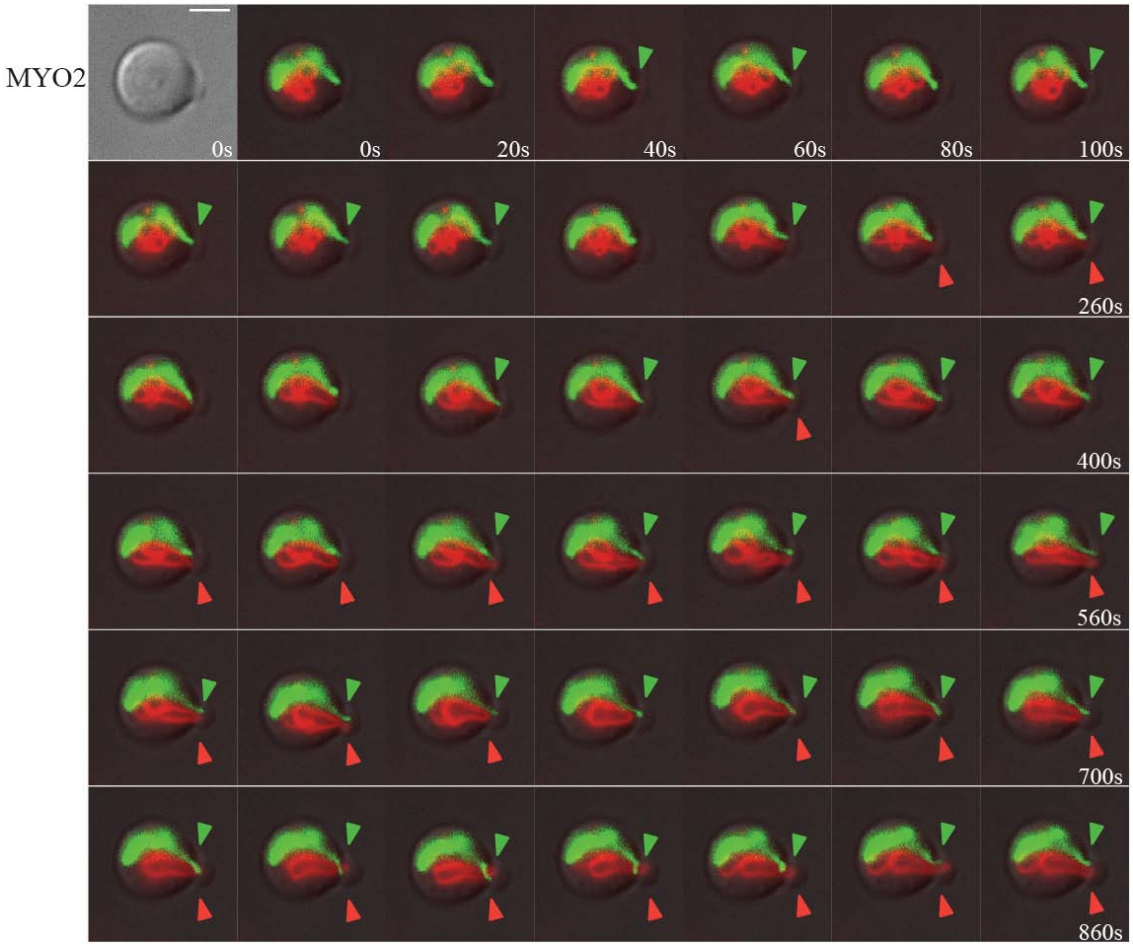

Figure 2.17
Time-lapse series of a wild-type cell. Time-lapse images were recorded from the cell analyzed in Figure 2.13(I) (top red-green pair) as mitochondria and vacuoles crossed the mother-bud neck into the bud. Images acquired every twenty seconds for a total of ~ thirteen minutes (860s). Color of arrow heads indicate an organelle in the bud. s, seconds. Bar = 1 μm.

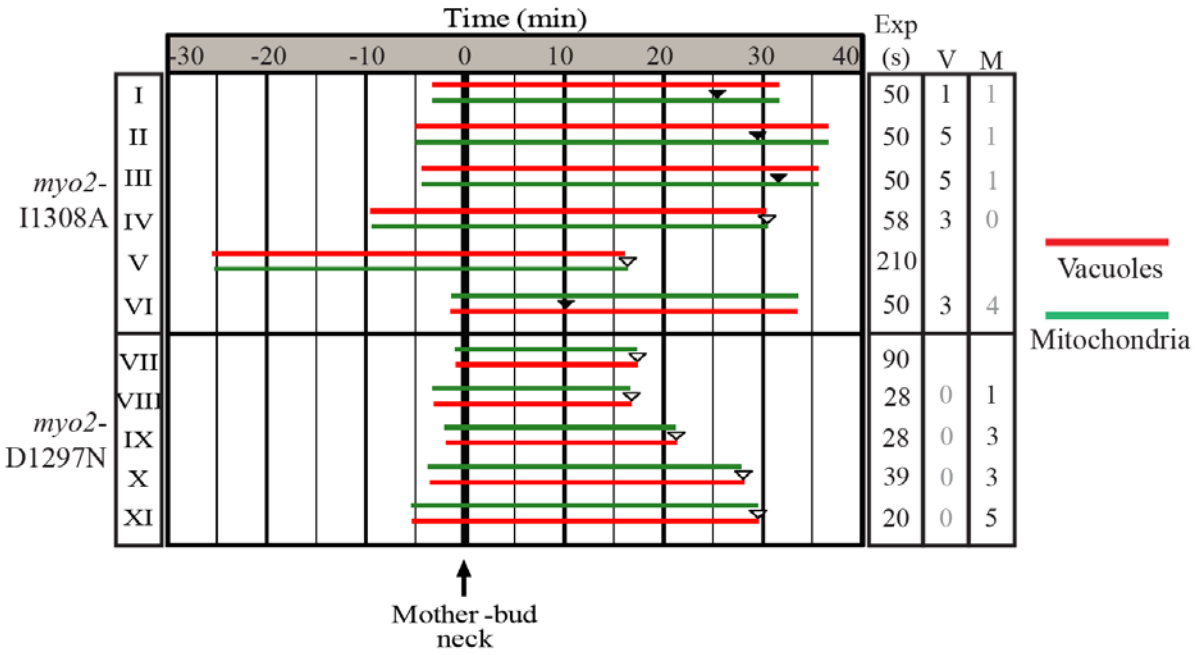

Figure 2.18
Vacuole or mitochondrial inheritance is delayed or disrupted in *myo2* mutants that disrupt Vac17 or Mmr1 binding. Vacuoles (FM4-64) and mitochondria (mitoGFP), were imaged in cells containing either *myo2*-I1308A or *myo2*-D1297N, expressed from a plasmid (CEN, HIS3) as the sole copy of *MYO2*. Zero (t=0), set for each pair, is the time that the first organelle (top bar in each pair) entered the bud. Arrowheads indicate the time that the lagging organelle entered the bud. *Top*: Five of six cells containing *myo2*-I1308A display a delay (I-III) or absence (IV-V) of mitochondrial inheritance. The bottom cell (VI) was wild-type-like. *Bottom*: Five cells containing *myo2*-D1297N showed an absence of vacuole inheritance (VII-XI). Right columns: Time (seconds) between each time-lapse exposure for each series; 'V' or 'M' indicate the number of times a vacuole tubule (V) or mitochondria tubule (M) crossed the mother-bud neck for the two time-lapse series that were less than 60 seconds between collected images.

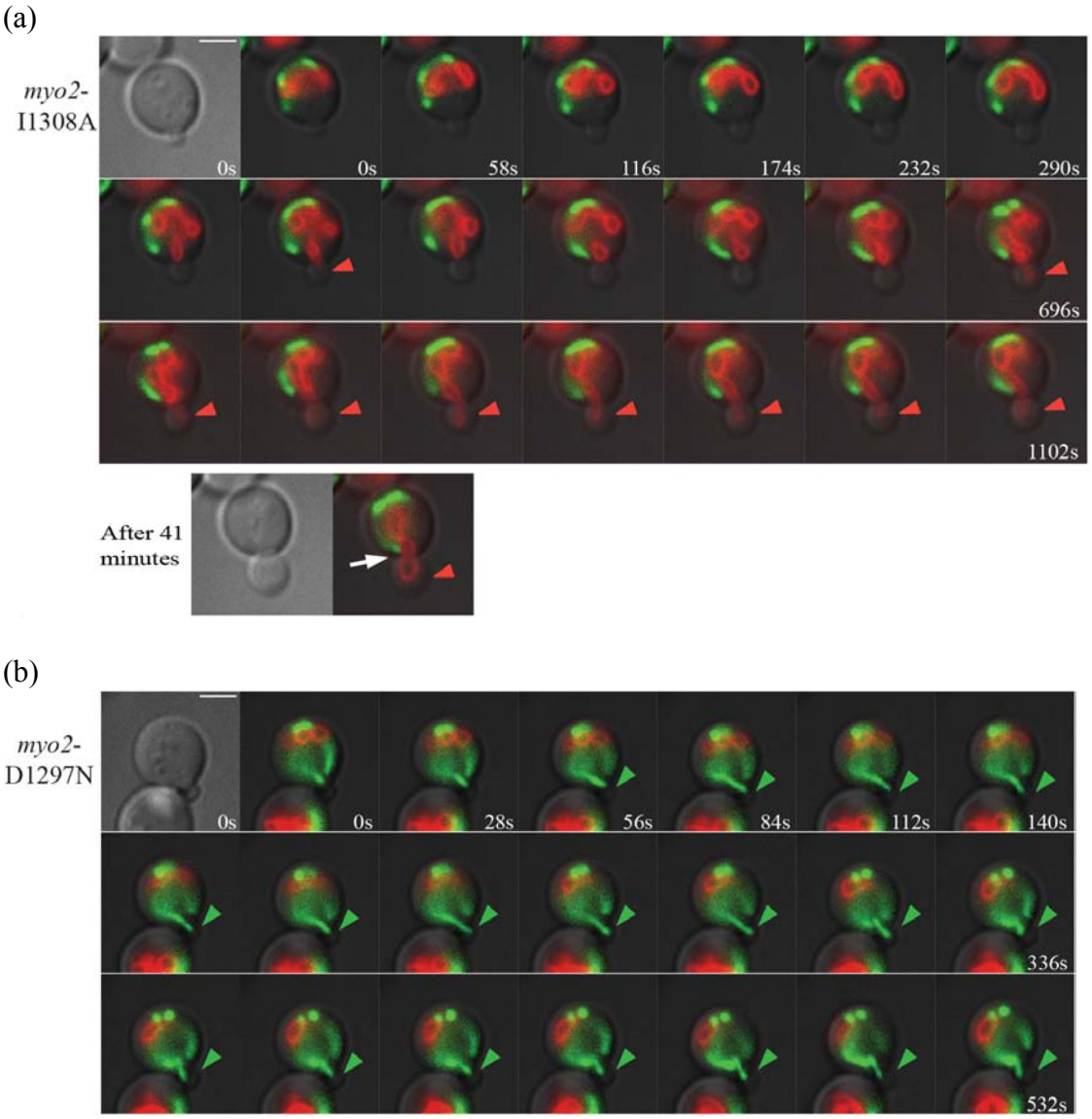

Figure 2.19
Time-lapse series micrographs of a cell containing *myo2*-I1308A or *myo2*-D1297N. (a) Time-lapse images (Figure 2.15 (IV)). Images acquired every 58 seconds for a total of ~ 41 minutes. Red arrowhead indicates when the vacuole was in the bud. After 41 minutes of imaging, the mitochondrial tubule moved toward the mother-bud neck region, yet did not pass into the bud (white arrow). (b) Time-lapse images (Figure 2.15 (VIII)). Images acquired every 28 seconds for a total of ~ 18 minutes. After about one minute, the mitochondrial tubule crossed the mother-bud neck while the vacuole remained toward the rear of the mother cell. s, seconds. Bar = 1 μm.

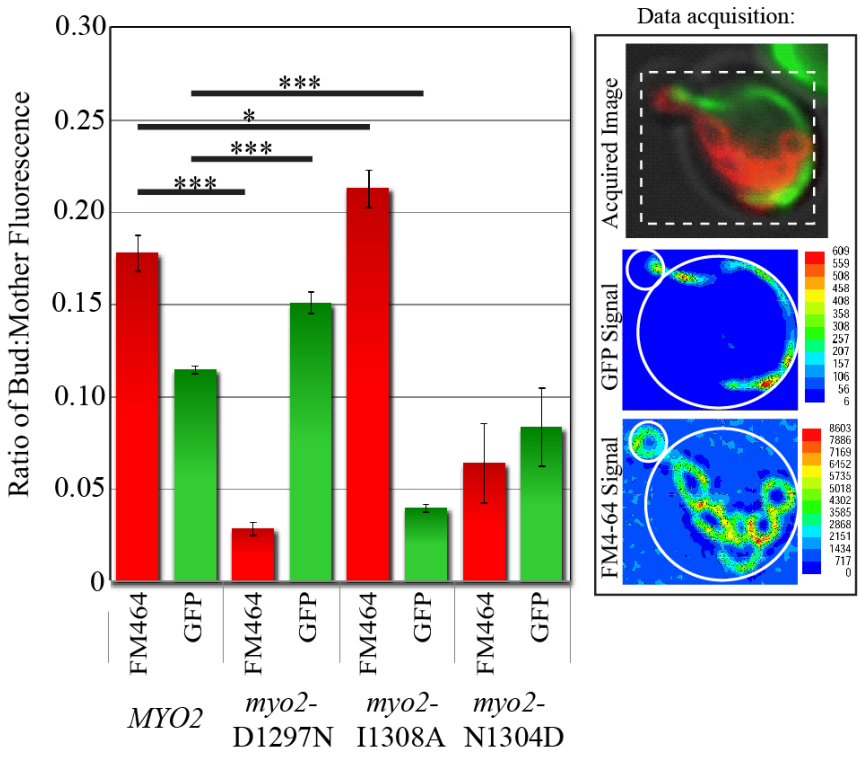

Figure 2.20
Quantitative analysis of vacuole and mitochondrial inheritance in *myo2* mutants reveals increased mitochondrial inheritance in *myo2*-D1297N and increased vacuole inheritance in *myo2*-I1308A. Small budded cells (bud diameter was ≤⅓ the diameter of the mother) were scored for relative levels of mitochondria (mitoGFP) and vacuole (FM4-64) signal in the bud compared to the mother. Right panel shows an example of linear intensity scales for mitochondria and vacuoles in a wild-type small budded cell. For each cell, fluorescence emitted at 528 nm (GFP) and 617 nm (FM4-64) in the mother and in the bud, with background subtracted, was determined. The bud-mother ratio of fluorescence is shown. Cells analyzed fit three criteria: [1] The bud was in focus. [2] Both vacuoles and mitochondria were visible in the mother cell. [3] The cell was free of surrounding cells on at least two sides which permitted background fluorescence measurement. Error bars represent standard deviation from the mean. * indicates $p<0.05$; *** indicates $p<0.001$ using Students T-test analysis. n=3; 33 small budded cells per strain, per experiment.

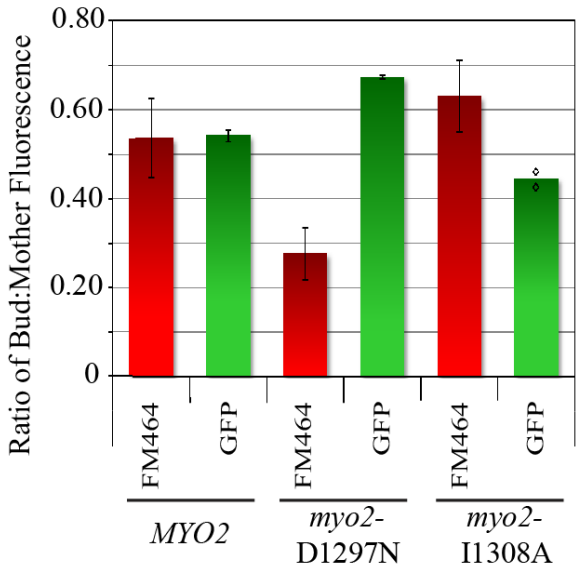

Figure 2.21
Quantitative analysis of the amount of mitochondria and vacuoles in large budded and unbudded cells. The bud:mother ratio of fluorescence emitted at 528 nm (GFP, mitochondria) and 617 nm (FM4-64, vacuoles) is shown. Cells analyzed fit the following criteria: [1] The bud was in focus. [2] Both vacuoles and mitochondria were visible in the mother cell. [3] The cell was free of surrounding cells on at least two sides. 33 budded cells per strain, per experiment. *n*=3, with the exception of *myo2*-I1308A (pmitGFP) where the values of two independent experiments are indicated (diamonds). Error bars represent the standard deviation from the mean.

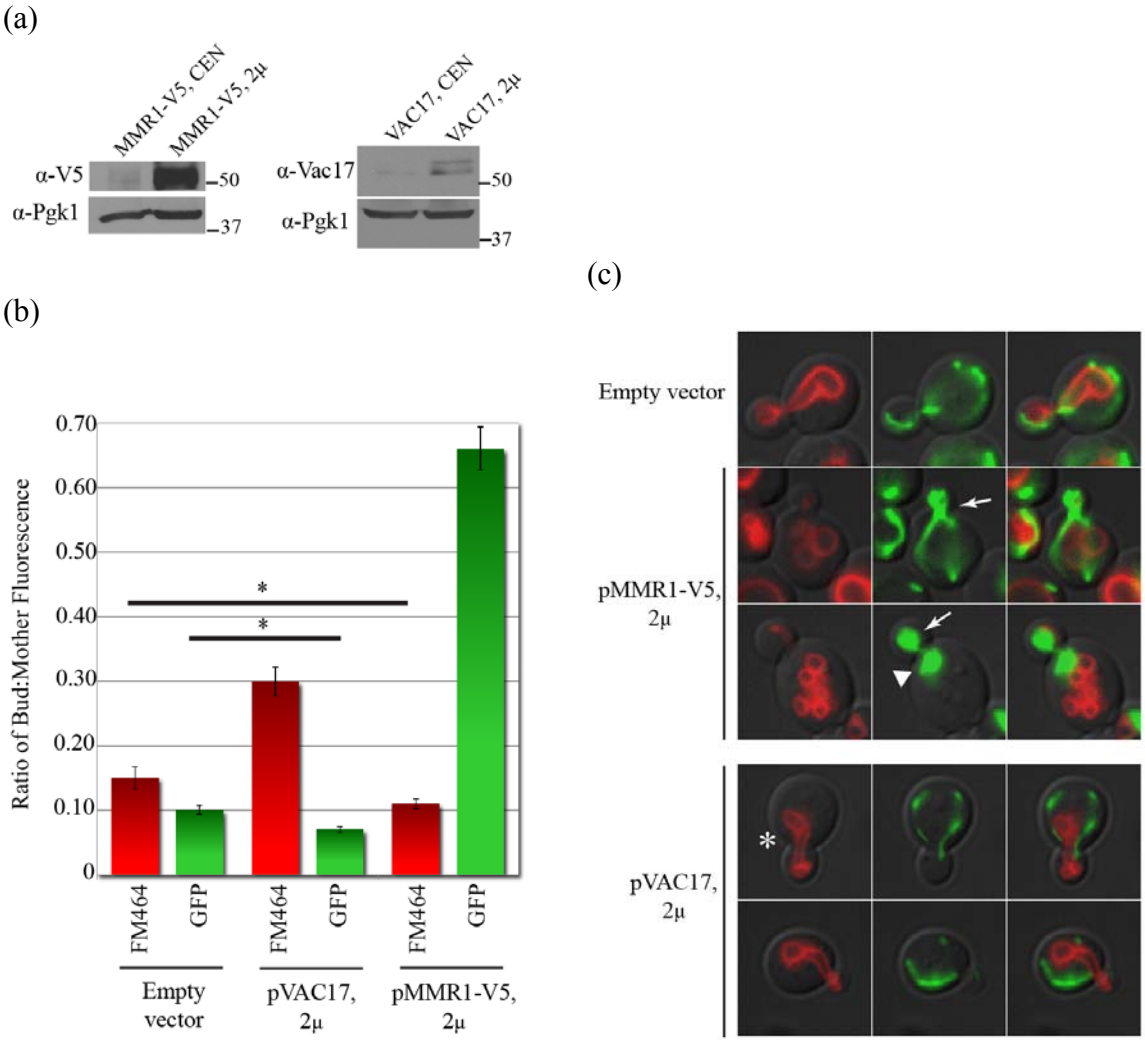

Figure 2.22
Over-expression of *MMR1* or *VAC17* reveals that Vac17 and Mmr1 proteins compete for access to Myo2 *in vivo*. (a) Wild-type cells transformed with single copy (CEN, URA3) or multicopy plasmids (2μ, URA3) as indicated. Whole cell lysates were prepared and separated by SDS-PAGE, then immunoblotted with anti-V5 or anti-Vac17 antibodies. Anti-Pgk1, loading control. (b-c) Wild-type cells were dual transformed with empty vector (2μ, URA3), pMMR1-V5 (2μ, URA3) or pVAC17 (2μ, URA3) multicopy plasmids and with pmitoGFP (2μ, LEU2) and grown in log phase before labeling with FM4-64 and subsequent imaging. (b) Quantitative fluorescence analysis of small and medium budded cells. *n*=3; 33 cells per experiment. Error bars represent standard deviation from the mean. (c) Micrograph images taken from one experiment in (b).

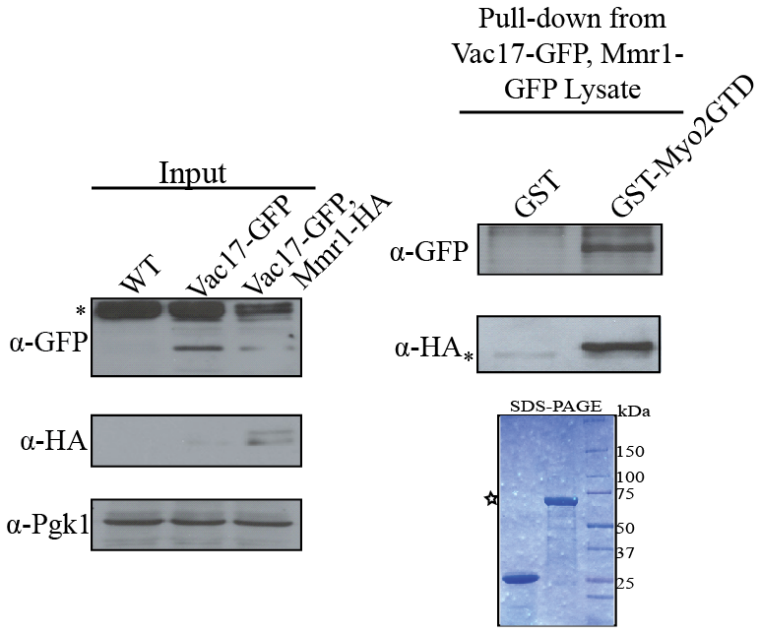

Figure 2.23
Recombinant Myo2 cargo binding domain pulls down Vac17-GFP and Mmr1-HA from yeast cell lysates. GST alone or GST-Myo2GTD (the cargo binding domain, residues 1131-1574) was expressed and purified from E. coli cell lysates (SDS-PAGE). Wild-type yeast cells expressing Vac17-GFP (CEN, URA3) and Mmr1-HA (CEN, TRP1) were lysed and GST or GST-Myo2GTD bound resin was incubated in the presence of yeast cell lysate. Input, ~8% of total loaded. Anti-Pgk1, loading control. Elutions from GST beads were separated and immunoblotted with anti-GFP or anti-HA antibody. Coomassie stain, star: GST-Myo2 (76 kDa). *Non-specific band.

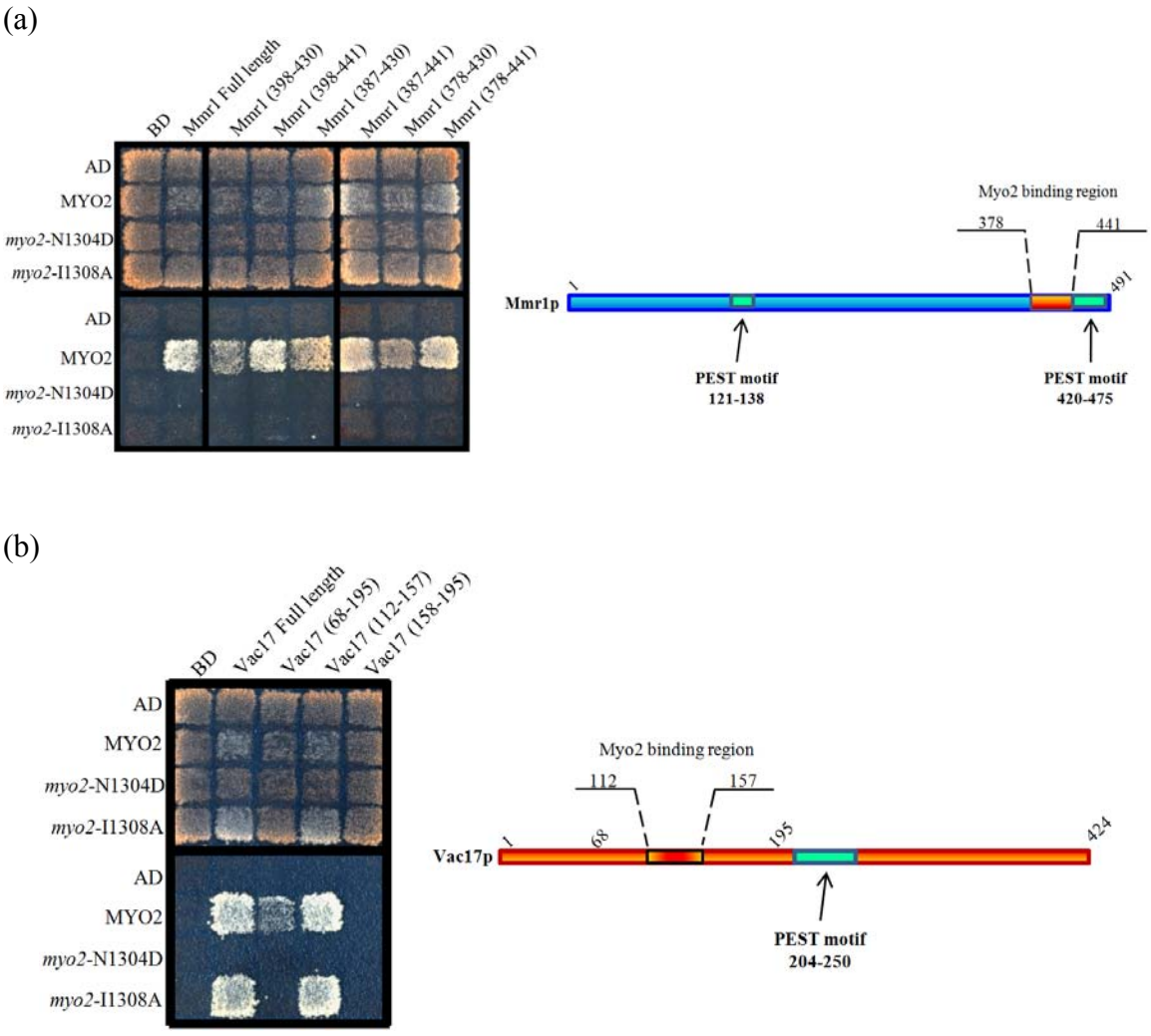

Figure 2.24
Yeast two-hybrid analysis to define the Myo2-binding region of Vac17 and Mmr1. (a) Yeast two-hybrid tests identified a region of Mmr1between residues 378 and 441 that showed specific interaction with wild-type Myo2 but not with Myo2 containing mutations that disturb mitochondrial inheritance (Figure 2.7) or Mmr1 binding (Figure 2.1). ePESTfind algorithm (Mobyle portal website of Pasteur Institute, France) identified two putative PEST sequences in Mmr1. (b) Yeast two-hybrid tests identified a region of 46 residues that interacts strongly with wild-type Myo2 and shows no binding to *myo2*-N1304D, a mutation that disrupts full-length Vac17 and vacuole inheritance (Figure 2.6). Vac17 PEST sequence was previously identified (Tang *et al*., 2003).

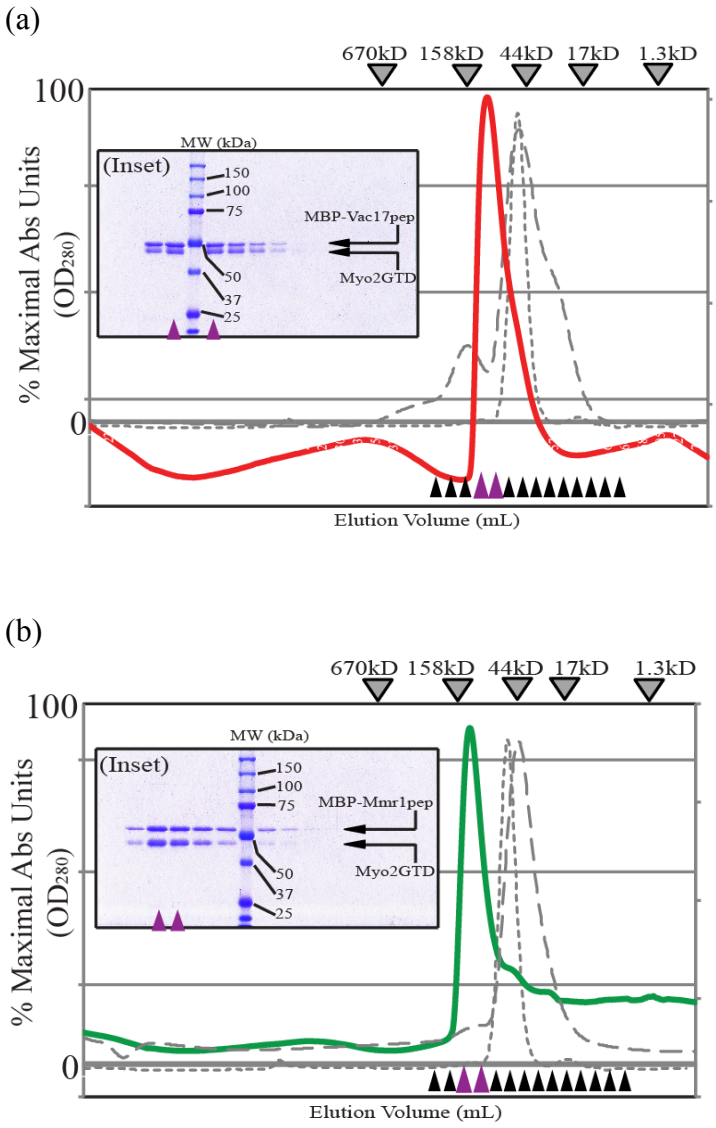

Figure 2.25
The Myo2 cargo binding domain interacts with Vac17 and Mmr1, *in vitro*. (a-b) Recombinant Myo2 cargo binding domain (Myo2GTD) and the Myo2-binding motif of either Vac17 (peptide of 46 residues) or Mmr1 (peptide of 44 residues) containing an N-terminal MBP tag (MBP-Vac17pep or MBP-Mmr1pep), were purified from *E. coli*. Myo2GTD was incubated in a 1:1 molar complex with MBP-Vac17pep (a; red line) or MBP-Mmr1pep (b; green line) and separated on a size exclusion chromatography column. Fractions collected (arrow heads) were separated via 10% SDS-PAGE (inset gels). Peak fractions: purple arrow heads. Molecular weight markers (in kDa) are indicated at the top. Chromatograms of separations of Myo2 GTD monomer (50.5 kDa; grey dashed line) and MBP monomer (42 kDa) plus Myo2 GTD (grey dotted line) are shown.

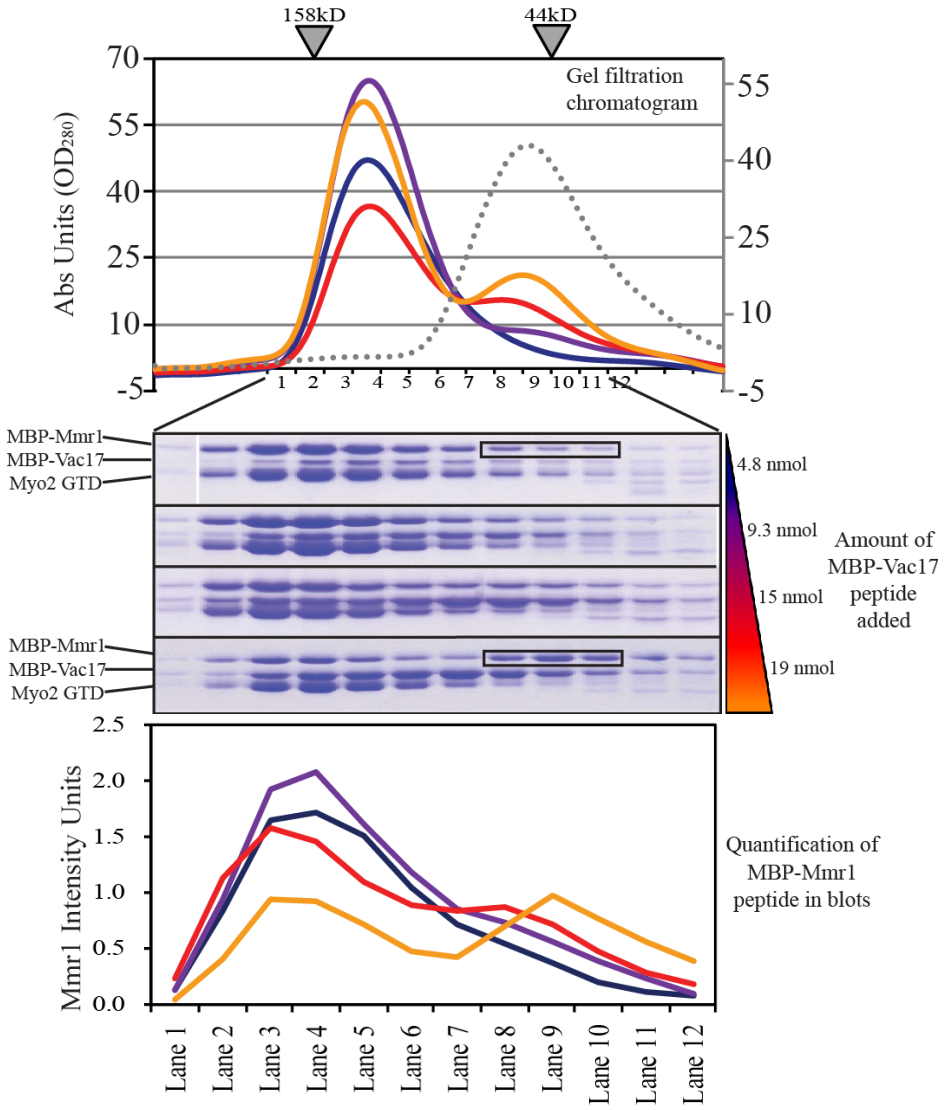

Figure 2.26
Vac17 and Mmr1 compete for access to Myo2, *in vitro*. Equal molar ratios of MBP-Mmr1peptide (11.7 nmol) and Myo2 CBD (11.4 nmol) were added together with increasing amounts of MBP-Vac17 peptide: 4.8 nmol, 9.3 nmol, 15 nmol, or 19 nmol (colored wedge) in four separate gel filtration experiments. Top: chromatogram of each separation. Grey dotted line indicates elution of MBP-Vac17peptide plus MBP-Mmr1peptide (1:1 molar ratio) as a control. Middle: Fractions 1 to 12 (indicated) were collected from each run; these correspond to proteins of molecular weight from approximately 180 kDa to 30 kDa. Bottom: Intensity of MBP-Mmr1peptide bands quantified from each gel.

(a)

(b)

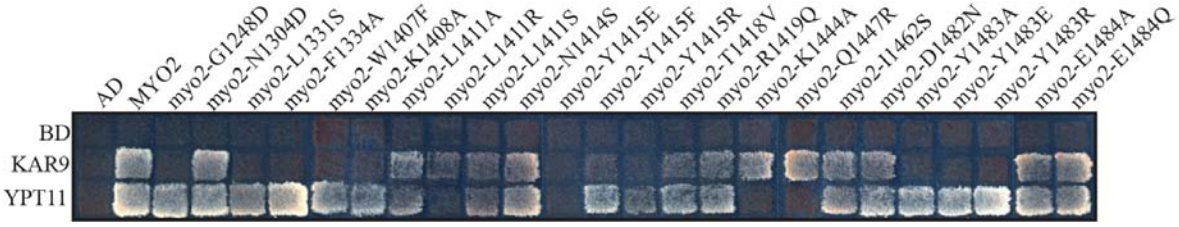

Figure 2.27
Mutations of the Myo2 cargo binding domain reveal that Ypt11 and Kar9 bind to an overlapping region with secretory vesicle Rab GTPases and Inp2. Yeast two-hybrid plates incubated at 24ºC for 4-5 days. Top and left test squares in each panel are empty vector controls. (a) myo2-L1301P, a mutation on helix six within the Mmr1/Vac17 binding region, also disrupts Kar9 and Smy1 binding. (b) Mutation analysis of surface residues surrounding Myo2-Y1415. This analysis was conducted on the basis of findings from Matthew J. Brunner and Dr. Yui Jin.

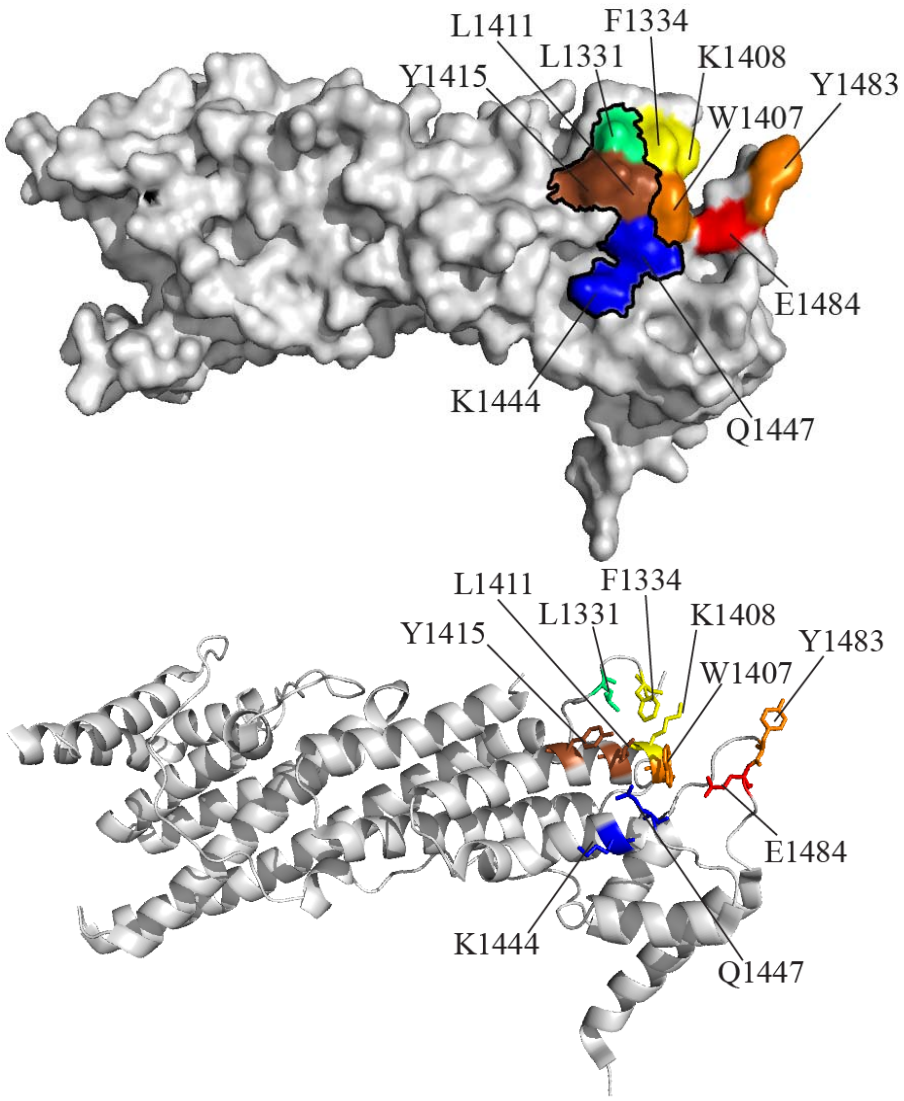

Figure 2.28
Surface (top) and ribbon (bottom) representation of the crystal structure of the Myo2 CBD indicating surface residues that interact with Kar9, Inp2, Ypt11 and Ypt31/Ypt32. Inp2 binding site (Fagarasanu *et al*., 2009); Ypt31/Ypt32 binding site (Lipatova *et al*., 2008). Rotated on the longitudinal axis 180° from the view in Figure 2.2. Black outline on the surface view represents the Ypt31/Ypt32 and Sec4 binding site. Red: Inp2 only; Orange: Kar9 and Inp2; Yellow: Kar9 only; Green: Kar9, Sec4 and Ypt31/Ypt32; Blue: Sec4, Ypt11 and Ypt31/32; Brown: Kar9, Inp2, Sec4, Ypt11 and Ypt31/Ypt32.

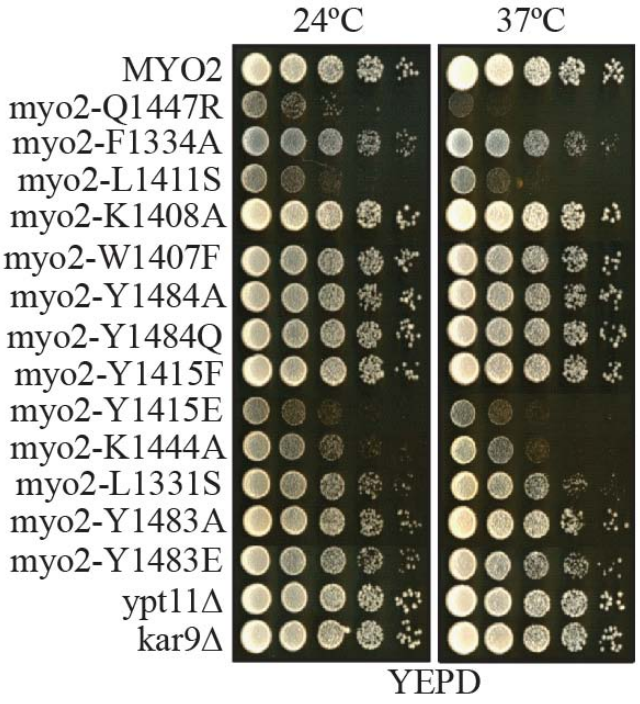

Figure 2.29
Myo2 mutants affecting Kar9 and Inp2 interactions had no effect on growth, whereas mutations in the Rab GTPase binding site had deleterious effects on growth. Strains containing *myo2* mutations were grown to log phase and serially diluted as indicated, and plated on rich media and incubated at 24°C or 37°C for 2-4 days.

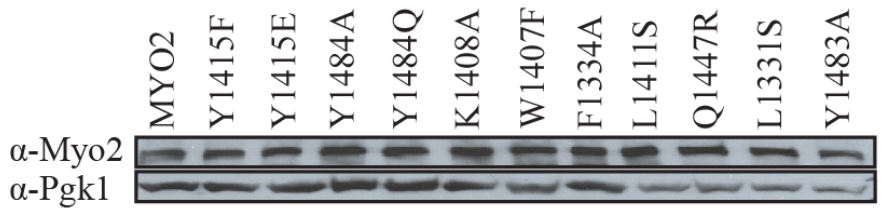

Figure 2.30
Expression levels of *myo2* mutants are similar to cells with wild-type *MYO2*. *myo2*Δ cells were transformed with either wild-type or mutant Myo2 plasmids (CEN, HIS3) under expression of the endogenous promoter. Cells were grown in log phase and protein extracts were extracted using TCA precipitation. Extracts were separated via 9% SDS-PAGE and immunoblotted with anti-Myo2 and anti-Pgk1 antibodies.

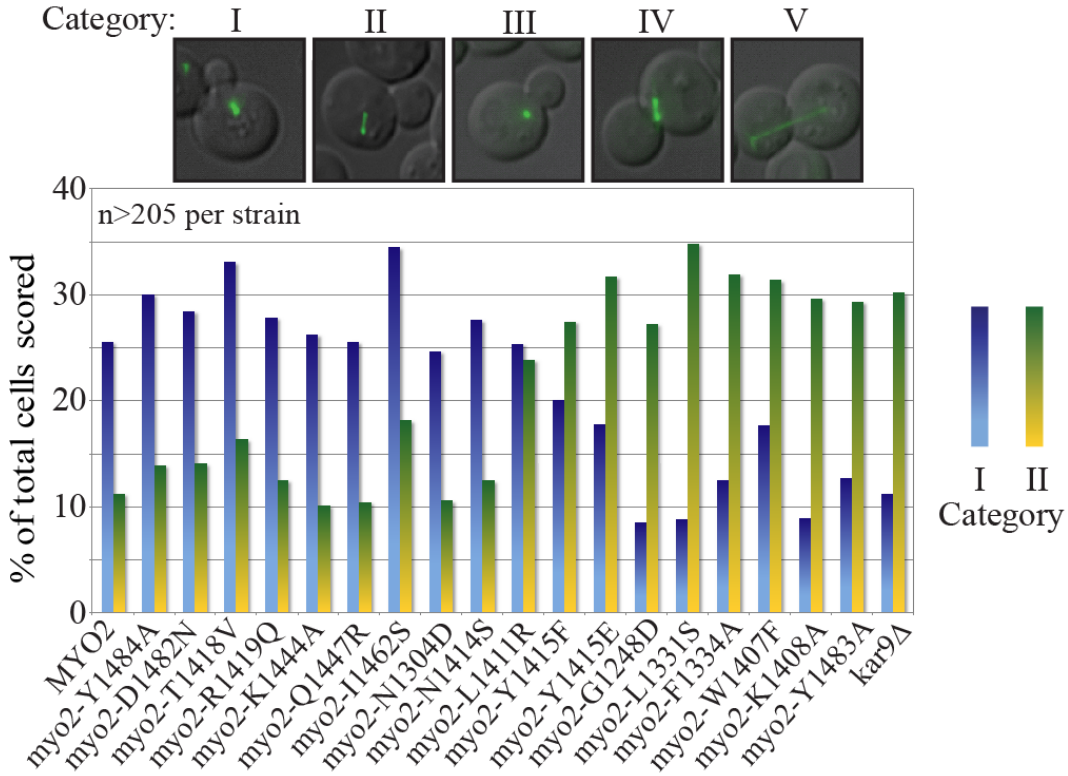

Figure 2.31
myo2 mutations that disrupt Kar9 binding in a yeast two-hybrid test also display a defect in spindle microtubule orientation. Residues L1331, F1334, W1407, K1408, Y1415 and Y1483 form the Kar9 binding site on Myo2 and are critical for proper orientation of the mitotic spindle. *myo2*Δ cells containing full-length wild-type *MYO2* or *myo2* mutant plasmids were transformed with pGFP-Tub1 and the orientation of spindle microtubules was scored according to 5 categories: [I] Microtubules properly aligned toward the bud; [II] Microtubules improperly aligned pointing away from the mother-bud neck; Categories III, IV and V were not informative and while they were scored, they are not shown. Categories I and II were plotted as percent of the total number of cells scored per all five categories. n=2; ≥215 cells scored per mutation.

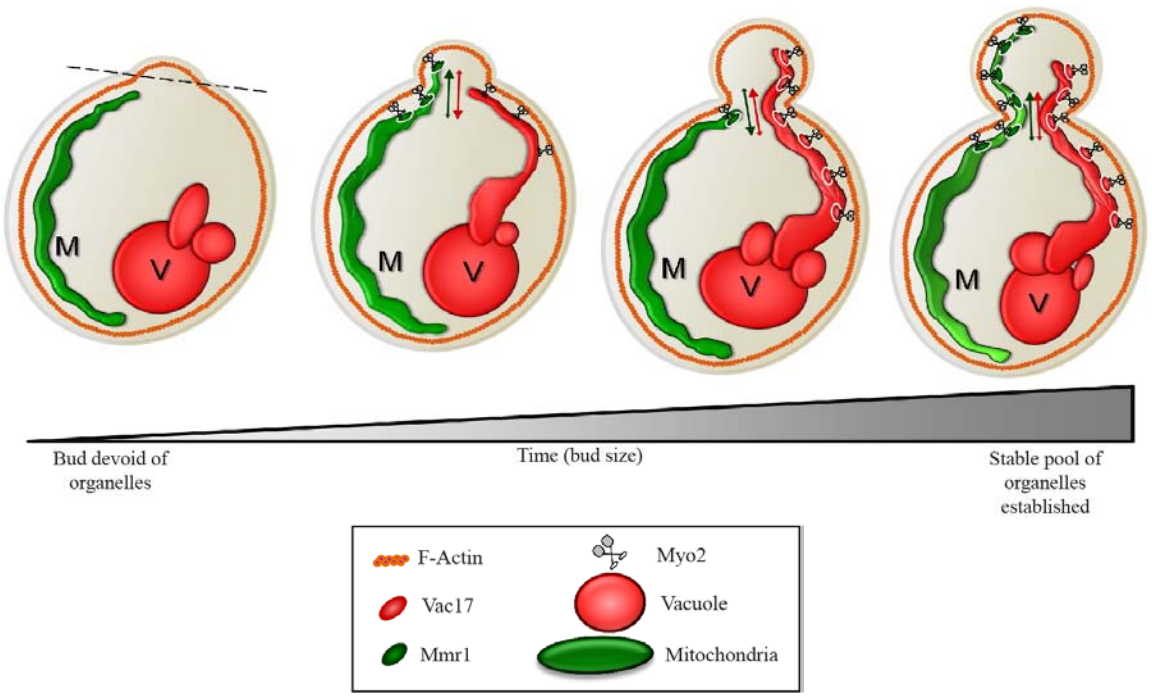

Figure 2.32
Model for how competition between Vac17 and Mmr1 contributes to the inheritance of vacuoles and mitochondria. Near the end of G1 phase, the bud emerges from the mother cell. Both mitochondria (M) and vacuoles (V) begin moving toward the bud at similar times. At the neck region, one organelle crosses the mother-bud neck before the other, a 50/50 chance for either a mitochondria or vacuole tubule. After moving into the bud, the organelle often retracts back into the mother cell before beginning movement further in the bud. In the model depicted above, a mitochondrial tubule crosses the neck first. In subsequent events, the other organelle, will move into the bud and back out. This "rocking" continues until a stable pool of each organelle is established in the bud.

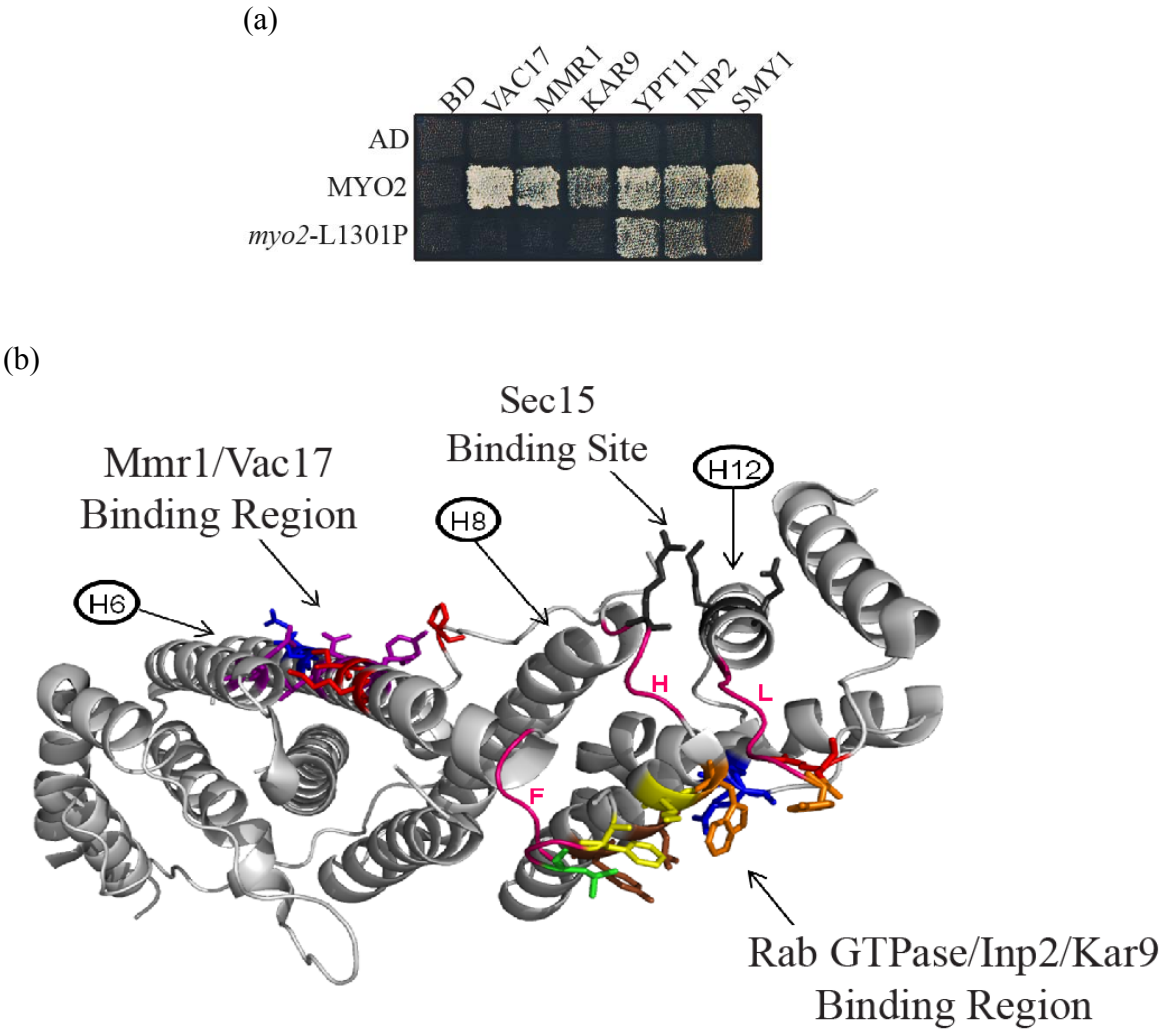

Figure 2.33
Binding cargo adaptors at the Rab GTPase/Inp2/Kar9, Vac17/Mmr1 binding regions or the Sec15 binding site may cause conformational changes in Myo2 that regulate the binding at other sites. (a) Binding of Kar9 and Smy1, in addition to Mmr1 and Vac17, are disrupted by mutation of Myo2-L1031 to *myo2*-L1301P. The residue L1301 is surface exposed. A mutation to proline likely produces a conformational change in helix 6 which affects the structure of the cargo binding domain. No other surface mutations in the Mmr1/Vac17 binding region affected the binding of Kar9 or Smy1. Plates incubated at 24ºC for 4 days. Top and left test squares are empty vector controls. (b) Ribbon view of the Myo2 cargo binding domain. Residues which affect binding interactions (stick view) are shown in color; colors are that of Figure 2.2 and 3.3. Three loops that may be critical for connection between binding sites are pink (Loops F, H and L).

CHAPTER 3

FUTURE DIRECTIONS

These thesis studies demonstrate that cargo adaptors bind to Myo2 at overlapping binding sites. Moreover they show that the overlap of Mmr1 and Vac17 regulate the volume of mitochondria and vacuoles inherited. Notably, the Rab GTPase/Inp2/Kar9 binding sites also overlap on Myo2, which strongly suggests that this overlap has functional significance. To gain further mechanistic insight into the functional significance of each overlapping binding site, it would be informative to determine the copy number of each adaptor relative to Myo2, their affinities for Myo2, and the precise *in vivo* localization for each cargo adaptor. Moreover analysis of the Myo2 structure suggests that it may change as a result of cargo adaptor binding or Myo2 phosphorylation. How cargo adaptor interactions integrate with other specific cellular processes and machinery is also important.

Do the contributions of cargo adaptor affinities and copy number account for cargo adaptor competition?

In addition to overlapping binding sites, other parameters regulate the inheritance of vacuoles and mitochondria. Importantly, the following discussion assumes that the adaptor proteins bind a cytoplasmic pool of Myo2 that is then recruited to the organelle. Moreover, the localization, copy number and binding affinity of Mmr1 and Vac17 for

Myo2 are important factors. As demonstrated in this thesis, Mmr1 and Vac17 localize to distinct pools at the bud-directed portions of mitochondria and vacuoles, respectively. As a first approach, since Mmr1 and Vac17 compete for access to Myo2, we tested whether the copy numbers of Mmr1 and Vac17 would be similar *in vivo*.

The total amount of Vac17 was found to be approximately 20 copies per cell (Tang *et al*., 2006). To determine the relative levels of Mmr1 to Vac17 *in vivo*, both Mmr1 and Vac17 were C-terminally tagged with GFP and expressed from their endogenous promoters. Protein extracts were made from log-phase cells and a western blot was performed of yeast extracts blotting with anti-GFP antibody (Figure 3.1). The linear range of anti-GFP signal was used to determine the relative levels of Vac17-GFP to Mmr1-GFP. The results indicate that Mmr1-GFP is present in the cell almost 4-fold higher than Vac17-GFP. This suggests that Mmr1 is expressed at at least 80 copies per cell.

The difference between Mmr1 and Vac17 steady-state levels was unexpected. While cell cycle regulation of Mmr1 is not well characterized, it may be that peak Vac17 levels are nearly equal to peak Mmr1 levels at overlapping times during organelle inheritance. This has yet to be tested. Another possible explanation for why Vac17 and Mmr1 compete for access to Myo2 even though their expression levels are ~4-fold different *in vivo* is that their binding affinities for Myo2 may not be the same. It is tempting to speculate that since Mmr1 is present ~4-fold higher than Vac17 *in vivo*, Vac17 may have a stronger binding affinity than Mmr1, for Myo2.

The binding affinity of a Vac17 peptide for the Myo2 cargo binding domain was determined. Recombinant Vac17(68-195) and Myo2(1131-1574) proteins were prepared

to high purity via size-exclusion chromatography. Myo2 was covalently modified with Alexafluor-532 and Vac17 was covalently attached to biotin affinity tags for use in the Flow Cytometry Protein Interaction Assay (Blazer *et al*., 2010; Figure 3.2a). A binding curve was obtained from a titration of Myo2 (amount held constant) with Vac17 (amount was varied). The dissociation constant (K_d) for Myo2/Vac17 was 53 nM (Figure 3.2b), which is within the range of dissociation constants for monoclonal antibodies bound to epitope (Kindt *et al*., 2007). To determine if Mmr1 binds Myo2 with a similar dissociation constant, the FCPIA assay can be utilized. Several suitable Mmr1 constructs have been identified (Figure 2.24) that are highly soluble *in vitro* and specifically interact with Myo2 CBD (Figure 2.25). Though the MBP tag remained attached to Mmr1 peptide in these experiments, MBP can be easily cleaved and removed using the TEV cleavage site within the expressed protein. Mmr1 peptide protein remains soluble after MBP cleavage (data not shown).

Do structural changes occur in Myo2 CBD upon cargo adaptor binding?

Allostery describes how protein binding at a specific binding site can regulate or affect a second, distinct binding site (Bu and Callaway 2011). Analysis of the structure of the Myo2 CBD suggests that cargo adaptor binding at the Rab GTPase/Inp2/Kar9 binding region may affect binding at the Mmr1/Vac17 binding region, and vice versa. Helix six, which contains most of the Mmr1/Vac17-binding residues, runs diagonally across the CBD. The C-terminus of helix six ends with a loop (Loop F; Figure 2.33) that connects to the Rab GTPase/Inp2/Kar9 binding region. It is appealing to speculate that the Myo2

CBD may structurally regulate cargo adaptor attachment to make binding at the other site less favorable.

To test whether cargo adaptor binding at one site regulates cargo adaptor binding at a distinct site, both *in vivo* and *in vitro* approaches can be utilized. Over-expression of Kar9 or Inp2 (using a 2μ plasmid) can be employed to test vacuole inheritance (using FM4-64) or mitochondria inheritance (using pmitoGFP). Further, over-expression of Vac17 or Mmr1 can be used to determine spindle orientation (Tub1-GFP), peroxisome inheritance (Pts1-GFP) or Golgi inheritance (Sec7-3xGFP). *In vitro* size-exclusion chromatography can be used to test if Vac17 peptide or Mmr1 peptides affect binding of Kar9 or Inp2 binding, and vice versa. While the *in vivo* approach would be more applicable to determine significance, the second approach may reveal if a direct structural change in the Myo2 CBD occurs.

Currently, *in vitro* studies and yeast two-hybrid mutational analysis suggests that a region in Vac17 between residues 112 and 157 (Figure 2.24) directly interact with the Myo2 CBD. The precise residues on Vac17 which directly contact Myo2 remain to be determined. To date, there is no high resolution structure of Vac17. At least four phosphorylation sites exist on Vac17 that enhance its interaction with Myo2 and are likely solvent-exposed. That these phosphorylation sites are located near or within the Myo2-binding region raises the possibility that they alter local Vac17 structure when phosphorylated, which in turn regulates binding to Myo2, Vac8 or other downstream partners in the vacuole inheritance pathway (e.g., protein(s) required for Vac17 turnover).

Knowing the structure of Vac17 bound to Myo2 would provide crucial insight into how the Vac17/Myo2 interaction is regulated. A structure of the complex would also

reveal if the Rab GTPase binding region has been altered when Vac17 binds Myo2. Studies have been initiated to determine the co-crystal structure of Myo2 CBD bound to Vac17(68-195), a region of Vac17 that likely includes all of the Myo2-binding domain. This Vac17 construct only interacts with wild-type Myo2 and not point mutants that disrupt full length Vac17 (Figure 3.3a). Using size-exclusion chromatography, the proteins were purified to homogeneity and several co-crystal structure screens were prepared to grow protein crystals. One screen, the Qiagen JCSC+ screen, yielded a small cluster of crystals of about 170 μm in length (Figure 3.3b). Birefringence (i.e., light rotation) indicates they are true crystals. The crystal was seeded at a protein concentration of 4 mg/ml. Unfortunately the individual crystals were too small to obtain a diffraction pattern. Additional promising conditions have been identified.

Future studies to determine the co-crystal structure of Myo2/Vac17 could also incorporate two new soluble peptides that were identified in this thesis work, Vac17 (112-157) and Mmr1 (387-430). However their binding affinities for Myo2 CBD have not been determined. New co-crystal screens from Hampton and Sigma companies are now available and may provide lead conditions to obtain crystals.

Identify additional Myo2 residues involved in cargo adaptor binding sites

The mapping of residues on Myo2 that are important for cargo adaptor binding is incomplete (Figure 3.4). Studies of the Myo2 surface, to date, suggests several open regions on the Myo2 CBD surface which may reveal extended binding sites of adaptor already identified. Further, that the Sec15 binding site was recently identified (Figure 3.4, dark grey residues), which is distinct from the two primary binding regions, suggests

additional binding sites on Myo2 are unknown. This is highlighted by Smy1. Smy1, a kinesin-like protein which does not likely have motor function, binds directly to Myo2. However a definitive binding site has not yet been identified. Similar to other cargo adaptors like Vac17, Mmr1 and Kar9, Smy1 binding to Myo2 is disrupted by *myo2-2* (*myo2*-G1248D) (unpublished results). Whether Smy1 binds an overlapping region with Sec15 should be tested.

How does the Myo2/Vac17/Vac8 complex get recruited to the proper subdomain on the vacuole membrane?

Segregation structures form at the region of the vacuole membrane closest to the emerging bud. Vac17 co-localizes with this structure and is often observed in the anterior portion of this structure. A screen for vacuole inheritance uncovered mutants related to Myo2 movement of vacuoles, as well as the pathway that generates the lipid phosphatidylinositol 3,5-bisphosphate ($PI(3,5)P_2$). $PI(3,5)P_2$ is a signaling lipid on the vacuole membrane that may serve to integrate location with downstream effects. However it is currently not known if and how these pathways interact.

An intriguing finding in a large-scale yeast two-hybrid screen suggested that Atg18, a $PI(3,5)P_2$ binding protein (Dove *et al*., 2008), interacts with Vac17 (Georgakopoulos *et al*., 2001). To validate results from the larger study, we tested and found that a slightly truncated form of Vac17 interacted with full length Atg18 but not truncated forms (Figure 3.5a). Atg18 is a WD repeat-containing protein that likely has a tertiary structure similar to β-barrel proteins. Thus, smaller domains of Atg18 may not bind to Vac17 because the entire structure is critical to its function. We narrowed the

domain of Vac17 required for this interaction to residues 260-425 (Figure 3.5b). This region of Vac17 includes the Vac8-binding region and the coiled-coil two (CC2) domain.

The finding that Atg18 interacts with Vac17 was not expected. In addition to binding $PI(3,5)P_2$, Atg18 is a negative regulator of the lipid kinase Fab1 (Efe *et al*., 2007). Fab1 converts PI(3)P to $PI(3,5)P_2$ via its 5' kinase catalytic domain. That Atg18 binds Vac17 suggests that Atg18 plays a role in the mechanism that links vacuole inheritance with the regulation of $PI(3,5)P_2$ levels.

Based on images of vacuoles in *atg18*Δ yeast, which show a single enlarged vacuole and an absence of segregation structures. Atg18 may function in membrane tubulation of the vacuole during vacuole inheritance. It is tempting to speculate that Atg18 functions at this same region to allow for membrane fission or membrane tubule formation the segregations structure.

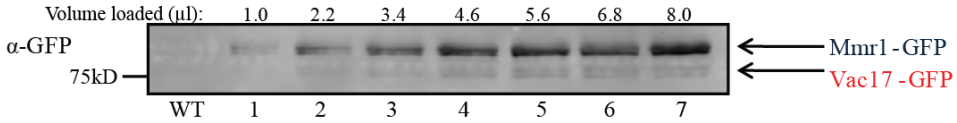

Lane	Vol	Mmr1	Vac17
1	1.0	12.37	4.47
2	2.2	16.59	7.67
3	3.4	17.88	9.17
4	4.6	20.87	11.56
5	5.8	21.82	14.87
6	7.0	23.67	15.47
7	8.2	28.97	15.07

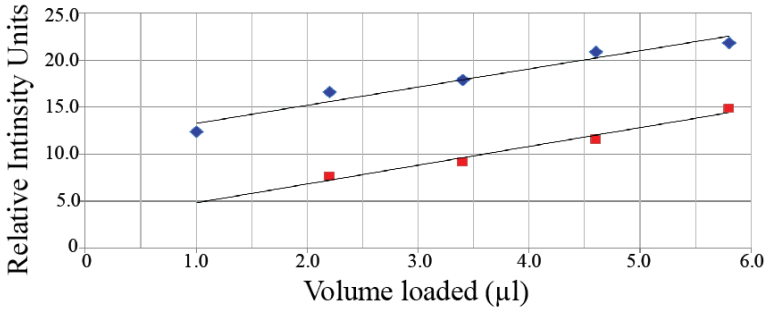

Figure 3.1
Mmr1 levels are approximately four-fold higher than Vac17 levels. The endogenous 3' end of *MMR1* and *VAC17* ORFs were tagged with GFP in the same strain and grown in log phase for several doublings. Indicated volumes of loaded yeast whole cell extract are at top; total volume loaded per lane was 8.2 µL. Lane 1 was loaded with 8.2 µL of wild-type cell extract as a control; Lane 2 was loaded with 1.0 µL of yeast lysate plus 7.2 µL of 1xSDS loading buffer, etc. Only data points within the linear range were plotted on the graph. Since the slopes are almost identical (Mmr1-GFP, m=2.32; Vac17-GFP, m=2.40), an increase in Mmr1-GFP signal corresponds to the same level of increase as Vac17-GFP for the range of each protein plotted on the graph. *Mmr1-GFP*, y=2.32x+11.0, x-int = -4.9; *for Vac17-GFP*, y=2.40x+2.4, x-int = -1.2. For example, at a y-value of 14, the x-value for Mmr1-GFP is 1.29 and Vac17-GFP is 4.83; therefore Mmr1 is ~3.8-times higher than Vac17.

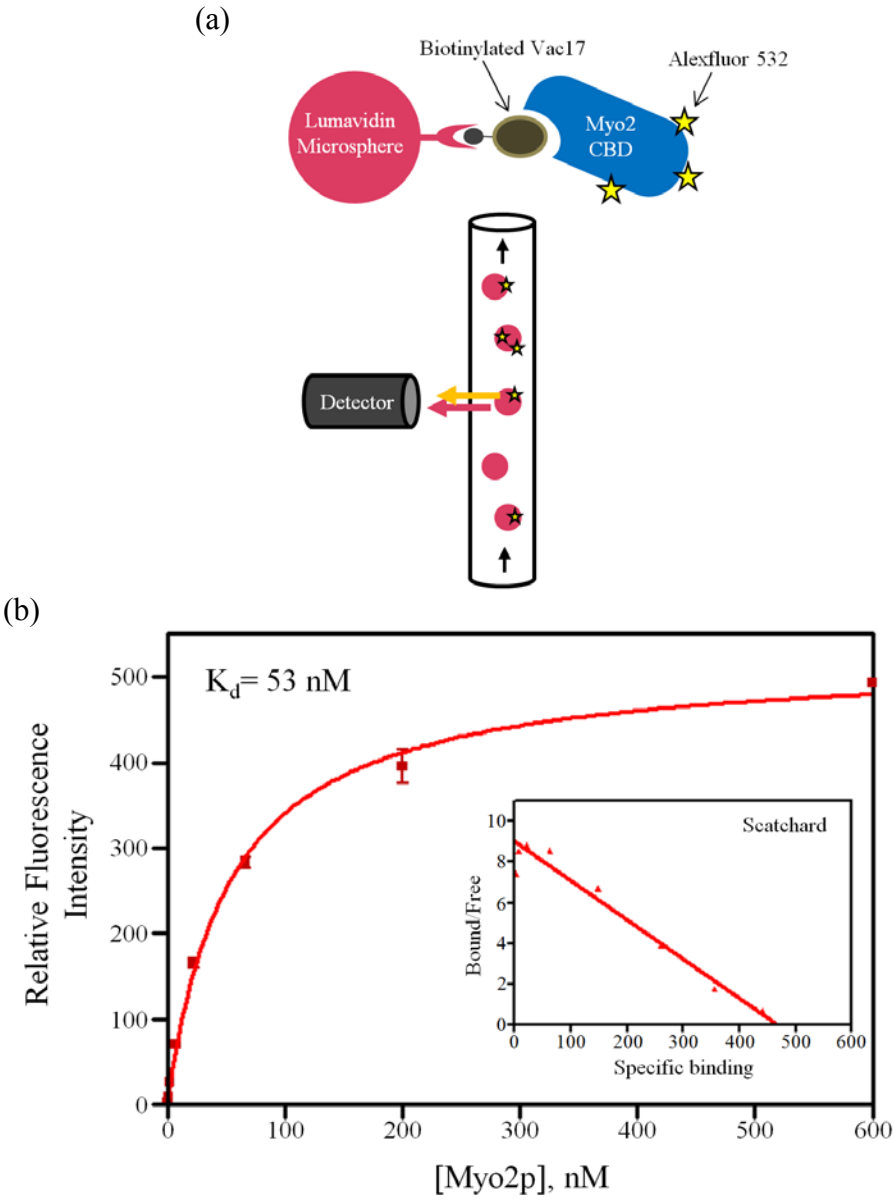

Figure 3.2
Myo2 cargo binding domain interacts with Vac17(68-195) with a 53 nM dissociation constant. (a) Luminescent Lumavidin microspheres (pink) bind biotinylated Vac17. Myo2, labeled with Alexa532, binds to Vac17. The flow cytometry detector simultaneously detects Lumavidin signal with Alexafluor 532 signal when Myo2 binds Vac17, and a dissociation constant can be calculated from titrations. (b) Recombinant Myo2 cargo binding domain purified from *E. coli* was covalently attached to ~three fluorescent Alexafluor-532 *n*-succidimidyl esters per protein. Vac17(68-195) purified from *E. coli* was covalently attached to ~two biotin *n*-succidimidyl esters per protein. Increasing concentrations of Myo2-AF532 bound to Vac17-biotin-microbeads allows generation of a binding curve. K_d=53 nM; B_{max}=479. Vac17(68-195) was originally found to bind Myo2 cargo binding domain by Dr. Natasha Pashkova.

(a)

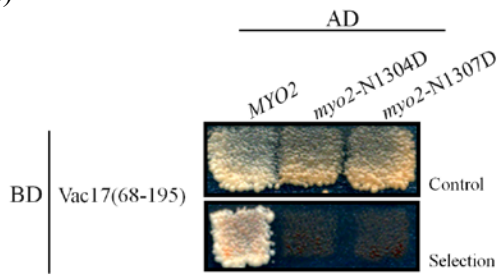

(b)

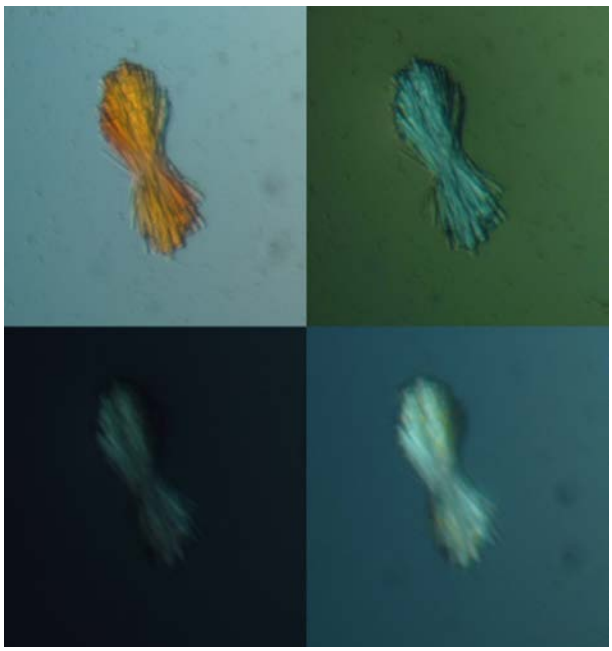

Figure 3.3
Myo2/Vac17 co-crystals identified in Qiagen JCSC+ Screen. (a) Vac17(68-195) interacts only with wild-type Myo2 and not point mutations which disrupt Myo2/Vac17 interactions. (b) The crystals were seeded in 2 µl; 1 µl mother liquor and 1 µl Myo2/Vac17 protein sample at 4 mg/ml. The mother liquor contained 0.1 M HEPES pH 7.50, 22% (w/v) polyacrylic acid-5100, 0.02 M $MgCl_2$. The hanging drop diffusion method was used. This condition was part of a tray set up on 7/31/2008; crystals were found on 11/26/2008 (118 days). 6His-Vac17(68-195) was constructed by Dr. Natasha Pashkova. This project was not pursued further because crystals were not obtained in a repetition of these conditions.

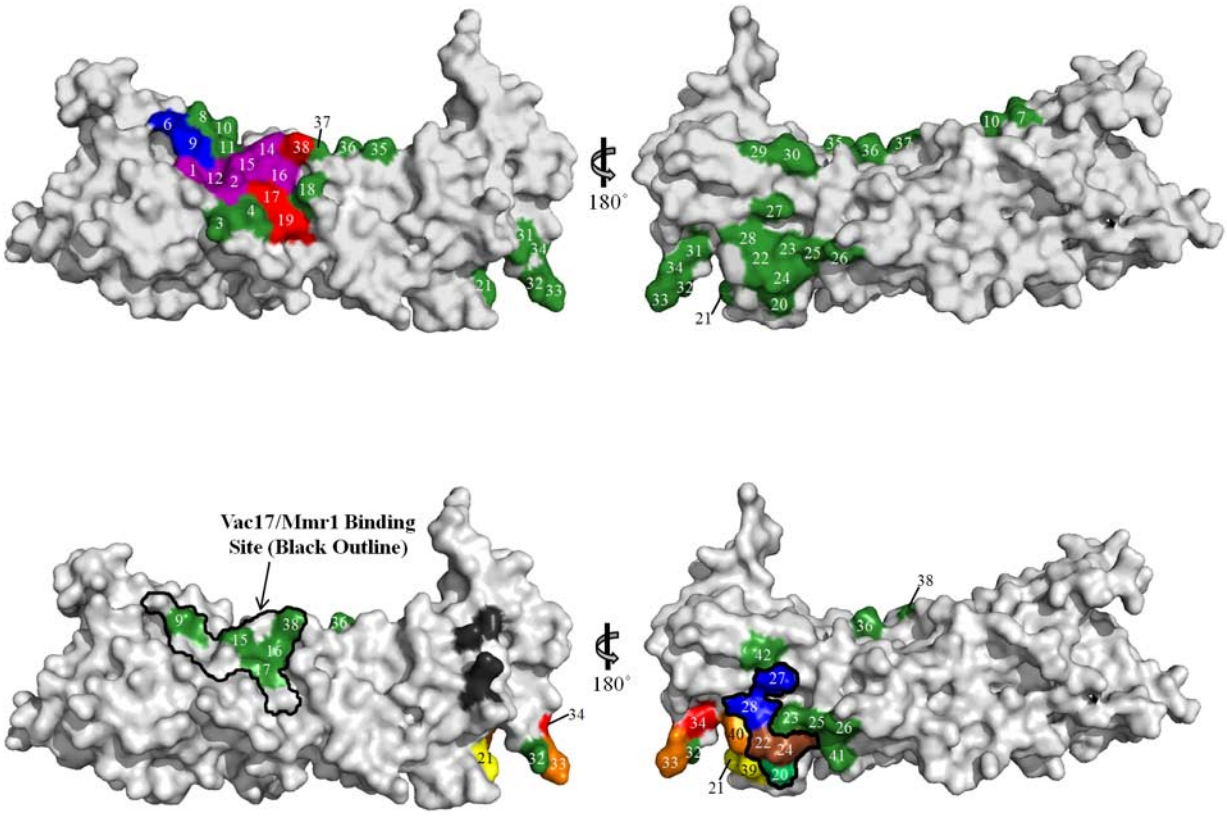

Figure 3.4
Surface representations Myo2 cargo binding domains showing all residues tested for at least one cargo adaptor. The binding sites for Myo2 cargo adaptors may extend beyond the tested residues. Note that, adjacent to each cargo adaptor region, there are white residues which have not been tested. Colors shown are those as previously shown in Figures 2.2 and 2.28. Green residues are mutations that did not perturb binding partners. Tested residues are as follows: **1**, 1229; **2**, 1233; **3**, 1234; **4**, 1237; **5**, 1248 (*myo2-2*; internal residue); **6**, 1293; **7**, 1295; **8**, 1296; **9**, 1297; **10**, 1299; **11**, 1300; **12**, 1301; **13**, 1302; **14**, 1303; **15**, 1304; **16**, 1307; **17**, 1308; **18**, 1311; **19**, 1312; **20**, 1331; **21**, 1408; **22**, 1411; **23**, 1414; **24**, 1415; **25**, 1418; **26**, 1422; **27**, 1444; **28**, 1447; **29**, 1461; **30**, 1464; **31**, 1480; **32**, 1482; **33**, 1483; **34**, 1484; **35**, 1525; **36**, 1526; **37**, 1528; **38**, 1529; **39**, 1334; **40**, 1407; **41**, 1419; **42**, 1462; **43**, 1539.

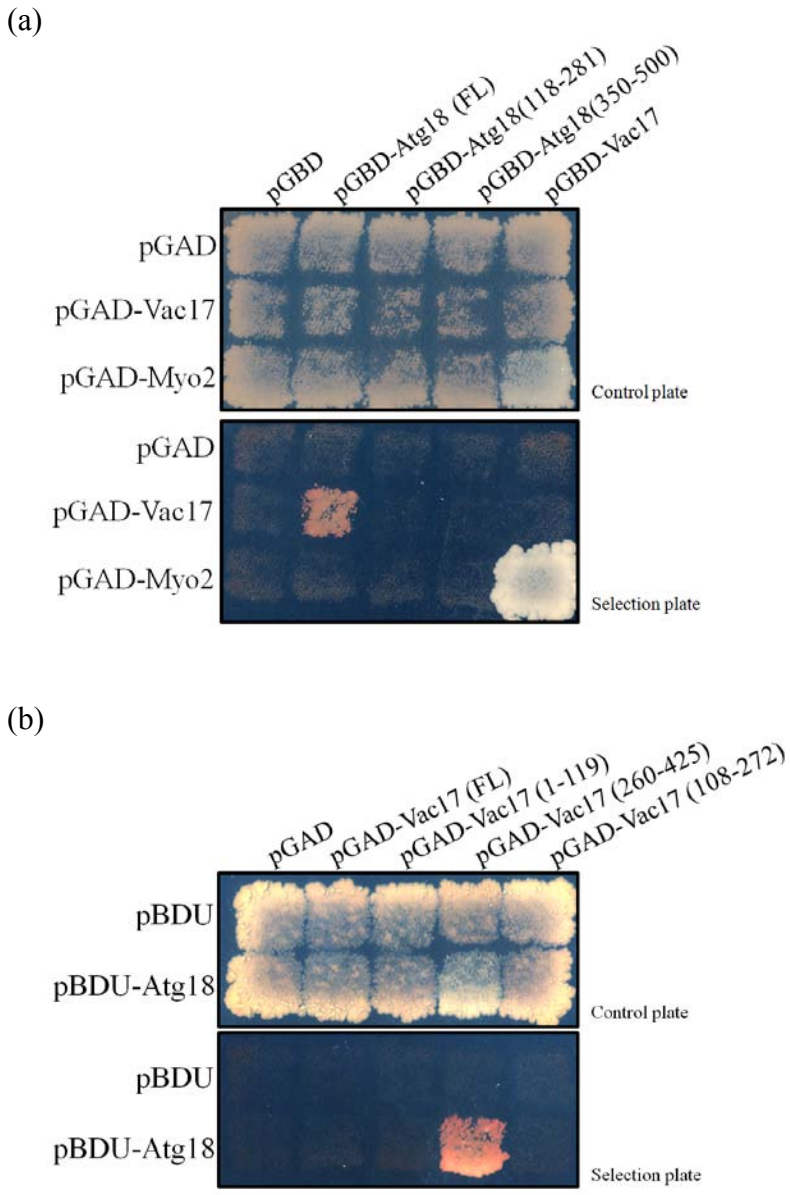

Figure 3.5
Full length Atg18 interacts with the Vac8-binding region of Vac17. Yeast two-hybrid plates incubated at 24˚C for 8-10 days until growth was seen on all control test squares. Top- and left-most test squares of both panels are empty vector controls. (a) Only full length Atg18 interacts with a truncated Vac17 construct (1-355). pGAD-Myo2 and pGBP-Vac17, positive control. (b) Full-length Atg18 interacts with the Vac8-binding region of Vac17 (residues 260-425). p*ATG18* plasmids were constructed by Jason Peterson. FL, full length.

CHAPTER 4

METHODS

Yeast strains and plasmids (Tables S1 and S2). Strains were grown at 24ºC unless indicated. *mmr1*Δ strain was constructed using PCR amplification of the endogenous kanamycin cassette from the YLR190W haploid knock out strain (Open Biosystems) and transformed into a diploid wild-type strain LWY9087, and sporulated to obtain the haploid knock out. *ypt11*Δ was constructed by PCR amplification of the endogenous kanamycin cassette from the YNL304W haploid knock out strain (Open Biosystems) and transformed into the haploid wt yeast strain LWY7235. Vac17-3xGFP was constructed using PCR with the plasmid PB1960 (from Dr. David Pellman, Harvard) and transformed into diploid yeast, sporulated and dissected (Jin *et al*., 2009). Vac17-3xGFP was used because endogenous Vac17 is of low abundance; approximately twenty copies per cell (Tang *et al.*, 2006). Mmr1-GFP was constructed using PCR amplification of the endogenous *GFP-HIS3* cassette containing flanking ends from the YLR190W ORF strain (Invitrogen) and transformed into the haploid wt yeast strain (Jin *et al.*, 2009). Mmr1-GFP is functional; cells expressing Mmr1-GFP expressed from the endogenous locus have normal inheritance of their mitochondria. In the Mmr1-GFP strain (LWY8867) transformed with mitoRFP (2µ, *URA3*) 80% of small and medium buds inherit mitochondria, versus wild-type cells transformed with mitoRFP (2µ, *URA3*) which

inherit mitochondria in 84% of small and medium buds (three independent experiments, a minimum of 33 cells analyzed per strain per experiment).

For generation of pRS416 *MMR1-V5*, a *Kpn*I-*Sac*II fragment (3.1 kb) of *MMR1* was subcloned into pBlueScript SK+ (pBS) at *Kpn*I and *Sac*II sites to generate pBS *MMR1*. A *Bgl*II site was generated at the C-terminus of *MMR1* by PCR using primers, (5'-GGA GAA GAA GGA AAA AaG Atc tGT CAA CTT CAA ATT AAA TTA AC-3') and (5'-GTT AAT TTA ATT TGA AGT TGA Cag aTC tTT TTT CCT TCT TCT CC-3') to generate pBS *MMR1-Bgl*II. To insert a V5 tag into the *Bgl*II site of pBS *MMR1-Bgl*II, annealed V5 primers encoded the V5 tag were used, (5'-GAT CTG GTA AGC CTA TCC CTA ACC CTC TCC TCG GTC TCG ATT CTA CGT GAG-3') and (5'-GAT CCT CAC GTA GAA TCG AGA CCG AGG AGA GGG TTA GGG ATA GGC TTA CCA-3') to generate pBS *MMR1-V5*. The resulting *Kpn*I-*Sac*II fragment was subcloned from pBS *MMR1-V5* into pRS416 at the *Kpn*I and *Sac*II sites.

Strains grown in rich media (1% yeast extract, 2% peptone, 2% dextrose), synthetic media (2% dextrose) lacking the indicated amino acid(s), or 5-fluoroorotic acid (5-FOA). *myo2* mutations were created with Stratagene Site Directed Mutatagenesis II kit following the manufacturer's protocol. For *myo2* plasmid-carrying strains, *myo2*Δ cells containing the *MYO2* (URA2, CEN) plasmid were transformed with mutant *myo2* plasmids (*HIS3*, CEN) and grown on 5-FOA. *myo2* plasmids in *myo2*Δ cells were maintained on rich media. Crystal structure representations of the Myo2 CBD (Pashkova *et al.*, 2006) PDB ID: 2F6H, were made using PyMOL Molecular Graphics System, Version 1.3 (Schrödinger, LLC) using the "cartoon" view.

Microscopy

Cultures were maintained at or below $5x10^6$ cells/ml for a minimum of six doubling times. Mitochondria were visualized by transformation of a mitochondrial-specific targeting peptide fused to GFP or RFP; mitoGFP/mitoRFP (Frederick *et al.*, 2008). For vacuoles, cells were incubated with 60 µg of FM4-64 for 45 min to 1 h in 2.5 ml of media, washed twice, and grown in 5 ml media for 1 doubling time (1.5-3hr). Images acquired on a DeltaVision Restoration system using an Olympus IX-71 inverted epifluorescence microscope with a Photometrics CoolSNAP HQ CCD camera. Widefield epifluorescence images were acquired without deconvolution using an Olympus 100X PlanApo objective. Following acquisition, fluorescence intensity was adjusted and applied to all images using DeltaVision softWoRx suite 3.5.1. Images converted to TIF format were overlaid and cropped in Adobe Photoshop. All budded cells in a given field were analyzed/scored if the bud was in focus using DIC, and the mother cell contained visible mitochondria and vacuoles that were in focus using fluorescence. Mitochondria inheritance was scored in small and medium budded cells according to 4 categories: [I] Mitochondria in the mother cell progressed to the mother bud neck only; [II] A small amount of mitochondria concentrated to the bud tip but not elsewhere in the bud; [III] Mitochondria progressed into the bud, but no more than halfway to the bud tip. [IV] Mitochondria distributed throughout the cortex up to the bud tip. Categories III-IV were scored as wild-type phenotypes. Small bud diameter ≤⅓ the diameter of the mother cell. Medium buds ⅓ to ½ the diameter of the mother cell. Large buds were greater than ½ the diameter of the mother. The large budded cell population included both budded and unbudded cells. The larger diameter cell in large budded cells was assumed to be the

mother. For quantitative fluorescence analysis, the softWoRx Data Inspector tool was used concurrently with the Measure Distance tool. For each channel, individual measurements of bud cell fluorescence were divided by mother cell fluorescence after subtracting background. Background was defined for each cell per channel by measuring detectable fluorescence next to the cell (Waters, 2009).

Live-Cell Time-Lapse Imaging

FM4-64 labeling was modified. Cells were labeled with 125 µg FM4-64 in 3 ml of fresh media for 1 hour. Cells were centrifuged once, supernatant was aspirated completely and cells were resuspended in 5 ml fresh media (without washing). Cells were grown for one doubling period (2-3 hours). Glass bottom chambers (Lab-Tek II; Nalge Nunc International) were treated overnight at 4ºC with concanavlin A dissolved at 1 mg/ml in 50 mM HEPES pH 7.5, 20 mM calcium acetate, 1 mM manganese sulfate, then air dried at least 30 min. Cells adsorbed to concanavalin-A-treated chambers for 2 min. Unbound cells were removed by aspiration and 250 µl fresh media was added. Cells were imaged at 23-24.5°C. Three criteria were applied to the cells imaged. (1) At the start, both organelles were absent from the bud; (2) both organelles were visible in the mother; (3) the cell remained in focus during imaging.

Yeast two-hybrid assays

S. cerevisiae strain PJ69-4A (James *et al.*, 1996) was co-transformed with *LEU2* and *TRP1* plasmids containing the GAL4 transcription factor activation domain (AD) and binding domain (BD), respectively. Colonies were grown for 3-4 days at 24 ºC on

synthetic complete (SC)-leu-trp media and patched onto SC-leu-trp agar plates before replica plating to selection media: SC–leu–trp, SC–leu–trp–ade–his and SC-leu-trp-Ade-his+3AT (3 mM 3-aminotriazole). Plates imaged after 3 to 10 days. Contrast and intensity settings were adjusted in Adobe Photoshop using the same settings for all images from a single experiment.

Western blot

TCA precipitation/NaOH method of protein extraction from whole cells was used. Briefly 4 x 10^8 cells were collected, washed with distilled, deionized H_2O and resuspended in ice cold 0.2 M NaOH. 50 µL of 100% trichloroacetic acid (TCA) was added, the sample centrifuged. 50-200 µL of 2xSDS loading buffer was added to the pellet, which was incubated at 70ºC, 5 min prior to loading on SDS-PAGE. Goat anti-Myo2 antibodies affinity purified and used at 1:1,500. Mouse monoclonal antibodies, anti-GFP (Roche) and anti-HA (Covance) was used at 1:5000 and 1:500, respectively. Mouse monoclonal anti-Pgk1 (Invitrogen) 1:10,000. Mouse anti-V5 antibody (Invitrogen) 1:1,000. Sheep Anti-Vac17 antibody, 1:500 (Tang *et al.*, 2003). HRP-conjugated donkey anti-goat antibody IgG, HRP-conjugated goat anti-sheep antibody IgG, and HRP-conjugated goat anti-mouse IgG (Jackson Immuno Research Laboratories) were used at 1:5,000.

In vitro purification, and binding and competition analysis with size-exclusion chromatography

Plasmids pMBP-Vac17(112-157)p, pMBP-Mmr1(378-430)p and pGST-Myo2(1131-1574)p were transformed into E.coli strain BL21/DE3/STAR and grown to Abs_{600nm} of 1.00 +/- 0.1 at 37ºC in Terrific broth (Invitrogen) containing Ampicillin and Spectinomycin, 100 µg/ml. Cells were cooled for 15 min then incubated at 20ºC for 14 hours in 1 mM isopropyl-β-D-thio-galactoside to induce expression. Cells were harvested at 4ºC. All subsequent steps took place at 0-4ºC. Cells were resuspended in 40 ml lysis buffer containing 20 mM HEPES pH 7.9, 200 mM NaCl, 1 mM EDTA, 0.05% β-mercaptoethanol. Lysis was performed using a probe sonicator with 6-8 repetitions of 10-15 sec, 50% intensity, in the presence of Roche Protease Inhibitor Cocktail (without EDTA; one tablet per 40 ml lysis buffer) and1 µM Pefabloc SC. Lysates were centrifuged at 40,000 rpm for 90 min in a Beckman Ti45 rotor. Lysate supernatants were incubated with the affinity matrix.

For GST-Myo2 CBD: Supernatants incubated with 2.5 ml glutathione sepharose 4B resin (GE Healthcare), 1 hour. GST was cleaved from the Myo2 CBD via incubation with 5 µL biotinylated thrombin (Thrombin Cleavage Capture Kit; Novagen) for 3.5 h in 1.5 ml thrombin buffer. Biotinylated thrombin was removed with streptavidin-linked agarose (Novagen). For MBP-conjugated peptides: Supernatants were incubated with 3.0 ml amylose resin (New England BioLabs), 1 hour. Resin was centrifuged, collected in 10 ml Polyprep columns (Bio-Rad) and washed in lysis buffer. MBP peptides eluted using lysis buffer containing 10 mM maltose.

Myo2 CBD and MBP-peptides were purified on a HiLoad 16/60 Superdex 200 prep-grade exclusion column (GE Healthcare). Purified proteins were analyzed on SDS-(10%) PAGE and visualized with Coomassie. Both BCA (Pierce) and Bradford (Bio-

Rad) assays were used to verify protein concentrations; a BSA standard curve was generated for each analysis. Myo2 CBD and MBP-peptide binding assays and competition assays were performed on a HiLoad 16/60 Superdex 200 analytical column (GE Healthcare).

Visualization of filamentous actin in fixed cells

Actin structures were visualized in fixed cells using rhodamine-phalloidin. Briefly, 5x10^6 cells/ml in log-phase were resuspended in 3.7% formaldehyde (final concentration) and incubated at RT for 10 minutes, washed and resuspended in PBS, pH 7.4 containing 3.7% formaldehyde. Rhodamine-phalloidin (Invitrogen) was dissolved in methonal and100 µl of fixed cells were mixed with 6.1 µM rhodamine-phalloidin (final concentration).

Table 1: Summary of Yeast Two-Hybrid and *In Vivo* Analyses

			Yeast two-hybrid test					*In vivo*	
	Myo2 Residue	Allele	Ypt11	Inp2	Kar9	Vac17	Mmr1	MTO	Viable
1	L1229	*L1229A*				+	+		
		L1229R				-	+		
2	Q1233	*Q1233R*				-	-		
3	K1234	*K1234A*				+	+		
4	T1237	*T1237A*				+	+		
5	G1248	*G1248D*	+	-	-	-	-	-	
6	E1293	*E1293K*				-	-		
7	K1295	*K1295S*				+			
8	D1296	*D1296N*				+	+		
9	D1297	*D1297N*	+	+		-	+		+
		D1297G				-			
10	E1299	*E1299Q*				+	+		
11	A1300	*A1300G*				+	+/-		+
12	L1301	*L1301P*	+	+/-	-	-	-		
		L1301R	+			-	-		
13	S1302	*S1302D*		+	+		+		
14	Y1303	*Y1303A*				-	-		
15	N1304	*N1304S*		+			-		
		N1304D	+	+	+	-	-	+	+
16	N1307	*N1307D*	+	+		-	-		
17	I1308	*I1308A*				+	-		+
18	K1311	*K1311A*				+	+		
19	K1312	*K1312S*				+	-		
		K1312A				+			+
20	L1331	*L1331S*	+/-	+	-	+	+	-	+/-
21	K1408	*K1408A*	+	+	-		+	-	+
22	L1411	*L1411R*	+	-	+		+	+/-	
		L1411S	+/-	+/-	+		+		-
		L1411A	+	-					
23	N1414	*N1414S*	+	+	+		+	+	
24	Y1415	*Y1415E*	-	-	-	+	+	-	-
		Y1415F	+	+	+/-	+	+	-	+
		Y1415R	+/-	-	+/-		+		
25	T1418	*T1418V*	+		+		+	+	
26	E1422	*E1422A*		+	+		+		
27	K1444	*K1444A*	-		+		+	+	-
28	Q1447	*Q1447R*	-		+		+	+	-
29	G1461	*G1461A*					+		
30	Y1464	*Y1464A*					+		
31	V1480	*V1480A*					+		
32	D1482	*D1482N*	+		+		+	+	
33	Y1483	*Y1483E*	+	-	-		+		+
		Y1483A	+	-				-	+
		Y1483R	+	+			+		
34	E1484	*E1484A*	+	+/-	+		+	+	+
		E1484Q	+	+			+		+
35	K1525	*K1525A*			+		+		
36	E1526	*E1526Q*				+			
37	G1528	*G1528A*				+	+		
38	P1529	*P1529A*	+	+	+	+	-		
39	F1334	*F1334A*	+	+	-			-	+
40	W1407	*W1407F*	+	-				-	+
41	R1419	*R1419Q*	+		+			+	
42	I1462	*I1462S*	+		+			+	

43	L1539	*L1539S*				+			

Key:	+	Interaction/WT phenotype
	+/-	Mild interaction/intermediate phenotype
	-	No interaction/mutant phenotype
		Blank = Not tested

MTO = Microtubule orientation ssay

Table 2: Yeast strains used in this thesis

Strain	Genotype	Source
LWY7235	*MAT* a, *ura3-52* , *leu2-3* , *his3-Δ200* , *trp1-Δ901* , *lys2-801* , *suc2-Δ9*	Catlett and Weisman, 1998
LWY2947	*MAT* α, *ura3-52* , *leu2-3* , *his3-Δ200* , *trp1-Δ901* , *lys2-801* , *suc2-Δ9,myo2Δ::TRP1, YCp50-MYO2*	Catlett and Weisman, 1998
PJ69-4A	*MAT* a, *trp1-901, leu2-3, ura3-52, his3-Δ200, Δgal4, Δgal80, LYS2::GAL1-HIS3, GAL2-ADE2, met::GAL7-lacZ*	James *et al* ., 1996
LWY9591	*MAT* a, , *ura3-52* , *leu2-3* , *his3-Δ200* , *trp1-Δ901* , *lys2-801* , *suc2-Δ9, ypt11Δ::KanMX6*	This study
LWY9579	*MAT* a, *ura3-52* , *leu2-3* , *his3-Δ200* , *trp1-Δ901* , *lys2-801* , *suc2-Δ9, mmr1Δ::KanMX6*	This study
LWY8944	*MAT* a, leu2-3,-112, his3-200, trp1-901, lys2-801, suc2-9, GFP-TUB1::URA3:: ura3-52, kar9Δ::kanMX6	Jin *et al* ., 2009
LWY5798	*MAT* a, *ura3-52* , *leu2-3* , *his3-Δ200* , *trp1-Δ901* , *lys2-801* , *suc2-Δ9, vac17Δ::TRP1*	Tang *et al* ., 2003
LWY8897	*MATa, ura3-52, leu2-3, his3-Δ200, trp1-Δ901, lys2-801, suc2-Δ9,GFP-TUB1::URA3*	This study
LWY10127	*MAT* α, *ura3-52* , *leu2-3* , *his3-Δ200* , *trp1-Δ901* , *lys2-801* , *suc2-Δ9,myo2Δ::TRP1, pRS413-MYO2*	This study
LWY10129	*MAT* α, *ura3-52* , *leu2-3* , *his3-Δ200* , *trp1-Δ901* , *lys2-801* , *suc2-Δ9,myo2Δ::TRP1, pRS413-myo2-K1311A*	This study
LWY10131	*MAT* α, *ura3-52* , *leu2-3* , *his3-Δ200* , *trp1-Δ901* , *lys2-801* , *suc2-Δ9,myo2Δ::TRP1, pRS413-myo2-K1234A*	This study
LWY10133	*MAT* α, *ura3-52* , *leu2-3* , *his3-Δ200* , *trp1-Δ901* , *lys2-801* , *suc2-Δ9,myo2Δ::TRP1, pRS413-myo2-P1529A*	This study
LWY10135	*MAT* α, *ura3-52* , *leu2-3* , *his3-Δ200* , *trp1-Δ901* , *lys2-801* , *suc2-Δ9,myo2Δ::TRP1, pRS413-myo2-D1297N*	This study
LWY10137	*MAT* α, *ura3-52* , *leu2-3* , *his3-Δ200* , *trp1-Δ901* , *lys2-801* , *suc2-Δ9,myo2Δ::TRP1, pRS413-myo2-I1308A*	This study
LWY10139	*MAT* α, *ura3-52* , *leu2-3* , *his3-Δ200* , *trp1-Δ901* , *lys2-801* , *suc2-Δ9,myo2Δ::TRP1, pRS413-myo2-L1229A*	This study
LWY10145	*MAT* α, *ura3-52* , *leu2-3* , *his3-Δ200* , *trp1-Δ901* , *lys2-801* , *suc2-Δ9,myo2Δ::TRP1, pRS413-myo2-A1300G*	This study
LWY10155	*MAT* α, *ura3-52* , *leu2-3* , *his3-Δ200* , *trp1-Δ901* , *lys2-801* , *suc2-Δ9,myo2Δ::TRP1, pRS413-myo2-K1312A*	This study
LWY10361	*MAT* α, *ura3-52* , *leu2-3* , *his3-Δ200* , *trp1-Δ901* , *lys2-801* , *suc2-Δ9,myo2Δ::TRP1, pRS413-myo2-N1304D*	This study
LWY10363	*MAT* α, *ura3-52* , *leu2-3* , *his3-Δ200* , *trp1-Δ901* , *lys2-801* , *suc2-Δ9,myo2Δ::TRP1, pRS413-myo2-L1301R*	This study
LWY10365	*MAT* α, *ura3-52* , *leu2-3* , *his3-Δ200* , *trp1-Δ901* , *lys2-801* , *suc2-Δ9,myo2Δ::TRP1, pRS413-myo2-E1293K*	This study

LWY10367	*MAT*α, *ura3-52* , *leu2-3* , *his3-*Δ*200* , *trp1-*Δ*901* , *lys2-801* , *suc2-*Δ*9,myo2*Δ*::TRP1, pRS413-myo2-Y1303E*	This study
LWY10369	*MAT*α, *ura3-52* , *leu2-3* , *his3-*Δ*200* , *trp1-*Δ*901* , *lys2-801* , *suc2-*Δ*9,myo2*Δ*::TRP1, pRS413-myo2-L1229R*	This study
LWY10371	*MAT*α, *ura3-52* , *leu2-3* , *his3-*Δ*200* , *trp1-*Δ*901* , *lys2-801* , *suc2-*Δ*9,myo2*Δ*::TRP1, pRS413-myo2-A1300R*	This study
LWY10976	*MAT*α, *ura3-52* , *leu2-3* , *his3-*Δ*200* , *trp1-*Δ*901* , *lys2-801* , *suc2-*Δ*9,myo2*Δ*::TRP1, pRS413-myo2-Q1447R*	This study
LWY10978	*MAT*α, *ura3-52* , *leu2-3* , *his3-*Δ*200* , *trp1-*Δ*901* , *lys2-801* , *suc2-*Δ*9,myo2*Δ*::TRP1, pRS413-myo2-F1334A*	This study
LWY10980	*MAT*α, *ura3-52* , *leu2-3* , *his3-*Δ*200* , *trp1-*Δ*901* , *lys2-801* , *suc2-*Δ*9,myo2*Δ*::TRP1, pRS413-myo2-L1411S*	This study
LWY10982	*MAT*α, *ura3-52* , *leu2-3* , *his3-*Δ*200* , *trp1-*Δ*901* , *lys2-801* , *suc2-*Δ*9,myo2*Δ*::TRP1, pRS413-myo2-K1408A*	This study
LWY10984	*MAT*α, *ura3-52* , *leu2-3* , *his3-*Δ*200* , *trp1-*Δ*901* , *lys2-801* , *suc2-*Δ*9,myo2*Δ*::TRP1, pRS413-myo2-W1407F*	This study
LWY10986	*MAT*α, *ura3-52* , *leu2-3* , *his3-*Δ*200* , *trp1-*Δ*901* , *lys2-801* , *suc2-*Δ*9,myo2*Δ*::TRP1, pRS413-myo2-Y1484A*	This study
LWY10988	*MAT*α, *ura3-52* , *leu2-3* , *his3-*Δ*200* , *trp1-*Δ*901* , *lys2-801* , *suc2-*Δ*9,* Δ*myo2::TRP1, pRS413-myo2-Y1484Q*	This study
LWY10990	*MAT*α, *ura3-52* , *leu2-3* , *his3-*Δ*200* , *trp1-*Δ*901* , *lys2-801* , *suc2-*Δ*9,myo2*Δ*::TRP1, pRS413-myo2-Y1415F*	This study
LWY10992	*MAT*α, *ura3-52* , *leu2-3* , *his3-*Δ*200* , *trp1-*Δ*901* , *lys2-801* , *suc2-*Δ*9,myo2*Δ*::TRP1, pRS413-myo2-Y1415E*	This study
LWY10994	*MAT*α, *ura3-52* , *leu2-3* , *his3-*Δ*200* , *trp1-*Δ*901* , *lys2-801* , *suc2-*Δ*9,myo2*Δ*::TRP1, pRS413-myo2-K1444A*	This study
LWY10996	*MAT*α, *ura3-52* , *leu2-3* , *his3-*Δ*200* , *trp1-*Δ*901* , *lys2-801* , *suc2-*Δ*9,myo2*Δ*::TRP1, pRS413-myo2-L1331S*	This study
LWY10998	*MAT*α, *ura3-52* , *leu2-3* , *his3-*Δ*200* , *trp1-*Δ*901* , *lys2-801* , *suc2-*Δ*9,myo2*Δ*::TRP1, pRS413-myo2-Y1483A*	This study
LWY11000	*MAT*α, *ura3-52* , *leu2-3* , *his3-*Δ*200* , *trp1-*Δ*901* , *lys2-801* , *suc2-*Δ*9,myo2*Δ*::TRP1, pRS413-myo2-Y1483E*	This study
LWY11140	*MAT*α, *ura3-52* , *leu2-3* , *his3-*Δ*200* , *trp1-*Δ*901* , *lys2-801* , *suc2-*Δ*9, MMR1-GFP::HIS3,* Δ*myo2::TRP1, pRS413-MYO2*	This study
LWY11141	*MAT*α, *ura3-52* , *leu2-3* , *his3-*Δ*200* , *trp1-*Δ*901* , *lys2-801* , *suc2-*Δ*9, MMR1-GFP::HIS3,* Δ*myo2::TRP1, pRS413-myo2-D1297N*	This study
LWY11142	*MAT*α, *ura3-52* , *leu2-3* , *his3-*Δ*200* , *trp1-*Δ*901* , *lys2-801* , *suc2-*Δ*9, MMR1-GFP::HIS3,* Δ*myo2::TRP1, pRS413-myo2-L1301R*	This study
LWY11143	*MAT*α, *ura3-52* , *leu2-3* , *his3-*Δ*200* , *trp1-*Δ*901* , *lys2-801* , *suc2-*Δ*9, MMR1-GFP::HIS3,* Δ*myo2::TRP1, pRS413-myo2-I1308A*	This study
LWY11144	*MAT*α, *ura3-52* , *leu2-3* , *his3-*Δ*200* , *trp1-*Δ*901* , *lys2-801* , *suc2-*Δ*9, MMR1-GFP::HIS3,* Δ*myo2::TRP1, pRS413-myo2-K1312A*	This study

LWY11145	*MAT* α, *ura3-52* , *leu2-3* , *his3-Δ200* , *trp1-Δ901* , *lys2-801* , *suc2-Δ9, MMR1-GFP::HIS3, Δmyo2::TRP1, pRS413-myo2-N1304D*	This study
LWY8737	*MAT* a, *ura3-52* , *leu2-3* , *his3-Δ200* , *trp1-Δ901* , *lys2-801* , *suc2-Δ9, VAC17-3xGFP::TRP1*	Jin *et al* ., 2009
LWY8867	*MAT* a, *ura3-52* , *leu2-3* , *his3-Δ200* , *trp1-Δ901* , *lys2-801* , *suc2-Δ9, MMR1-GFP::HIS3*	This study
LWY11413	*MAT* a, *ura3-52* , *leu2-3* , *his3-Δ200* , *trp1-Δ901* , *lys2-801* , *suc2-Δ9, VAC17-3xGFP::TRP1, myo2Δ::TRP1, pRS413-MYO2*	This study
LWY11414	*MAT* a, *ura3-52* , *leu2-3* , *his3-Δ200* , *trp1-Δ901* , *lys2-801* , *suc2-Δ9, VAC17-3xGFP::TRP1, myo2Δ::TRP1, pRS413-myo2-D1297N*	This study
LWY11415	*MAT* a, *ura3-52* , *leu2-3* , *his3-Δ200* , *trp1-Δ901* , *lys2-801* , *suc2-Δ9, VAC17-3xGFP::TRP1, myo2Δ::TRP1, pRS413-myo2-L1301R*	This study
LWY11416	*MAT* a, *ura3-52* , *leu2-3* , *his3-Δ200* , *trp1-Δ901* , *lys2-801* , *suc2-Δ9, VAC17-3xGFP::TRP1, myo2Δ::TRP1, pRS413-myo2-N1304D*	This study
LWY11417	*MAT* a, *ura3-52* , *leu2-3* , *his3-Δ200* , *trp1-Δ901* , *lys2-801* , *suc2-Δ9, VAC17-3xGFP::TRP1, myo2Δ::TRP1, pRS413-myo2-I1308A*	This study
LWY11418	*MAT* a, *ura3-52* , *leu2-3* , *his3-Δ200* , *trp1-Δ901* , *lys2-801* , *suc2-Δ9, VAC17-3xGFP::TRP1, myo2Δ::TRP1, pRS413-myo2-K1312A*	This study

Table 3: Plasmids used in this thesis

Plasmid	Description	Source
pRS413-MYO2	CEN, HIS3	Catlett and Weisman, 1998
pRS413-*myo2*-Q1447R	CEN, HIS3	Pashkova *et al*., 2006
pRS413-*myo2*-F1334A	CEN, HIS3	This study
pRS413-*myo2*-L1411S	CEN, HIS3	Pashkova *et al*., 2006
pRS413-*myo2*-K1408A	CEN, HIS3	This study
pRS413-*myo2*-W1407F	CEN, HIS3	Pashkova *et al*., 2006
pRS413-*myo2*-Y1484A	CEN, HIS3	This study
pRS413-*myo2*-Y1484Q	CEN, HIS3	This study
pRS413-*myo2*-Y1415E	CEN, HIS3	Pashkova *et al*., 2006
pRS413-*myo2*-Y1415F	CEN, HIS3	This study
pRS413-*myo2*-Y1415R	CEN, HIS3	Pashkova *et al*., 2006
pRS413-*myo2*-K1444A	CEN, HIS3	Pashkova *et al*., 2006
pRS413-*myo2*-L1331S	CEN, HIS3	Pashkova *et al*., 2006
pRS413-*myo2*-Y1483A	CEN, HIS3	Fagarasanu *et al*., 2009
pRS413-*myo2*-Y1483E	CEN, HIS3	This study
pRS413-*myo2*-E1293K	CEN, HIS3	This study
pRS413-*myo2*-Q1233R	CEN, HIS3	Pashkova *et al*., 2006
pRS413-*myo2*-L1229A	CEN, HIS3	This study
pRS413-*myo2*-L1229R	CEN, HIS3	This study
pRS413-*myo2*-D1297N	CEN, HIS3	Ishikawa *et al*., 2003
pRS413-*myo2*-L1301R	CEN, HIS3	This study
pRS413-*myo2*-Y1303A	CEN, HIS3	This study
pRS413-*myo2*-N1304D	CEN, HIS3	This study
pRS413-*myo2*-N1307D	CEN, HIS3	This study
pRS413-*myo2*-I1308A	CEN, HIS3	This study
pRS413-*myo2*-K1312A	CEN, HIS3	This study
pGAD-C1	2µ, LEU2	James *et al*., 1996
pGAD-C1-MYO2	2µ, LEU2	Pashkova *et al*., 2005
pGAD-C1-*myo2*-G1248D	*myo2-2,* 2µ, LEU2	Ishikawa *et al*., 2003
pGAD-C1-*myo2*-L1331S	2µ, LEU2	This study
pGAD-C1-*myo2*-F1334A	2µ, LEU2	This study
pGAD-C1-*myo2*-W1407F	2µ, LEU2	This study
pGAD-C1-*myo2*-K1408A	2µ, LEU2	This study
pGAD-C1-*myo2*-L1411A	2µ, LEU2	This study
pGAD-C1-*myo2*-L1411R	2µ, LEU2	This study
pGAD-C1-*myo2*-L1411S	2µ, LEU2	This study
pGAD-C1-*myo2*-N1414S	2µ, LEU2	This study
pGAD-C1-*myo2*-Y1415E	2µ, LEU2	This study
pGAD-C1-*myo2*-Y1415F	2µ, LEU2	This study
pGAD-C1-*myo2*-Y1415R	2µ, LEU2	This study
pGAD-C1-*myo2*-T1418V	2µ, LEU2	This study
pGAD-C1-*myo2*-R1419Q	2µ, LEU2	This study
pGAD-C1-*myo2*-K1444A	2µ, LEU2	This study
pGAD-C1-*myo2*-Q1447R	2µ, LEU2	This study

pGAD-C1-*myo2*-I1462S	2μ, LEU2	This study
pGAD-C1-*myo2*-D1482N	2μ, LEU2	This study
pGAD-C1-*myo2*-Y1483A	2μ, LEU2	This study
pGAD-C1-*myo2*-Y1483E	2μ, LEU2	This study
pGAD-C1-*myo2*-Y1483R	2μ, LEU2	This study
pGAD-C1-*myo2*-E1484A	2μ, LEU2	This study
pGAD-C1-*myo2*-E1484Q	2μ, LEU2	This study
pGAD-C1-*myo2*-L1229A	2μ, LEU2	This study
pGAD-C1-*myo2*-L1229R	2μ, LEU2	This study
pGAD-C1-*myo2*-Q1233R	2μ, LEU2	This study
pGAD-C1-*myo2*-K1234A	2μ, LEU2	This study
pGAD-C1-*myo2*-T1237A	2μ, LEU2	This study
pGAD-C1-*myo2*-E1293K	2μ, LEU2	This study
pGAD-C1-*myo2*-D1296N	2μ, LEU2	This study
pGAD-C1-*myo2*-D1297N	2μ, LEU2	Ishikawa *et al*., 2003
pGAD-C1-*myo2*-E1299Q	2μ, LEU2	This study
pGAD-C1-*myo2*-A1300G	2μ, LEU2	This study
pGAD-C1-*myo2*-L1301P	2μ, LEU2	Ishikawa *et al*., 2003
pGAD-C1-*myo2*-L1301R	2μ, LEU2	This study
pGAD-C1-*myo2*-Y1303A	2μ, LEU2	This study
pGAD-C1-*myo2*-N1304D	2μ, LEU2	Ishikawa *et al*., 2003
pGAD-C1-*myo2*-N1304S	2μ, LEU2	Ishikawa *et al*., 2003
pGAD-C1-*myo2*-N1307D	2μ, LEU2	This study
pGAD-C1-*myo2*-I1308A	2μ, LEU2	This study
pGAD-C1-*myo2*-K1311A	2μ, LEU2	This study
pGAD-C1-*myo2*-K1312A	2μ, LEU2	This study
pGAD-C1-*myo2*-G1528A	2μ, LEU2	This study
pGAD-C1-*myo2*-P1529A	2μ, LEU2	This study
pGAD-C1-*myo2*-P1529S	2μ, LEU2	This study
pGAD-C1-*myo2*-V1189A	2μ, LEU2	This study
pGAD-C1-*myo2*-V1288G	2μ, LEU2	This study
pGAD-C1-*myo2*-K1500M	2μ, LEU2	This study
pGAD-C1-*myo2*-E1546G	2μ, LEU2	This study
pGAD-C1-*myo2*-K1559R	2μ, LEU2	This study
pGBD-C1-MMR1	2μ, TRP1	This study
pGBD-C1-VAC17	2μ, TRP1	Ishikawa *et al*., 2003
pGBD-C1-KAR9	2μ, TRP1	Pashkova *et al*., 2005
pGBD-C1-YPT11	2μ, TRP1	This study
pGBD-C1-INP2	2μ, TRP1	Fagarasanu *et al*., 2009
pGBD-C1-SMY1	2μ, TRP1	Pashkova *et al*., 2005
pGBD-C1-Mmr1(398-430)	2μ, TRP1	This study
pGBD-C1-Mmr1(398-441)	2μ, TRP1	This study
pGBD-C1-Mmr1(387-430)	2μ, TRP1	This study
pGBD-C1-Mmr1(387-441)	2μ, TRP1	This study
pGBD-C1-Mmr1(378-430)	2μ, TRP1	This study
pGBD-C1-Mmr1(378-441)	2μ, TRP1	This study
pGBD-C1-Vac17(68-195)	2μ, TRP1	This study

pGBD-C1-Vac17(158-195)	2μ, TRP1	This study
pRS416	CEN, URA3	Sikorski and Hieter, 1989
pRS416-MMR1-V5	CEN, URA3	This study
pVT102-MMR1-V5	2μ, URA3	This study
pmitoGFP	CEN, LEU2	Frederick *et al* ., 2008
pmitoRFP	CEN, URA3	Frederick *et al* ., 2008
pRS416-VAC17	CEN, URA3	Tang *et al* ., 2003
pVT102-VAC17	2μ, URA3	This study
pMBP-Parallel-1	Amp^r	Sheffield *et al.,* 1999
pMBP-Vac17(112-157)p	Amp^r	This study
pMBP-Mmr1(378-430)p	Amp^r	This study
pGST-Myo2(1131-1574)p	Amp^r	Pashkova *et al* ., 2006
pUC19-TUB1-GFP	CEN, LEU2	Song and Lee, 2001

REFERENCES

Altmann, K., M. Frank, et al. (2008). "The class V myosin motor protein, Myo2, plays a major role in mitochondrial motility in Saccharomyces cerevisiae." J Cell Biol **181**(1): 119-130.

Amon, A. (1999). "The spindle checkpoint." Curr Opin Genet Dev **9**(1): 69-75.

Arai, S., Y. Noda, et al. (2008). "Ypt11 functions in bud-directed transport of the Golgi by linking Myo2 to the coatomer subunit Ret2." Curr Biol **18**(13): 987-991.

Armstrong, J. (2010). "Yeast vacuoles: more than a model lysosome." Trends Cell Biol **20**(10): 580-585.

Ayscough, K. R., J. Stryker, et al. (1997). "High rates of actin filament turnover in budding yeast and roles for actin in establishment and maintenance of cell polarity revealed using the actin inhibitor latrunculin-A." J Cell Biol **137**(2): 399-416.

Babour, A., A. A. Bicknell, et al. (2010). "A surveillance pathway monitors the fitness of the endoplasmic reticulum to control its inheritance." Cell **142**(2): 256-269.

Beach, D. L., J. Thibodeaux, et al. (2000). "The role of the proteins Kar9 and Myo2 in orienting the mitotic spindle of budding yeast." Curr Biol **10**(23): 1497-1506.

Beningo, K. A., S. H. Lillie, et al. (2000). "The yeast kinesin-related protein Smy1p exerts its effects on the class V myosin Myo2p via a physical interaction." Mol Biol Cell **11**(2): 691-702.

Blasius, T. L., D. Cai, et al. (2007). "Two binding partners cooperate to activate the

molecular motor Kinesin-1." J Cell Biol **176**(1): 11-17.

Blazer, L. L., D. L. Roman, et al. (2010). "Use of flow cytometric methods to quantify protein-protein interactions." Curr Protoc Cytom **Chapter 13**: Unit 13 11 11-15.

Boldogh, I. R., S. L. Ramcharan, et al. (2004). "A type V myosin (Myo2p) and a Rab-like G-protein (Ypt11p) are required for retention of newly inherited mitochondria in yeast cells during cell division." Mol Biol Cell **15**(9): 3994-4002.

Boldogh, I. R., H. C. Yang, et al. (2001). "Arp2/3 complex and actin dynamics are required for actin-based mitochondrial motility in yeast." Proc Natl Acad Sci U S A **98**(6): 3162-3167.

Bu, Z. and D. J. Callaway (2011). "Proteins move! Protein dynamics and long-range allostery in cell signaling." Adv Protein Chem Struct Biol **83**: 163-221.

Buvelot Frei, S., P. B. Rahl, et al. (2006). "Bioinformatic and comparative localization of Rab proteins reveals functional insights into the uncharacterized GTPases Ypt10p and Ypt11p." Mol Cell Biol **26**(19): 7299-7317.

Byrd, D. T., M. Kawasaki, et al. (2001). "UNC-16, a JNK-signaling scaffold protein, regulates vesicle transport in C. elegans." Neuron **32**(5): 787-800.

Catlett, N. L., J. E. Duex, et al. (2000). "Two distinct regions in a yeast myosin-V tail domain are required for the movement of different cargoes." J Cell Biol **150**(3): 513-526.

Catlett, N. L. and L. S. Weisman (1998). "The terminal tail region of a yeast myosin-V mediates its attachment to vacuole membranes and sites of polarized growth." Proc Natl Acad Sci U S A **95**(25): 14799-14804.

Catlett, N. L. and L. S. Weisman (2000). "Divide and multiply: organelle partitioning in

yeast." Curr Opin Cell Biol **12**(4): 509-516.

Chang, J., A. Fagarasanu, et al. (2007). "Peroxisomal peripheral membrane protein YlInp1p is required for peroxisome inheritance and influences the dimorphic transition in the yeast Yarrowia lipolytica." Eukaryot Cell **6**(9): 1528-1537.

Chang, J., F. D. Mast, et al. (2009). "Pex3 peroxisome biogenesis proteins function in peroxisome inheritance as class V myosin receptors." J Cell Biol **187**(2): 233-246.

Chang, W., R. F. Zaarour, et al. (2008). "Myo2p, a class V myosin in budding yeast, associates with a large ribonucleic acid-protein complex that contains mRNAs and subunits of the RNA-processing body." RNA **14**(3): 491-502.

Cheney, R. E. and O. C. Rodriguez (2001). "Cell biology. A switch to release the motor." Science **293**(5533): 1263-1264.

Colanzi, A., C. Hidalgo Carcedo, et al. (2007). "The Golgi mitotic checkpoint is controlled by BARS-dependent fission of the Golgi ribbon into separate stacks in G2." EMBO J **26**(10): 2465-2476.

Coy, D. L., M. Wagenbach, et al. (1999). "Kinesin takes one 8-nm step for each ATP that it hydrolyzes." J Biol Chem **274**(6): 3667-3671.

De La Cruz, E. M., A. L. Wells, et al. (2000). "Actin and light chain isoform dependence of myosin V kinetics." Biochemistry **39**(46): 14196-14202.

Diaz, F. and C. T. Moraes (2008). "Mitochondrial biogenesis and turnover." Cell Calcium **44**(1): 24-35.

Dove, S. K., R. C. Piper, et al. (2004). "Svp1p defines a family of phosphatidylinositol 3,5-bisphosphate effectors." EMBO J **23**(9): 1922-1933.

Du, Y., S. Ferro-Novick, et al. (2004). "Dynamics and inheritance of the endoplasmic

reticulum." J Cell Sci **117**(Pt 14): 2871-2878.

Duex, J. E., J. J. Nau, et al. (2006). "Phosphoinositide 5-phosphatase Fig 4p is required for both acute rise and subsequent fall in stress-induced phosphatidylinositol 3,5-bisphosphate levels." Eukaryot Cell **5**(4): 723-731.

Duex, J. E., F. Tang, et al. (2006). "The Vac14p-Fig4p complex acts independently of Vac7p and couples PI3,5P2 synthesis and turnover." J Cell Biol **172**(5): 693-704.

Dunn, B. D., T. Sakamoto, et al. (2007). "Myo4p is a monomeric myosin with motility uniquely adapted to transport mRNA." J Cell Biol **178**(7): 1193-1206.

Efe, J. A., R. J. Botelho, et al. (2007). "Atg18 regulates organelle morphology and Fab1 kinase activity independent of its membrane recruitment by phosphatidylinositol 3,5-bisphosphate." Mol Biol Cell **18**(11): 4232-4244.

Ernst, R., J. H. Claessen, et al. (2011). "Enzymatic blockade of the ubiquitin-proteasome pathway." PLoS Biol **8**(3): e1000605.

Eshel, D., L. A. Urrestarazu, et al. (1993). "Cytoplasmic dynein is required for normal nuclear segregation in yeast." Proc Natl Acad Sci U S A **90**(23): 11172-11176.

Estrada de Martin, P., P. Novick, et al. (2005). "The organization, structure, and inheritance of the ER in higher and lower eukaryotes." Biochem Cell Biol **83**(6): 752-761.

Fagarasanu, A., M. Fagarasanu, et al. (2006). "The peroxisomal membrane protein Inp2p is the peroxisome-specific receptor for the myosin V motor Myo2p of Saccharomyces cerevisiae." Dev Cell **10**(5): 587-600.

Fagarasanu, A., M. Fagarasanu, et al. (2007). "Maintaining peroxisome populations: a story of division and inheritance." Annu Rev Cell Dev Biol **23**: 321-344.

Fagarasanu, A., F. D. Mast, et al. (2009). "Myosin-driven peroxisome partitioning in S. cerevisiae." J Cell Biol **186**(4): 541-554.

Fagarasanu, A., F. D. Mast, et al. (2010). "Molecular mechanisms of organelle inheritance: lessons from peroxisomes in yeast." Nat Rev Mol Cell Biol **11**(9): 644-654.

Fagarasanu, A. and R. A. Rachubinski (2007). "Orchestrating organelle inheritance in Saccharomyces cerevisiae." Curr Opin Microbiol **10**(6): 528-538.

Fortsch, J., E. Hummel, et al. (2011). "The myosin-related motor protein Myo2 is an essential mediator of bud-directed mitochondrial movement in yeast." J Cell Biol **194**(3): 473-488.

Foth, B. J., M. C. Goedecke, et al. (2006). "New insights into myosin evolution and classification." Proc Natl Acad Sci U S A **103**(10): 3681-3686.

Frederick, R. L., K. Okamoto, et al. (2008). "Multiple pathways influence mitochondrial inheritance in budding yeast." Genetics **178**(2): 825-837.

Garcia-Rodriguez, L. J., D. G. Crider, et al. (2009). "Mitochondrial inheritance is required for MEN-regulated cytokinesis in budding yeast." Curr Biol **19**(20): 1730-1735.

Georgakopoulos, T., G. Koutroubas, et al. (2001). "Functional analysis of the Saccharomyces cerevisiae YFR021w/YGR223c/YPL100w ORF family suggests relations to mitochondrial/peroxisomal functions and amino acid signalling pathways." Yeast **18**(12): 1155-1171.

Grava, S., F. Schaerer, et al. (2006). "Asymmetric recruitment of dynein to spindle poles and microtubules promotes proper spindle orientation in yeast." Dev Cell **10**(4):

425-439.

Grosshans, B. L., D. Ortiz, et al. (2006). "Rabs and their effectors: achieving specificity in membrane traffic." Proc Natl Acad Sci U S A **103**(32): 11821-11827.

Haken, H. (1983). Advanced synergetics : instability hierarchies of self-organizing systems and devices. Berlin ; New York, Springer-Verlag.

Hakimi, M. A., D. W. Speicher, et al. (2002). "The motor protein kinesin-1 links neurofibromin and merlin in a common cellular pathway of neurofibromatosis." J Biol Chem **277**(40): 36909-36912.

Hammer, J. A., 3rd and J. R. Sellers (2012). "Walking to work: roles for class V myosins as cargo transporters." Nat Rev Mol Cell Biol **13**(1): 13-26.

Hetzer, M. W. (2010). "The nuclear envelope." Cold Spring Harb Perspect Biol **2**(3): a000539.

Hetzer, M. W. (2010). "The role of the nuclear pore complex in aging of post-mitotic cells." Aging (Albany NY) **2**(2): 74-75.

Heuck, A., T. G. Du, et al. (2007). "Monomeric myosin V uses two binding regions for the assembly of stable translocation complexes." Proc Natl Acad Sci U S A **104**(50): 19778-19783.

Heuck, A., I. Fetka, et al. (2010). "The structure of the Myo4p globular tail and its function in ASH1 mRNA localization." J Cell Biol **189**(3): 497-510.

Hill, K. L., N. L. Catlett, et al. (1996). "Actin and myosin function in directed vacuole movement during cell division in Saccharomyces cerevisiae." J Cell Biol **135**(6 Pt 1): 1535-1549.

Hirokawa, N. and R. Takemura (2005). "Molecular motors and mechanisms of

directional transport in neurons." Nat Rev Neurosci **6**(3): 201-214.

Hodges, A. R., C. S. Bookwalter, et al. (2009). "A nonprocessive class V myosin drives cargo processively when a kinesin- related protein is a passenger." Curr Biol **19**(24): 2121-2125.

Hou, J. C., L. Min, et al. (2009). "Insulin granule biogenesis, trafficking and exocytosis." Vitam Horm **80**: 473-506.

Houdusse, A., J. F. Gaucher, et al. (2006). "Crystal structure of apo-calmodulin bound to the first two IQ motifs of myosin V reveals essential recognition features." Proc Natl Acad Sci U S A **103**(51): 19326-19331.

Huh, W. K., J. V. Falvo, et al. (2003). "Global analysis of protein localization in budding yeast." Nature **425**(6959): 686-691.

Hutchins, M. U., M. Veenhuis, et al. (1999). "Peroxisome degradation in Saccharomyces cerevisiae is dependent on machinery of macroautophagy and the Cvt pathway." J Cell Sci **112 (Pt 22)**: 4079-4087.

Ishikawa, K., N. L. Catlett, et al. (2003). "Identification of an organelle-specific myosin V receptor." J Cell Biol **160**(6): 887-897.

Itoh, T., E. A. Toh, et al. (2004). "Mmr1p is a mitochondrial factor for Myo2p-dependent inheritance of mitochondria in the budding yeast." EMBO J **23**(13): 2520-2530.

Itoh, T., A. Watabe, et al. (2002). "Complex formation with Ypt11p, a rab-type small GTPase, is essential to facilitate the function of Myo2p, a class V myosin, in mitochondrial distribution in Saccharomyces cerevisiae." Mol Cell Biol **22**(22): 7744-7757.

James, P., J. Halladay, et al. (1996). "Genomic libraries and a host strain designed for

highly efficient two-hybrid selection in yeast." Genetics **144**(4): 1425-1436.

Jeffries, T. R., S. K. Dove, et al. (2004). "PtdIns-specific MPR pathway association of a novel WD40 repeat protein, WIPI49." Mol Biol Cell **15**(6): 2652-2663.

Jin, Y., A. Sultana, et al. (2011). "Myosin V transports secretory vesicles via a Rab GTPase cascade and interaction with the exocyst complex." Dev Cell **21**(6): 1156-1170.

Jin, Y., P. Taylor Eves, et al. (2009). "PTC1 is required for vacuole inheritance and promotes the association of the myosin-V vacuole-specific receptor complex." Mol Biol Cell **20**(5): 1312-1323.

Johnston, G. C., J. A. Prendergast, et al. (1991). "The Saccharomyces cerevisiae MYO2 gene encodes an essential myosin for vectorial transport of vesicles." J Cell Biol **113**(3): 539-551.

Kaiser, P., W. Seufert, et al. (1994). "A human ubiquitin-conjugating enzyme homologous to yeast UBC8." J Biol Chem **269**(12): 8797-8802.

Kamal, A., G. B. Stokin, et al. (2000). "Axonal transport of amyloid precursor protein is mediated by direct binding to the kinesin light chain subunit of kinesin-I." Neuron **28**(2): 449-459.

Kanai, Y., N. Dohmae, et al. (2004). "Kinesin transports RNA: isolation and characterization of an RNA-transporting granule." Neuron **43**(4): 513-525.

Karcher, R. L., J. T. Roland, et al. (2001). "Cell cycle regulation of myosin-V by calcium/calmodulin-dependent protein kinase II." Science **293**(5533): 1317-1320.

Kindt, T. J., R. A. Goldsby, et al. (2007). Kuby immunology. New York, W.H. Freeman.

Kirwan, J. P., S. C. Kwok, et al. (2009). "Unique role of clusters of electrostatic

attractions in controlling the stability of two-stranded alpha-helical coiled-coils." Adv Exp Med Biol **611**: 77-78.

Korinek, W. S., M. J. Copeland, et al. (2000). "Molecular linkage underlying microtubule orientation toward cortical sites in yeast." Science **287**(5461): 2257-2259.

Kornmann, B., E. Currie, et al. (2009). "An ER-mitochondria tethering complex revealed by a synthetic biology screen." Science **325**(5939): 477-481.

Kornmann, B., C. Osman, et al. (2011). "The conserved GTPase Gem1 regulates endoplasmic reticulum-mitochondria connections." Proc Natl Acad Sci U S A **108**(34): 14151-14156.

Kornmann, B. and P. Walter (2010). "ERMES-mediated ER-mitochondria contacts: molecular hubs for the regulation of mitochondrial biology." J Cell Sci **123**(Pt 9): 1389-1393.

Krementsova, E. B., A. R. Hodges, et al. (2011). "Two single-headed myosin V motors bound to a tetrameric adapter protein form a processive complex." J Cell Biol **195**(4): 631-641.

Kurihara, L. J., C. T. Beh, et al. (1994). "Nuclear congression and membrane fusion: two distinct events in the yeast karyogamy pathway." J Cell Biol **126**(4): 911-923.

Lee, L., J. S. Tirnauer, et al. (2000). "Positioning of the mitotic spindle by a cortical-microtubule capture mechanism." Science **287**(5461): 2260-2262.

Legesse-Miller, A., S. Zhang, et al. (2006). "Regulated phosphorylation of budding yeast's essential myosin V heavy chain, Myo2p." Mol Biol Cell **17**(4): 1812-1821.

Leisner, C., D. Kammerer, et al. (2008). "Regulation of mitotic spindle asymmetry by SUMO and the spindle-assembly checkpoint in yeast." Curr Biol **18**(16):

1249-1255.

Lillie, S. H. and S. S. Brown (1998). "Smy1p, a kinesin-related protein that does not require microtubules." J Cell Biol **140**(4): 873-883.

Lipatova, Z., A. A. Tokarev, et al. (2008). "Direct interaction between a myosin V motor and the Rab GTPases Ypt31/32 is required for polarized secretion." Mol Biol Cell **19**(10): 4177-4187.

Liu, J., D. W. Taylor, et al. (2006). "Three-dimensional structure of the myosin V inhibited state by cryoelectron tomography." Nature **442**(7099): 208-211.

Longtine, M. S., A. McKenzie, 3rd, et al. (1998). "Additional modules for versatile and economical PCR-based gene deletion and modification in Saccharomyces cerevisiae." Yeast **14**(10): 953-961.

Lowe, M. and F. A. Barr (2007). "Inheritance and biogenesis of organelles in the secretory pathway." Nat Rev Mol Cell Biol **8**(6): 429-439.

Mast, F. D., A. Fagarasanu, et al. (2010). "Peroxisome biogenesis: something old, something new, something borrowed." Physiology (Bethesda) **25**(6): 347-356.

Meednu, N., H. Hoops, et al. (2008). "The spindle positioning protein Kar9p interacts with the sumoylation machinery in Saccharomyces cerevisiae." Genetics **180**(4): 2033-2055.

Menetrey, J., A. Bahloul, et al. (2005). "The structure of the myosin VI motor reveals the mechanism of directionality reversal." Nature **435**(7043): 779-785.

Merlini, L. and S. Piatti (2011). "The mother-bud neck as a signaling platform for the coordination between spindle position and cytokinesis in budding yeast." Biol Chem **392**(8-9): 805-812.

Miller, R. K., S. C. Cheng, et al. (2000). "Bim1p/Yeb1p mediates the Kar9p-dependent cortical attachment of cytoplasmic microtubules." Mol Biol Cell **11**(9): 2949-2959.

Moore, J. K. and R. K. Miller (2007). "The cyclin-dependent kinase Cdc28p regulates multiple aspects of Kar9p function in yeast." Mol Biol Cell **18**(4): 1187-1202.

Moseley, J. B. and B. L. Goode (2006). "The yeast actin cytoskeleton: from cellular function to biochemical mechanism." Microbiol Mol Biol Rev **70**(3): 605-645.

Munson, M. and P. Novick (2006). "The exocyst defrocked, a framework of rods revealed." Nat Struct Mol Biol **13**(7): 577-581.

Neumuller, R. A. and J. A. Knoblich (2009). "Dividing cellular asymmetry: asymmetric cell division and its implications for stem cells and cancer." Genes Dev **23**(23): 2675-2699.

Pashkova, N., N. L. Catlett, et al. (2005). "A point mutation in the cargo-binding domain of myosin V affects its interaction with multiple cargoes." Eukaryot Cell **4**(4): 787-798.

Pashkova, N., N. L. Catlett, et al. (2005). "Myosin V attachment to cargo requires the tight association of two functional subdomains." J Cell Biol **168**(3): 359-364.

Pashkova, N., Y. Jin, et al. (2006). "Structural basis for myosin V discrimination between distinct cargoes." EMBO J **25**(4): 693-700.

Peng, Y., F. Tang, et al. (2006). "Palmitoylation plays a role in targeting Vac8p to specific membrane subdomains." Traffic **7**(10): 1378-1387.

Peng, Y. and L. S. Weisman (2008). "The cyclin-dependent kinase Cdk1 directly regulates vacuole inheritance." Dev Cell **15**(3): 478-485.

Peraza-Reyes, L., D. G. Crider, et al. (2010). "Mitochondrial manoeuvres: latest insights and hypotheses on mitochondrial partitioning during mitosis in Saccharomyces cerevisiae." Bioessays **32**(12): 1040-1049.

Prendergast, J. A., L. E. Murray, et al. (1990). "Size selection identifies new genes that regulate Saccharomyces cerevisiae cell proliferation." Genetics **124**(1): 81-90.

Pruyne, D. and A. Bretscher (2000). "Polarization of cell growth in yeast." J Cell Sci **113 (Pt 4)**: 571-585.

Pruyne, D., L. Gao, et al. (2004). "Stable and dynamic axes of polarity use distinct formin isoforms in budding yeast." Mol Biol Cell **15**(11): 4971-4989.

Pruyne, D., A. Legesse-Miller, et al. (2004). "Mechanisms of polarized growth and organelle segregation in yeast." Annu Rev Cell Dev Biol **20**: 559-591.

Rechsteiner, M. and S. W. Rogers (1996). "PEST sequences and regulation by proteolysis." Trends Biochem Sci **21**(7): 267-271.

Reck-Peterson, S. L., M. J. Tyska, et al. (2001). "The yeast class V myosins, Myo2p and Myo4p, are nonprocessive actin-based motors." J Cell Biol **153**(5): 1121-1126.

Richards, T. A. and T. Cavalier-Smith (2005). "Myosin domain evolution and the primary divergence of eukaryotes." Nature **436**(7054): 1113-1118.

Rietdorf, J., A. Ploubidou, et al. (2001). "Kinesin-dependent movement on microtubules precedes actin-based motility of vaccinia virus." Nat Cell Biol **3**(11): 992-1000.

Rodriguez, O. C. and R. E. Cheney (2000). "A new direction for myosin." Trends Cell Biol **10**(8): 307-311.

Rodriguez, O. C. and R. E. Cheney (2002). "Human myosin-Vc is a novel class V myosin expressed in epithelial cells." J Cell Sci **115**(Pt 5): 991-1004.

Rogers, S. L., R. L. Karcher, et al. (1999). "Regulation of melanosome movement in the cell cycle by reversible association with myosin V." J Cell Biol **146**(6): 1265-1276.

Rossanese, O. W. and B. S. Glick (2001). "Deconstructing Golgi inheritance." Traffic **2**(9): 589-596.

Rossanese, O. W., C. A. Reinke, et al. (2001). "A role for actin, Cdc1p, and Myo2p in the inheritance of late Golgi elements in Saccharomyces cerevisiae." J Cell Biol **153**(1): 47-62.

Santiago-Tirado, F. H., A. Legesse-Miller, et al. (2011). "PI4P and Rab inputs collaborate in myosin-V-dependent transport of secretory compartments in yeast." Dev Cell **20**(1): 47-59.

Schliwa, M. and G. Woehlke (2003). "Molecular motors." Nature **422**(6933): 759-765.

Schott, D. H., R. N. Collins, et al. (2002). "Secretory vesicle transport velocity in living cells depends on the myosin-V lever arm length." J Cell Biol **156**(1): 35-39.

Segev, N. (2001). "Ypt and Rab GTPases: insight into functions through novel interactions." Curr Opin Cell Biol **13**(4): 500-511.

Segev, N. (2001). "Ypt/rab gtpases: regulators of protein trafficking." Sci STKE **2001**(100): re11.

Setou, M., D. H. Seog, et al. (2002). "Glutamate-receptor-interacting protein GRIP1 directly steers kinesin to dendrites." Nature **417**(6884): 83-87.

Sheltzer, J. M. and M. D. Rose (2009). "The class V myosin Myo2p is required for Fus2p transport and actin polarization during the yeast mating response." Mol Biol Cell **20**(12): 2909-2919.

Shepard, K. A., A. P. Gerber, et al. (2003). "Widespread cytoplasmic mRNA transport in yeast: identification of 22 bud-localized transcripts using DNA microarray analysis." Proc Natl Acad Sci U S A **100**(20): 11429-11434.

Shimizu, H. and H. Haken (1983). "Co-operative dynamics in organelles." J Theor Biol **104**(2): 261-273.

Swayne, T. C., C. Zhou, et al. (2011). "Role for cER and Mmr1p in anchorage of mitochondria at sites of polarized surface growth in budding yeast." Curr Biol **21**(23): 1994-1999.

Tang, F., E. J. Kauffman, et al. (2003). "Regulated degradation of a class V myosin receptor directs movement of the yeast vacuole." Nature **422**(6927): 87-92.

Tang, F., Y. Peng, et al. (2006). "Vac8p, an armadillo repeat protein, coordinates vacuole inheritance with multiple vacuolar processes." Traffic **7**(10): 1368-1377.

Taylor, K. A. (2007). "Regulation and recycling of myosin V." Curr Opin Cell Biol **19**(1): 67-74.

Terrak, M., G. Rebowski, et al. (2005). "Structure of the light chain-binding domain of myosin V." Proc Natl Acad Sci U S A **102**(36): 12718-12723.

Terrak, M., G. Wu, et al. (2003). "Two distinct myosin light chain structures are induced by specific variations within the bound IQ motifs-functional implications." EMBO J **22**(3): 362-371.

Tewari, R., E. Bailes, et al. (2010). "Armadillo-repeat protein functions: questions for little creatures." Trends Cell Biol **20**(8): 470-481.

Theesfeld, C. L., J. E. Irazoqui, et al. (1999). "The role of actin in spindle orientation changes during the Saccharomyces cerevisiae cell cycle." J Cell Biol **146**(5):

1019-1032.

Vale, R. D. (2003). "The molecular motor toolbox for intracellular transport." Cell **112**(4): 467-480.

Veenhuis, M., F. A. Salomons, et al. (2000). "Peroxisome biogenesis and degradation in yeast: a structure/function analysis." Microsc Res Tech **51**(6): 584-600.

Veigel, C., F. Wang, et al. (2002). "The gated gait of the processive molecular motor, myosin V." Nat Cell Biol **4**(1): 59-65.

Verger, A., J. Perdomo, et al. (2003). "Modification with SUMO. A role in transcriptional regulation." EMBO Rep **4**(2): 137-142.

Verhey, K. J. and J. W. Hammond (2009). "Traffic control: regulation of kinesin motors." Nat Rev Mol Cell Biol **10**(11): 765-777.

Verhey, K. J., D. Meyer, et al. (2001). "Cargo of kinesin identified as JIP scaffolding proteins and associated signaling molecules." J Cell Biol **152**(5): 959-970.

Walker, M. L., S. A. Burgess, et al. (2000). "Two-headed binding of a processive myosin to F-actin." Nature **405**(6788): 804-807.

Warren, G. and W. Wickner (1996). "Organelle inheritance." Cell **84**(3): 395-400.

Waters, J. C. (2009). "Accuracy and precision in quantitative fluorescence microscopy." J Cell Biol **185**(7): 1135-1148.

Watson, R. T. and J. E. Pessin (2001). "Intracellular organization of insulin signaling and GLUT4 translocation." Recent Prog Horm Res **56**: 175-193.

Watson, R. T. and J. E. Pessin (2001). "Subcellular compartmentalization and trafficking of the insulin-responsive glucose transporter, GLUT4." Exp Cell Res **271**(1): 75-83.

Weisman, L. S. (2003). "Yeast vacuole inheritance and dynamics." Annu Rev Genet **37**: 435-460.

Weisman, L. S. (2006). "Organelles on the move: insights from yeast vacuole inheritance." Nat Rev Mol Cell Biol **7**(4): 243-252.

Weisman, L. S. and W. Wickner (1992). "Molecular characterization of VAC1, a gene required for vacuole inheritance and vacuole protein sorting." J Biol Chem **267**(1): 618-623.

Wong, Y. L. and S. E. Rice (2010). "Kinesin's light chains inhibit the head- and microtubule-binding activity of its tail." Proc Natl Acad Sci U S A **107**(26): 11781-11786.

Yildiz, A., J. N. Forkey, et al. (2003). "Myosin V walks hand-over-hand: single fluorophore imaging with 1.5-nm localization." Science **300**(5628): 2061-2065.

Yin, H., D. Pruyne, et al. (2000). "Myosin V orientates the mitotic spindle in yeast." Nature **406**(6799): 1013-1015.